

Practically string stable, lateral control solution for a homogeneous platoon of vehicles

A Centralized vs Distributed MPC approach.

J. A. de Geus

Master of Science Thesis



**Practically string stable,
lateral control solution for a
homogeneous platoon of vehicles**
A Centralized vs Distributed MPC approach.

MASTER OF SCIENCE THESIS

For the degree of Master of Science in Mechanical Engineering at Delft
University of Technology

J. A. de Geus

January 8, 2021

Faculty of Mechanical, Maritime and Materials Engineering (3mE) · Delft University of
Technology

The work in this thesis was supported by Siemens Digital Industries AG. Their cooperation is hereby gratefully acknowledged.



Copyright © Mechanical Engineering (Track: Vehicle Engineering)
All rights reserved.

Abstract

The world is becoming increasingly congested due to a continuous growth of world population and overall wealth. Current road capacity limitations will lead to a significant decrease of traffic flow accompanied by a serious increase in global fuel consumption and air pollution. Ever-expanding road infrastructure is not expected to be a sustainable and long-term solution, thus other solutions are sought. Amongst these solutions is the concept letting Automated Vehicle (AV) drive closer together, cooperatively. A flock of vehicles that coordinates collective movement while maintaining short inter-vehicle distances is defined as *platooning*. Evidently, in order to achieve safe platooning, a thorough understanding of both longitudinal and lateral behaviour of the platoon system and its dynamics is required.

The longitudinal aspect of platooning concerned with the design of spacing policies (i.e., distance keeping) has been broadly researched in the past decades. As a consequence, numerous valid applications exist. Whereas for the lateral aspect, the subject has not been researched as extensive. Hence a considerable amount of knowledge on this side is still needed to meet strict conditions and requirements for platooning applications. One of the major bottlenecks obstructing robust lateral platoon control is the ability to assure the lateral string stability for the complete platoon.

String stability implies that errors propagating in an upstream direction of inter-connected vehicles forming the vehicular platoon, do not amplify. Specifically, lateral string stability implies that initially bounded lateral errors will remain bounded between ever pair of consecutive vehicles along the string of vehicles. Propagating errors are therefore attenuated during, e.g. the execution of a lane change. Henceforth, when Lateral String Stability for a platoon can be guaranteed, so is the reassurance that a platoon can safely perform certain manoeuvres such as a collective lane change.

This thesis endeavours to develop a string stable, lateral controller for a homogeneous platoon of vehicles using a Model Predictive Control (MPC) approach. In the process two different control strategies tightly linked with the information flow topology, being *centralized* and *distributed*, are designed and compared in terms of reference tracking performance, noise- and disturbance rejection and practical implementation.

Lastly, the developed controllers are simulated and validated using Siemens' Simcenter Prescan software, after which the results are thoroughly discussed. Results have indicated that for the application discussed in this work, the centralized controller outperformed its competitor in the field of tracking performance and noise rejection, but not by a great margin. Furthermore, the novel developed definition of Practical Lateral String Stability (PLSS) guarantees stability for a platoon of $n = 5$ vehicles while using both controllers. To this end, the distributed controller is seen as worthy competitor and more workable solution due to the centralized controller's issue of practical implementation. As part of anticipated future work, we plan testing the proposed approach with field experiments to validate the proposed method in real life.

Glossary

List of Acronyms

ADAS	Advanced Driver Assistance Systems
ALSS	Absolute Lateral String Stability
AV	Automated Vehicle
CACC	Cooperative Adaptive Cruise Control
DARE	Discrete time Algebraic Ricatti Equation
DLC	Double Lane Change
IFT	Information Flow Topology
ITS	Intelligent Transportation Systems
LKA	Lane Keeping Assist
LTI	Linear Time Invariant
MPC	Model Predictive Control
V2I	Vehicle-To-Infrastructure
V2V	Vehicle-To-Vehicle
ZMWN	Zero Mean White Noise

List of Symbols

α_f	[rad]	Front slip angle.
α_r	[rad]	Rear slip angle.
β_i	[rad]	Sideslip angle.
δ	[rad]	Steering angle.
$\dot{\psi}$	[rad/s]	Yaw rate.
$\dot{\psi}_{e,i}$	[rad/s]	Rate of change in yaw-angle error of vehicle i .

$\dot{y}_{e,i}$	[m/s]	Rate of change of lateral error of vehicle i .
\mathcal{B}_i	[-]	Body-fixed coordinate frame for vehicle i .
\mathcal{C}	[-]	Orthogonal projection on reference trajectory coordinate frame.
\mathcal{N}^g	[-]	World-fixed, global coordinate frame.
\mathcal{T}	[-]	Reference trajectory.
\mathcal{U}	[-]	Set containing all the possible input states of $u \in \mathbb{R}^n$.
\mathcal{X}	[-]	Set containing all the possible vehicle states of $x \in \mathbb{R}^n$.
$\psi_{e,i}$	[rad]	Heading error of vehicle i .
ψ_i	[rad]	Yaw angle of vehicle i .
ε_i	[-]	Propagation of lateral error from platoon member $i - 1$ to i .
\vec{V}	[m/s]	Vehicle velocity vector.
A_d	[-]	Discretized System matrix of A, likewise for B, C and D.
C	[-]	Vehicle Center of Gravity.
C_f	[N/rad]	Front tire cornering stiffness.
C_r	[N/rad]	Rear tire cornering stiffness.
d_i	[m]	Inter-vehicle distance between platoon member $i - 1$ and i .
f	[-]	Contact point of front wheel with ground.
$F(x, N)$	[-]	Terminal cost function over prediction horizon N .
F_{xf}	[N]	Longitudinal front tire force.
F_{xr}	[N]	Longitudinal rear tire force.
I_z	[kgm ²]	Vehicle mass moment of inertia.
J	[-]	MPC-controller cost function.
j	[-]	Complex part of a number.
L	[m]	Wheelbase.
L_f	[m]	Distance from vehicle COG to front axle.
L_r	[m]	Distance from vehicle COG to rear axle.
m	[kg]	Total vehicle mass.
N	[-]	Prediction Horizon.
r	[-]	Contact point of rear wheel with ground.
$R_{\mathcal{B} \rightarrow \mathcal{N}}(\psi)$	[rad]	Rotation matrix around the z -axis for mapping from \mathcal{B} to \mathcal{N} .
v_x	[m/s]	Longitudinal velocity component.
v_y	[m/s]	Lateral velocity component.
X_f	[-]	Terminal set of terminal cost function.
$y_{e,i}$	[m]	Lateral error of vehicle i .
Γ_i	[-]	String stability complementary sensitivity function in the Laplace domain.
λ	[-]	Weighing matrix on the input vector $[u(k), \dots, u(k + N)]^T$.
Ω	[-]	Weighing matrix on the state vector $[x(k), \dots, x(k + N)]^T$.
ω	[rad/s]	Frequency.
sup	[-]	Supremum.

Table of Contents

Glossary	iii
List of Acronyms	iii
List of Symbols	iii
Acknowledgements	xi
1 Introduction	1
1-1 Motivation for Vehicular Platooning	1
1-2 Vehicular Platooning; a brief overview	2
1-2-1 Information Flow Topology	3
1-3 The Concept of String Stability	4
1-3-1 Longitudinal String Stability	4
1-3-2 Lateral String Stability	5
1-4 Problem statement and contribution	5
1-5 Scope and limitations	6
1-6 Thesis outline	7
2 Review of Lateral Control Methods	9
2-1 Lateral Control approaches	9
2-1-1 Look Down: Centerline tracking	10
2-1-2 Look Ahead: Lane Following	10
2-1-3 Look Ahead: Vehicle Following	10
2-2 Model Predictive Control	12
2-2-1 An overview of MPC theory	12
2-2-2 Motivation for MPC-approach	15
2-3 Conclusion	16

3	Vehicle System Dynamics	17
3-1	Single track bicycle model	17
3-1-1	State-Space Equation for a single vehicle	21
3-2	Error dynamics	22
3-2-1	$\dot{\psi}_{e,i}$ -derivation	23
3-2-2	$\dot{y}_{e,i}$ -derivation	24
3-2-3	State-Space Equation including error dynamics	25
3-3	Platoon model	26
3-3-1	State-Space Equation for preceding- and following vehicle	27
3-3-2	Centralized Platoon Model	28
4	Proposed control solution	31
4-1	String Stability: a mathematical definition	32
4-1-1	\mathcal{L}_p stability	33
4-1-2	\mathcal{L}_∞ -stability	34
4-2	From Theoretical to Practical String Stability	36
4-3	Control Objectives	38
4-4	Centralized- vs. Distributed strategy	38
4-5	Designing controller architecture	40
4-5-1	Discretization of the system matrices	41
4-5-2	Cost function	42
4-5-3	Predictor	43
4-5-4	Constraints	44
4-5-5	Terminal sets and terminal costs	46
4-5-6	Full problem formulation	46
5	Simulation and results	49
5-1	Simulation setup	49
5-1-1	Simcenter Prescan	49
5-1-2	Test Vehicles	50
5-1-3	Scenario 1: Double Lane Change (DLC)	51
5-1-4	Scenario 2: Highway Turn	51
5-1-5	Scenario 3: Double Lane Change during constant curve	52
5-1-6	Noise and disturbance conditions	52
5-1-7	Gust of wind	53
5-1-8	Decision variables for guaranteeing Practical Lateral String Stability	53
5-2	Simulation Results	54
5-3	Discussion and comparison	69
6	Conclusions and Future Work	75
6-1	Conclusions	75
6-2	Recommendations for further research	77

A Linear Tire Behaviour	79
B Proof of \mathcal{L}_∞-stability	81
C Simulation result plots	83
C-0-1 Double Lane Change Scenario, normal conditions, $v_x = 100$ km/h	83
C-0-2 Constant Curve Scenario, normal conditions, $v_x = 80$ km/h	84
C-0-3 Lane Change in Constant Curve, normal conditions, $v_x = 80$ km/h	85
Bibliography	87

List of Figures

1-1	Homogeneous platoon of five interconnected vehicles	2
1-2	Four possible platoon topologies; 1. Predecessor following (PF), 2. Bi-directional (BD), 3. Two-Predecessors Following (TPF), 4. Leader Following (LF) [1]	3
1-3	Slinky effect occurring in the longitudinal aspect of platooning	4
1-4	Lateral error accumulation along a platoon, y-position against time	5
2-1	Corner-cutting phenomenon	11
2-2	Path-Based Vehicle Following method	12
2-3	Visualization of the concept of Model Predictive Control [2]	13
2-4	Control structure for MPC	14
3-1	Single Track Bicycle Model	17
3-2	Relevant parameters and conventions for error dynamics	22
3-3	Relevant parameters and conventions for vehicle following	26
3-4	Relevant parameters and conventions for the centralized platoon model	29
4-1	Centralized control topology for platooning application	39
4-2	Distributed control topology for platooning application	40
5-1	Screenshots of a double lane change scenario simulation	50
5-2	Parameter values used in simulation	50
5-3	Scenario 1: Double Lane Change at $v_x = 100$ km/h	51
5-4	Scenario 2: Constant Curve ($r=400$ m) at $v_x = 80$ km/h	51
5-5	Disturbed signal (e.g. yaw rate)	52
5-6	Relevant dimensions for road and test vehicles	53
A-1	Lateral tire force against slip [3]	79

Acknowledgements

After seven beautiful years of studying Mechanical Engineering at the Delft University of Technology, my time here has come to an end. Over the course of these years, I have had the privilege to be enriched with an incredible amount of amazing experiences, good memories and close friends. Therefore, I would like to take this opportunity to thank some people.

My first word of thanks goes out to my TU Delft supervisor, Laura Ferranti. Laura, during the long process I could always count on your knowledge, experiences and sharp insights. By providing these, you helped me greatly with valuable and solid advice during meetings in order for me to finalize this thesis. For which again I'd like to say, thank you.

Secondly, I'd like to express my gratitude towards my supervisors at Siemens Digital Industries AG, Joan Roca Nuñez, Mohsen Alirezeai and Koen Bussemakers. Joan, under your guidance at Siemens I felt trust and responsibility which extremely motivated me into working hard and passionately on the subject. I very much enjoyed the nice and friendly working environment at the office and gained an enormous amount of working experience during the internship. Mohsen, your expertise, deep understanding of the subject and feedback you provided was on all fronts extremely useful. Thank you for making time to help me further whenever I got stuck and for letting me reflect on my own work, critically. Koen, I'd like to thank you dearly for the fun conversations and consultation sessions we've had the last 9 months. You have been of great help when I needed you and were always down for some laughing.

During the process, I also reached out to fellow students for some second opinions and insights. Daniel, Joost and Nino, thank you guys for stretching out your helping hand when I asked you for it.

Special thanks goes out to my dear parents and brother Kevin. Without you always being there for me over all the years of my life, I would not stand where I am today. For this, I will be eternally grateful. My roommates, Stefan and Vito, thanks for providing me with the necessary laughter and encouragement when times got tougher and motivation was lower.

Last but certainly not least, I'd like to thank my amazing girlfriend, Annemarieke, for her immense love and continuous emotional support. All along the process, you gave me energy, inspiration and reminded me to always give my best in order to finish this work.

"We are continually faced by great opportunities brilliantly disguised as insoluble problems."

— *Lee Iacocca*

Chapter 1

Introduction

1-1 Motivation for Vehicular Platooning

Ever since the development of the first Advanced Driver Assistance Systems (ADAS) aiming to increase driving comfort and safety, technological improvements in all aspects of autonomous driving have advanced at a quick pace. A next step forward in the ongoing evolution of transportation is to enable cooperative driving, also known as platooning. In recent years, it has become clear many benefits are to be achieved from this promising concept [4],[5],[6].

As the world population and overall wealth increases, at the same time does the societal demand for personal-, public- and freight-transportation. Consequently, this growth has led to a serious increase of road use and is expected to keep growing in the near future [7]. When the limits of current road capacities are reached, traffic-flow efficiency significantly reduces leading to severe congestion. Expansion of the existing road network is considered to be only a costly and short-term solution. On the other hand, by allowing vehicles to drive maintaining short inter-vehicle distances, optimal use of the existing road network can be accomplished; improving traffic throughput and eliminating so called phantom traffic jams [8]. The rise of Intelligent Transportation Systems (ITS) in the last decade has cleared the path for solutions employing Vehicle-to-Vehicle (V2V) and Vehicle-to-Infrastructure (V2I) communication in order to achieve such short inter-vehicle distances.

The increase of traffic-flow efficiency is not the only advantage vehicular platooning has to offer. Various studies have shown (truck-)platooning significantly reduces fuel consumption due to decrease in aerodynamic drag forces when incorporating short inter-vehicle distances [9], [10]. Additionally, optimized acceleration/deceleration control reinforces this effect. Accordingly, vehicular platooning will positively contribute to current environmental concerns by realizing a reduction of fossil fuel usage while at the same time lowering levels of air pollution. Likewise for commercial purposes; platooning can also be applied to Heavy Duty Vehicles. Reducing fuel consumption will yield substantial savings for companies that are engaged freight-transportation of products and services.

Another crucial benefit autonomous driving provides is improved safety for all road users. In [11], [12] it has been concluded more than 70% of accidents are caused by human errors that could have been prevented. Driver fatigue, driver distractions and audacious driving behaviour are most contributing factors to fatalities in these situations. Henceforth, one can safely assume (cooperative) autonomous driving increases safety, reliability and driving comfort by abolishing unfavorable human-error effects and taking away dynamic driving tasks from the human controller. Summarizing, one may conclude that platooning would undoubtedly benefit society. Unfortunately until today challenges remain and as a consequence much knowledge is still to be gained.

Section 1-2 introduces the concept of vehicular platooning and briefly states some concepts of which understanding is needed in order to pose the research question, detailed in Section 1-4. Section 1-5 highlights the scope and limitations for this work. The structure for the remainder of this thesis is mentioned in Section 1-6.

1-2 Vehicular Platooning; a brief overview

A vehicular platoon can be defined as a fleet of interconnected sub-systems (i.e., the vehicles) that coordinate collective movement while maintaining short inter-vehicle distance. The collective movement is realized through measurements of other platoon members and via wireless, inter-vehicle communication of vehicle states. The cooperative approach allows the vehicles to accelerate and brake simultaneously as well as following a constant trajectory. A vehicular platoon consists of one lead vehicle and n followers, indexed by $i = \{1, 2, \dots, n\}$ consecutively along the string of vehicles, whilst maintaining a certain inter-vehicle distance, d_i . The platoon leader can either be operated by a human controller, or be programmed to follow a certain reference trajectory, implying the platoon is fully autonomous.

By interconnecting vehicles to a form platoon, one simultaneously couples the dynamics of the sub-systems to a whole. Therefore, a thorough understanding of not only a single vehicle's dynamical properties in the longitudinal and lateral domain are required, but also of the full flock. A platoon for which all vehicles have the same dynamics, saturations and physical limits (i.e., all identical vehicles) is defined as a homogeneous platoon. A platoon for which this is not the case, i.e., non-identical vehicles are utilized, the platoon is defined to be heterogeneous. In this thesis, only homogeneous platoons will be considered. Figure 1-1 depicts such a homogeneous platoon of five interconnected vehicles. Every platoon member is equipped with various sensors, controllers and communication devices in order to enable the cooperative driving.

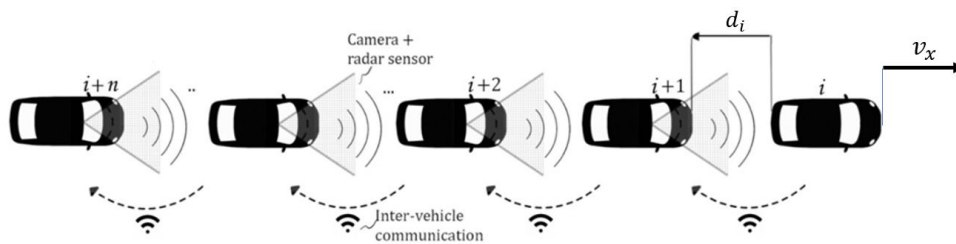


Figure 1-1: Homogeneous platoon of five interconnected vehicles

For the longitudinal automation, i.e., distance keeping, the AVs are equipped with forward-looking radar sensors as applied in conventional Cooperative Adaptive Cruise Control (CACC) systems. These sensors keep track of the preceding vehicle and continuously measure its vehicle states as reliable as possible. Embedded controllers and actuators together with incorporated spacing policies decide whether an individual vehicle in the platoon should accelerate or brake slightly to respect the distance-keeping criteria.

For the lateral automation, the AVs are usually equipped with camera sensors that again through object detection can identify lane markings and preceding vehicles in order to keep the vehicle in the center of the lane, as seen in conventional Lane Keeping Assist (LKA) systems. The data retrieved by the sensors along with a platoon member's own vehicle state parameters (i.e., position, velocity, longitudinal and lateral acceleration and steering angle) may be communicated to other AVs in the platoon, depending whichever Information Flow Topology (IFT) is incorporated.

1-2-1 Information Flow Topology

To achieve safe platooning, wireless, inter-vehicle communication may be utilized to improve system reliability. This communication can be applied using several strategies. The method in which vehicles share their data with other vehicles in the platoon is defined as the Information Flow Topology and is conceptualized with graph theory. Several studies [1], [13] have been conducted on platoon topologies in order to find the best topology for certain platooning applications. Figure 1-2 visualizes four possible platoon topologies. One commonly used topology in literature is that the lead vehicle exchanges data with other member in the platoon separately. This *centralized* topology is defined as a Leader Following (LF). Another commonly used approach is that a vehicle in the platoon gets data solely from the preceding vehicle, in order to achieve faster processing of data and thus allows smaller inter-vehicle distances to be possible, a *distributed* approach incorporating a Predecessor following (PF) topology. At this point there is no effective analysis method for general IFTs yet and thus no superior solution for a specific platoon formation stands out. At the same time one must be careful selecting a certain topology, as it may greatly affect string stability behaviour because of communication delay worsening the string stability properties of a platoon [14].

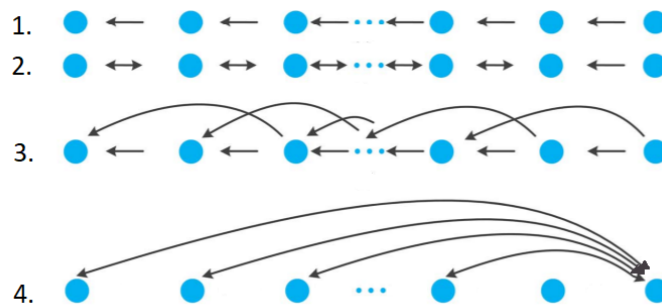


Figure 1-2: Four possible platoon topologies; 1. Predecessor following (PF), 2. Bi-directional (BD), 3. Two-Predecessors Following (TPF), 4. Leader Following (LF) [1]

1-3 The Concept of String Stability

When a vehicular platoon is to perform, for example, a lane change, it is critical to ensure that all members of the platoon perform the same manoeuvre and do not swerve off the road during the execution. For this reason the complete system of interconnected vehicles must respect the stability criteria, and not just stay within the stability margins of its own subsystem. This concept is denoted as *String Stability* and is defined for both in the longitudinal as well as in the lateral sense. Even though in literature slightly different definitions of the term are given, the phenomenon can best be described by; "*The attenuation of errors propagating in an upstream direction of interconnected vehicles forming a platoon*" [15]. More specifically, initially bounded lateral- or spacing errors will remain bounded between every pair of vehicles, hence safe platooning can be guaranteed if the criteria are met. String stability analysis is the principal assessment criterion for determining whether a platoon executes desired behaviour. In literature, several distinct methods in assessing platoon behaviour and assessing string stability have been identified [16]. However, a vast majority of these methods consist from complex, theoretical mathematics in the analysis of the integrated system model. In this work, such a method is cumbersome and thus a more practical definition that guarantees stability for the selected purpose is sought.

1-3-1 Longitudinal String Stability

The longitudinal aspect of string stability is concerned with the regulation of distance keeping between two consecutive platoon members. Braking or accelerating without inter-vehicle communication will result in oscillations between vehicles i and $i - 1$ that will propagate further down the platoon. This phenomenon is also known as the *slinky effect* [17] and is illustrated in Figure 1-3. If the platoon leader ($i = 0$) brakes, the distance to the first following vehicle (i), being d_1 , decreases. When vehicle ($i + 1$) also then brakes, d_2 decreases. As a result, d_1 then increases again. Evidently, this process creates a propagating oscillation along the platoons inter-vehicle distances. In addition, large delays in communication, slow sensor data processing and actuator lag may further amplify the slinky effect. A longitudinal, string stable controller ensures the phenomenon is attenuated and spacing errors stay within stable margins, respecting the platoon's spacing policy. Throughout this thesis a longitudinal distance controller is assumed to be present in the experimentation and therefore the concept of longitudinal string stability is not taken into account.

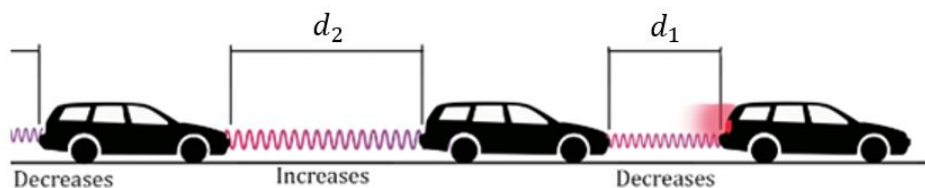


Figure 1-3: Slinky effect occurring in the longitudinal aspect of platooning

1-3-2 Lateral String Stability

The concept of Lateral String Stability (LSS) ensures the amplification of lateral deviation along the platoon measured from the preceding vehicle's centerline, stays bounded. The completely coupled platooning system must respect the string stability criteria in order to ensure all members will always stay within their designated lane, do not swerve off the road or enter a neighboring lane. Figure 1-4 depicts the accumulation of lateral errors ε_1 , ε_2 , ε_3 and ε_4 for a lane change manoeuvre in a platoon consisting of five vehicles. Lateral string stability requirements must assure the summation of lateral errors, $\sum \varepsilon_i \forall i = \{1, 2, \dots, n\}$, does not override system bounds. In theory, this can be achieved by limiting the amplification of lateral errors, i.e., $|\frac{\varepsilon_i}{\varepsilon_{i+1}}| \leq 1$.

Against the classical definition of string stability, for practical purposes, sometimes a slight amplification can be accepted as long as it remains between the imposed system bounds. In Chapter 4, the overall concept of Lateral String Stability, the mathematical definition and a novel, more practical definition of the concept denoted as Practical Lateral String Stability will be further elaborated.

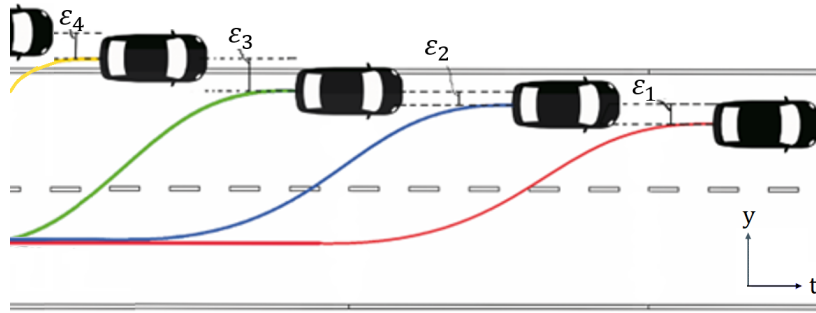


Figure 1-4: Lateral error accumulation along a platoon, y-position against time

1-4 Problem statement and contribution

After performing a literature survey prior to this work [16], it has been identified that the longitudinal aspect of platooning, concerned with the design of spacing policies (i.e., distance keeping) has been broadly researched in the past decades. As a consequence, a vast understanding of the required knowledge is present and valid applications exist. Whereas for the lateral aspect, the subject has not been researched as extensive and therefore progress on this field has been slow. A considerable amount of knowledge on this side is still needed to meet the strict conditions and requirements for platooning applications. One of the major bottlenecks obstructing robust lateral platoon control is the guarantee of Lateral String Stability issue as mentioned in Section 1-3-2.

Furthermore, it has been found a wide range of control strategies for lateral automation exists, but not all methods used for conventional LKA-systems are directly applicable for vehicular platooning. When these are extended to form a path follower for multiple vehicles, new challenges arise. One attractive option as lateral controller for a platoon of vehicles; is Model Predictive Control (MPC).

This MSc thesis contributes to the State Of The Art by bringing forward a threefold of assets;

1. Additional knowledge to the field of lateral control solutions for vehicular platooning: we develop two different MPC strategies both tightly linked to the Information Flow Topologies for which no superior solution exists yet. Due to the work executed in this thesis, remarks can now be made on the performance and applicability of two of such methods. This reveals new insights for future research using MPC as the selected control method.
2. A novel definition: instead of using complex, theoretical mathematics in order to attempt guaranteeing Lateral String Stability, a novel definition of the concept of string stability will be developed. This new definition, entitled Practical Lateral String Stability (PLSS) can guarantee string stability in the lateral sense for a platoon up to n vehicles by sometimes allowing amplifications of lateral disturbances as long as they remain bounded between the imposed system bounds.
3. Extensive testing: the results in this work have been obtained using the high-fidelity simulation environment of Simcenter Prescan. Using such an extensive and reliable simulation tool, confidence is stirred the findings in this work might be practically feasible for real-life applications. Namely, results have indicated excellent tracking performance and noise rejection.

1-5 Scope and limitations

The aim of this thesis lies on the development of a practically string stable, lateral control solution for a homogeneous platoon of n vehicles for highway driving applications. Two strategies concerning the communication between the platoon members, being centralized and distributed, are compared in terms of their performance, computation time and noise-rejection properties to determine the superior solution.

The value for $n = 5$ has been selected based on outcome of multiple studies having found platoons of large n are difficult to control in the lateral sense [18],[19],[20] and that stability quickly decreases with an increasing n . In literature, platoon sizes between 5 and 10 are commonly found and possibly most practical for first real-life applications.

Furthermore, as the main focus of this work lies in the lateral domain, longitudinal dynamics (including pitching and diving caused by accelerating and braking) that influence vehicle behaviour will not be considered. Moreover, a constant longitudinal velocity ($v_x = 100$ km/h) and a constant inter-vehicle distance ($d_i = 20m$) are incorporated during the development and simulation. This implies the inter-vehicle time of $t_i \approx 0.72$ s is significantly less than the 2 s safety guideline handled on the Dutch national highways [21] for human controlled strings, thus proving that road capacity would be significantly improved.

In addition, it was mentioned that the platooning application discussed in this thesis represent highway-driving only. Therefore, assumptions for linearizing the vehicle model and small angle approximations can be made. These will be further elaborated in Chapter 3, where the Vehicle System Dynamics are discussed.

Lastly, in this thesis it is assumed that (perfect) wireless V2V-communication is present and perfect sensor measurement are obtained amongst the platoon. Platoon members can therefore communicate data on their states to the other platoon members without latency and too large sensor errors.

1-6 Thesis outline

The upcoming chapters in this work are structured as follows. Chapter 2 reviews the existing lateral control options as utilized in current platooning applications. First, different path-following strategies are highlighted and compared. Then, a summary on the theory behind Model Predictive Control, the selected control solution, is given along with the accompanying motivation. Hereafter, in Chapter 3, the equations that describe the vehicle- and platoon's lateral dynamics are discussed. The state-space equations for a single vehicle and the error dynamics to the reference trajectory are derived. Next, this state-space equation is extended with the dynamics that describe a vehicle's relation to its predecessor. Finally, the complete, generalized platoon model is drafted.

We proceed with covering the proposed control solution in Chapter 4. The chapter starts with different view on string stability; the concept is further explained in a more mathematical fashion in order to understand the principles. Then, a novel, more practical definition of the concept that is more relevant for the application discussed in this work is made clear. Hereafter the design process of all necessary features of MPC for both the centralized and the distributed controller are clarified. In Chapter 5 we deal with the setup of the experimental simulations for testing the controllers in terms of performance, robustness and noise rejection. Three different scenarios are proposed that resemble everyday highway driving, subjected to both normal and disturbed conditions. Results of the extensive testing of both controllers are also thoroughly discussed in this chapter. Lastly, in Chapter 6, conclusions on the developed controllers are drawn. Hereafter, the thesis is closed with recommendations in case further research on the topic is considered.

Review of Lateral Control Methods

As mentioned in the introduction, only limited research has been conducted on the topic of lateral control and lateral string stability for vehicular platooning. This chapter first reviews the lateral control options available for platooning applications in the current state of the art. Then, an overview of theory and motivation on the selected control method used in this work, Model Predictive Control (MPC), is provided.

2-1 Lateral Control approaches

At its core, lateral control embodies the concept of letting a vehicle drive a desired reference trajectory. In other words, letting a vehicle follow a (curved) path of preference, e.g. a road centerline. This can be achieved by adjusting the steering wheel based on certain input signals that are collected by the means of various sensors. For single vehicles, plentiful lateral control algorithms have been developed. However, when attempting to let a complete platoon of vehicles track a certain reference trajectory, several challenges arise. Various different strategies can be incorporated, each with their own benefits, drawbacks and applicational limits.

When incorporating a lateral control method, the first step is to determine how a vehicle determines its reference trajectory. Generally, this is done by the means of data collection via embedded sensors. The sensing strategies are classified into a Look Down- and a Look Ahead approach, depending where the AV tries to 'find' the reference trajectory. When the sensing strategy for a single vehicle is determined, one can establish how to extend the lateral control method to a platoon of vehicles. This section discusses concretely one Look Down and two Look Ahead options.

2-1-1 Look Down: Centerline tracking

In the Look Down method of centerline tracking, the AVs uses sensors to determine the road centerline by looking down at the road surface and reducing the measured lateral offset to this centerline, y_e , to zero. At an early stage of lateral automation research in the 90s, one tried experimenting with embedding magnetic reference signals in the the road surface for the vehicle to follow [22]. The downside of such a method is that adaptation becomes quite costly, as infrastructural changes need to be applied. Furthermore, bad lighting and weather conditions such as snow, ice and hail could lead to unreliable measurements from embedded sensors. Therefore Look Ahead Methods such as the Lane Following and Vehicle Following were quickly preferred.

2-1-2 Look Ahead: Lane Following

Lane following methods ([23],[24],[25]) rely on the detection of lane markings on the road surface to calculate the position of the lane centerline at a certain Look Ahead distance. Such methods yield an absolute reference value for the lateral error, y_e , used as input on the steering wheel angle in order to let the vehicles drive over the reference trajectory. For lane following methods, when extending this method to a platoon, the lateral dynamics of the complete platoon will not be interconnected as all vehicles follow a certain fixed reference hence lateral errors do not accumulate along the string of vehicles. However, the major drawback for this approach becomes clear when applied to a platoon incorporating very small inter-vehicle distances. In this case only limited information on the upcoming road can be detected, as the look ahead distance is blocked by the preceding vehicle. Consequently, ultra fast processing and communication is a strict requirement for this approach. In addition, hardly-visible lane markings and bad weather conditions may lead to poor measurements and in make it difficult for the controller to accurately track the reference path. This in turn could possibly leading to dangerous situations when reliable path tracking can not be guaranteed.

2-1-3 Look Ahead: Vehicle Following

Vehicle Following relies on continuous measurements of the preceding vehicle and evaluation of its states. Accordingly, the lateral position yields a relative reference value of lateral offset, y_e , to be used as input for the lateral controller. Considering that for vehicle following methods every vehicle essentially follows only its predecessor, the lateral dynamics are coupled together. Consequently, lateral disturbances may propagate throughout the platoon. As a consequence, strict conditions and analysis on string stability is required. The vehicle following approach can be further divided into two different strategies; distinguishing Direct Vehicle Following and Path-based Vehicle Following.

Direct Vehicle Following

The concept behind Direct Vehicle Following ([26],[27]) is to steer a vehicle directly towards a reference point that is located on the preceding vehicle after it is detected by the following vehicle's radar- and camera sensors.

Essentially, this reference point then is the relative position of the preceding vehicle as measured from the following vehicle in its local coordinate system. This method has also been described 'virtual tow-bar'-method, as the vehicle is 'towed' towards the reference point in the shortest, direct manner.

Direct Vehicle Following has been the most frequently implemented strategy in this approach, as it is perceived to be the simplest of the two solutions. This simplicity is mainly caused by the fact that the measured current relative position of preceding vehicle is the only input variable to the controller. As a consequence, this simplicity also brings forward the main disadvantage of this method defined as the 'Corner-cutting phenomenon', which is illustrated in Figure 2-1.

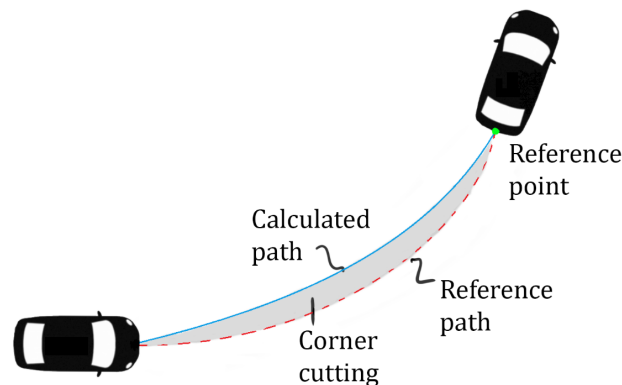


Figure 2-1: Corner-cutting phenomenon

It can be observed from the figure that the path driven by the following vehicle differs from the path that its predecessor drove. Evidently, this path-error will occur for every vehicle in the platoon and will thus accumulate along the string of vehicles. If the platoon counts many members, some vehicles could heavily undercut the path, possibly leading to dangerous situations.

Path-based Vehicle Following

The Path-Based Vehicle Following strategy ([28],[29]) relies on the construction of an estimated path driven by a vehicle's predecessor. The embedded radar- and camera sensors measure a reference point in 3D-coordinates from the preceding vehicle at every timestep, in the ego-vehicle's coordinate system. Hereafter the path is reconstructed using interpolation techniques. Lastly, this constructed path is used as input for the following vehicle's lateral controller, in the same way a lane following method is implemented. Evidently, this method adds significant complexity to the system in the form of additional computational efforts depending on the sample rate and look ahead distance. However, results have indicated controller performance significantly improved compared to Direct Vehicle Following methods [28]. Another considerable advantage of this method is that Path-Based Vehicle Following controllers do not experience the same corner-cutting phenomenon found in Direct Vehicle Following methods.

Figure 2-2 depicts such a Path Based Vehicle Following method.

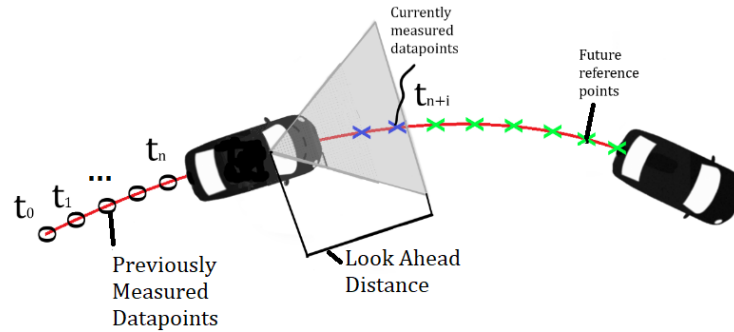


Figure 2-2: Path-Based Vehicle Following method

Clearly, the type of lateral control strategy incorporated for a platoon has a significant effect on the performance and Lateral String Stability conditions. Moreover, both approaches have their advantages and disadvantages in terms of performance, complexity and applicability.

In this thesis, a highway-driving application for the vehicular platoon is discussed. Therefore, slight effects of the corner cutting phenomenon are accepted and, in order to further reduce system complexity and speed up computation, incorporating Direct Vehicle Following-like method has been chosen based for this work.

2-2 Model Predictive Control

The literature survey prior to this work has reviewed different control strategies and has selected MPC to be an interesting option due to the nature of its algorithm and its rarity for platooning applications [16]. Section 2-2-2 discusses a brief motivation on why MPC was chosen as the superior solution.

2-2-1 An overview of MPC theory

Model Predictive Control is a control strategy in which an optimal input from the controller is computed at each time step for a discretized plant model to follow a certain desired reference value of the plant output. This optimal input is calculated using a cost function over a prediction horizon while only the current input is implemented at each time step k . When the next measurements become available at $k + 1$, this process is re-iterated. A model of the plant is used to make predictions about the future plant output behaviour such that the consequences of the implemented control input are taken into account by the means of weights. The calculations done in the prediction step are based on current measurements as well as predictions of the future values of the output. Figure 2-3 depicts the basic concept of an MPC in which the predicted output approaches the reference output.

The cost function is implemented to obtain an optimisation objective, based on the difference between the reference states and the measured/predicted states. It can be interpreted as the inverse of the desired control behaviour; hence a penalty is given to undesired behaviour using the weights. This control input is calculated by repeatedly solving finite-time optimal control problems over a specified prediction horizon N -steps in the future.

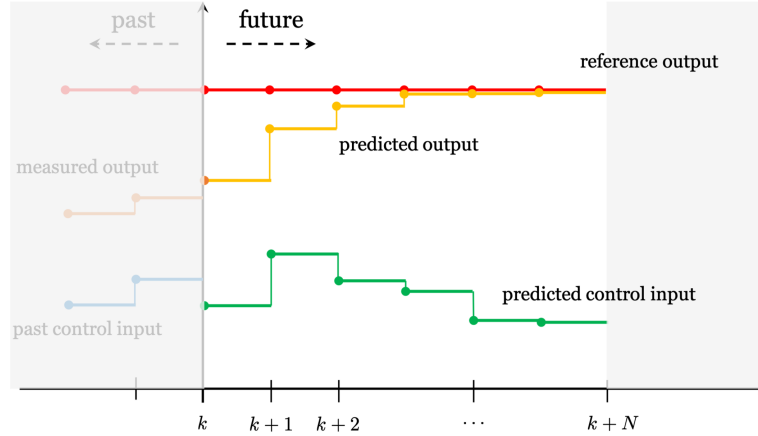


Figure 2-3: Visualization of the concept of Model Predictive Control [2]

Additionally, constraints can be added to the optimization problem to ensure certain system bounds are not overridden. These are conventionally added to achieve desired performance and desired stability. Equation 2-1 shows a general formulation of such an optimal control problem solved by the MPC at every time step. First, we define the state and input vector for the optimization problem of the MPC as;

1. $\tilde{x}(k|k) = [x(k+1|k)^T, x(k+2|k)^T, \dots, x(k+N|k)^T]^T$
2. $\tilde{u}(k|k) = [u(k|k)^T, u(k+1|k)^T, \dots, u(k+N-1|k)^T]^T$

Then the optimization problem can be written as;

$$\begin{aligned}
 & \min_{\tilde{u}(k)} J(\tilde{x}(k), \tilde{u}(k)) \\
 & \text{s.t.} \\
 & x(k+p|k) = f(x(k+p-1|k), u(k+p-1|k)) \\
 & x(k|k) = x(0) \\
 & x(k) \in \mathcal{X}, \quad u(k) \in \mathcal{U} \\
 & p = 1, \dots, N
 \end{aligned} \tag{2-1}$$

where and In this formulation, the states and inputs are contained in convex sets $\mathcal{X} = \{x \in \mathbb{R}^m \mid x_{\min} \leq x \leq x_{\max}\}$ and $\mathcal{U} = \{u \in \mathbb{R}^m \mid u_{\min} \leq u \leq u_{\max}\}$. All imposed constraints need to be satisfied in order to find a feasible solution. The cost function J can be drafted to the designer's preference, depending on the nature of the plant model and control objectives. In MPC-applications, the cost function is conventionally chosen to resemble a (convex) Linear Quadratic Regulator (LQR), e.g:

$$J(k+p) = \sum_{p=1}^{N-1} (\|x(k+p) - x_r(k+p)\|_{\Omega}^2 + \|u(k+p) - u_r(k+p)\|_{\lambda}^2) \tag{2-2}$$

Herein, x_r denotes the reference state vector, u_r denotes the reference control input. The iterations for predicting future states and minimizing the cost function are done for the current timestep until the end of the prediction horizon N , i.e. $p = \{1, \dots, N\}$.

What's more, Ω and λ denote (positive semidefinite) weighing matrices on respectively the state- and input vector. The height of this weight corresponds with the importance of the state to be tracked or the input to be penalized; the lower the values, the more emphasis lies on this parameter. A feasible solution is found when both x_r and u_r are kept within the interior of the product of the sets \mathcal{X} and \mathcal{U} .

MPC adopts a certain framework that is defined as the receding horizon. This framework implies that the same steps are repeated iteratively until the end of the simulation. Throughout the process, the length of this prediction horizon stays constant. The receding horizon framework operates iteratively repeating the following five steps:

1. Measure current state $x(k|k)$ and output $y(k|k)$.
2. Calculate the optimal control signals $\tilde{u}(k|k)$ over horizon N by minimizing cost function $J(\tilde{x}(k), \tilde{u}(k))$. By optimizing the control inputs, future states and outputs are predicted using the prediction model.
3. Apply the first optimal control input from $\tilde{u}(k|k)$ to the plant model at time instant k .
4. Await the next time instant, i.e. wait until $k = k + 1$.
5. Repeat from step 1.

The control structure that handles this iterative scheme is visualized in Figure 2-4. Here one can observe that the constraints and the cost function are directly imposed on the optimizer, and that plant (i.e. the vehicle- or platoon model) output is directly fed back to the predictor as well as to compare it with reference y_{ref} value.

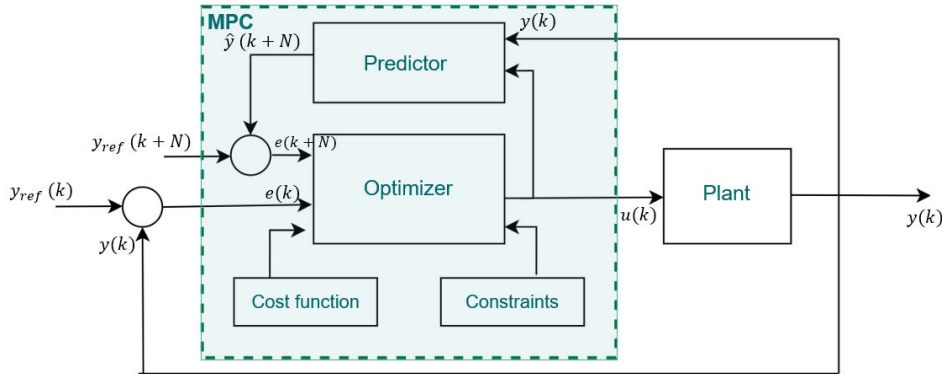


Figure 2-4: Control structure for MPC

For stability analysis in MPC-related problems, conventionally a Lyapunov stability function is used. It was found in [30] that a value function of a finite horizon optimal control problem could be used instead of a Lyapunov function to establish guaranteed controller stability. This was done by employing a terminal cost function at the end of the prediction horizon, $F(x, N)$, to the cost function and a terminal set, X_f , to the constraints. By doing so, stability can be guaranteed if an optimal solution is found. Moreover, employing terminal sets and costs can be used to stabilize systems that cannot be stabilized with continuous feedback controllers.

The general MPC-problem formulation from Equation 2-1 can be extended with the terminal set and cost to obtain:

$$\begin{aligned}
& \min_{\tilde{u}(k)} J(\tilde{x}(k), \tilde{u}(k)) + F(x(N, x_0)) \\
& \text{s.t.} \\
& x(k+p|k) = f(x(k+p-1|k), u(k+p-1|k)) \\
& x(k|k) = x(0) \\
& x(k) \in \mathcal{X}, \quad u(k) \in \mathcal{U}, \quad x(N, x_0) \in X_f, \\
& p = 1, \dots, N
\end{aligned} \tag{2-3}$$

The choice of $F(x)$ and X_f can highly influence the system performance. For most MPC applications, $F(x)$ is designed as the solution (P_N) to the finite horizon, Discrete time Algebraic Ricatti Equation (DARE), such that N approaches infinity. The DARE is denoted in Equation 2-4.

$$0 = \Omega + A^T P_N A - A^T P_N B (\lambda + B^T P_N B)^{-1} B^T P_N A \tag{2-4}$$

Lastly, there are several different types of MPC that can be adopted depending on the system characteristics, the dynamics where the controller is to act upon and physical application, e.g. (Non-)linear MPC, Hybrid MPC, LTV-MPC, Offline- or Explicit MPC. The type of MPC utilized is of great significance on the performance and computational loads, hence choosing the right type for the right application is an important design variable. This thesis handles a linearized vehicle model, and therefore a Linear MPC will be adopted.

2-2-2 Motivation for MPC-approach

The first criterion where MPC outperformed its competitors on is tracking performance. The control approach is well known as being one of the most reliable multi-objective control methods in terms of accuracy due to its predicting-and-correction nature. This allows for high-performance reference tracking and robustness, as opposed to other reviewed methods. This directly reveals the control method's main *raison d'être*; the on-line approach into handling control laws will always outperform conventional off-line methods using pre-computed control laws. However, it must be noted this past is also a limitation as it effects increased computational efforts [2]. Beside the high-performance reference tracking, the prediction-and-correction nature also allows for noise- and disturbance rejection as these are not incorporated in the prediction of future states.

A second attractive property is its constraint-handling characteristic. Whereas some methods reviewed could not deal with constraints, MPC can. This implies that physical limits and saturations that arise from vehicle dynamics or environmental factors such as road- and weather conditions can be taken into account for this method. For this work, this is an extremely important property as a novel definition for Lateral String Stability is sought which can use this property to its advantage; imposing the constraints as certain performance and stability bounds.

Furthermore, the method is known as being an easy-to-tune method, as compared to other control methods [31]. Essentially, when tuning an MPC-controller, the sole task required is adjusting weights in the cost function; a simple and intuitive process to achieve desired performance. Besides, in recent years MPC has become a very prominent solution as found in several automotive applications [32], and therefore also interesting option for a platooning applications.

However, like any other control method, there are a few disadvantages for this control approach. The major drawback of this control approach comes from the computational efforts that are quite high as a consequence of the high-performance tracking. This might lead to slow processing and higher computational costs. Another point of attention when working with MPC is found in the fact that considerable accurate model of the system dynamics is required. For complex systems, this might be difficult to realize and thus might affect performance. However for this thesis, a sufficiently accurate dynamics model is obtained and therefore the choice for MPC is justified.

2-3 Conclusion

It was previously concluded that little knowledge on lateral automation for platooning applications is present. This chapter has briefly reviewed the current State Of The Art on several control methods and strategies to be used for highway-platooning.

Based on the available knowledge, a Direct Vehicle Following-like method with two different Linear MPC structures are designed in this work. More specifically, two different IFT-structures, being distributed and centralized, are incorporated in the MPC. By comparing the distributed and centralized approach, deeper understanding of lateral control using this method is reached, and knowledge on how this method handles reference tracking, noise- and disturbance rejection is gathered. Furthermore, the constraint-handling property of the selected control approach paves the way to a novel definition of Lateral String Stability in a practical sense. Therefore, the proposed controller as will be thoroughly discussed in Chapter 4, fills up some of the required knowledge in this field in order to make widespread platooning a reality.

As mentioned in the scope and limitations section, it is assumed that pitching, lifting and rolling behaviour are neglected in this model. This assumption can be made because longitudinal and lateral accelerations in highway-driving are generally insignificant enough to conclude load transfer phenomena do not influence vehicle behaviour.

In the model, both the front and rear axle are represented by one single wheel. Each wheel has a contact point with the ground, respectively defined as f (front) and r (rear) where longitudinal and lateral tire forces (F_{ij} with $i \in \{x, y\}$ and $j \in \{f, r\}$) are generated to act on the vehicle dynamics. The vehicle's center of gravity is found in point C and divides the vehicle's wheelbase L into L_f and L_r ; the distances from the center of gravity to each axle. Vector \vec{V} represents the vehicle's absolute velocity and contains a magnitude and a direction, whilst acting from point C . Moreover, this vector is decomposed into its longitudinal (or forward) component, v_x , and the lateral velocity, v_y , with the aim to clarify the derivation of equations of motion. Lastly, the sideslip angle β_i defines the angle between the vehicle velocity vector at each wheel and the vehicle's longitudinal axis, i.e. centerline. They are calculated using Equation 3-1.

$$\beta_i = \arctan\left(\frac{v_{y,i}}{v_{x,i}}\right), \quad i \in \{f, r\} \quad (3-1)$$

In order to reliably derive the kinematic equations, first a local, Body-fixed coordinate system is defined. This coordinate system, \mathcal{B}_i , has its origin, \mathcal{O}^l in the center of gravity of the vehicle at point C . The unit vector \vec{e}_x^l is aligned with the vehicle's longitudinal axis and unit vector \vec{e}_y^l lies perpendicular to this centerline. However, to be able to establish all kinematic equations, not only the vehicle's local coordinate system needs to be defined, but also a global, world-fixed coordinate system is required. This coordinate system is defined as \mathcal{N}^g . Using both of these coordinate systems, it is possible to describe vehicle trajectories from the body-fixed frame in terms of the world-fixed frame [34].

The set of vectors that describes the space spanned by the unit vectors of the both coordinate frames is denoted by;

$$\mathcal{B} : \underline{e}^l = (\vec{e}_x^l \quad \vec{e}_y^l)^T \quad \mathcal{N} : \underline{e}^g = (\vec{e}_x^g \quad \vec{e}_y^g)^T$$

The mapping from one coordinate system to another can be performed using a rotation matrix around the z -axis, $R_{\mathcal{B} \rightarrow \mathcal{N}}(\psi)$. The transformation of a position vector from the body-fixed frame into the world-fixed frame is denoted as can be observed in Equation 3-2 ¹.

$$\begin{aligned} \vec{e}^l &= R(\psi)^T \vec{e}^g \\ \underline{e}^l &= \begin{pmatrix} \cos \psi & -\sin \psi \\ \sin \psi & \cos \psi \end{pmatrix} \underline{e}^g \end{aligned} \quad (3-2)$$

¹the subscript of $\mathcal{B} \rightarrow \mathcal{N}$ will from now onwards be disregarded for the sake of clarity

Now, the position vector from the origin of the world-fixed frame, \mathcal{O}^g , to the vehicle's center of gravity, $r_{\vec{C}}$, is defined as;

$$r_{\vec{C}} = (x \ y) \underline{e}^g$$

Taking the first derivative of this vector will yield the velocity vector of point C as;

$$\begin{aligned} \dot{r}_{\vec{C}} &= [\dot{x} \ \dot{y}] \underline{e}^g \\ \dot{r}_{\vec{C}} &= [v_x \ v_y] \underline{e}^l \end{aligned} \quad (3-3)$$

To obtain the acceleration vector of point C , the second derivative of $r_{\vec{C}}$ is taken with respect to time and then the chain rule is applied to yield;

$$\ddot{r}_{\vec{C}} = (v_x \ v_y) \dot{\underline{e}}^l + (v_x \ v_y) \underline{e}^l \quad (3-4)$$

Using Equation 3-2 and applying once again the chain rule, the following relation can be derived for $\dot{\underline{e}}^l$;

$$\begin{aligned} \dot{\underline{e}}^l &= \dot{R}(\psi)^T \underline{e}^g + R(\psi)^T \dot{\underline{e}}^g \\ &= \dot{\psi} \begin{pmatrix} 0 & 1 \\ -1 & 0 \end{pmatrix} \begin{pmatrix} \cos \psi & -\sin \psi \\ \sin \psi & \cos \psi \end{pmatrix} \underline{e}^g \\ &= \begin{pmatrix} 0 & \dot{\psi} \\ -\dot{\psi} & 0 \end{pmatrix} \underline{e}^l \end{aligned} \quad (3-5)$$

Herein, $\dot{\psi}$ represents the vehicle yaw rate about its center of gravity. Substitution of Equation 3-5 into Equation 3-4 leads to the final expression for acceleration of point C as seen from the world-fixed frame;

$$\ddot{r}_{\vec{C}} = (v_x - \dot{\psi} v_y \ v_y + \dot{\psi} v_x) \underline{e}^l \quad (3-6)$$

Having established the expression for acceleration in 3-6, the equations of motion can be obtained when this expression is applied to Newton's second law to include forces that are generated by the contact between tires and road surface;

$$\sum \vec{F}_C = m \ddot{r}_{\vec{C}}.$$

in which m represents the total mass of the vehicle. For both the longitudinal and lateral tire forces, the Newton laws are expressed as;

$$\sum F_x = m(v_x - \dot{\psi} v_y) \quad (3-7)$$

$$\sum F_y = m(v_y + \dot{\psi} v_x) \quad (3-8)$$

Moreover, it is stated in [3] that for highway driving, the small angle approximation for steering angle δ can be applied. This approximation implies that for small values of δ , it can be assumed that $\sin \delta \approx \delta$ and $\cos \delta \approx 1$. From this assumption it directly follows that for equilibrium of all tire forces along both the longitudinal and lateral component, sum of front and rear tire forces add up to $\sum F_x = F_{xf} + F_{xr}$ and $\sum F_y = F_{yf} + F_{yr}$. All of these force create a moment about the vehicle center of gravity at point C about the z -axis that is equal to $\sum M_z = L_f F_{yf} - L_r F_{yr}$. Finally, this sum of moments can be expressed as the product of the vehicle's mass moment of inertia I_z about the z -axis and the derivative of the yaw rate such that;

$$\sum M_z = I_z \ddot{\psi} \quad (3-9)$$

This leads to the set of equations of motion as seen in 3-10 to 3-12 required to describe lateral dynamics for a single vehicle using the bicycle model;

$$m(\dot{v}_x - \dot{\psi}v_y) = F_{xf} + F_{xr} \quad (3-10)$$

$$m(\dot{v}_y + \dot{\psi}v_x) = F_{yf} + F_{yr} \quad (3-11)$$

$$I_z \ddot{\psi} = L_f F_{yf} - L_r F_{yr} \quad (3-12)$$

Next, the slip angles α_f and α_r are computed. The slip angle for each wheel describes the difference between each wheels velocity vector and the orientation of the wheel, similar to the sideslip angle β . It is calculated using Equation 3-13.

$$\alpha_i = -\beta = \arctan\left(\frac{v_{yi}}{v_{xi}}\right), \quad i \in \{f, r\} \quad (3-13)$$

Here it directly follows from geometry as can be observed in Figure 3-1 that;

$$\alpha_f = \delta - \beta_f \quad (3-14)$$

$$\alpha_r = -\beta_r \quad (3-15)$$

As in this work only highway driving is considered, once again the assumption can be made that only very small values of slip angles occur during driving [3]. This implies each tire operates within the linear region (typically between 0 and 15% of maximum slip) and thus may we assume a linear relation between longitudinal tire force and slip angle through constants defined as the front- and rear cornering stiffness of the tires, C_f and C_r . These constants measure how much lateral force a tire generates per radian of wheel rotation. The linear tire relation along with some additional remarks can be observed in Appendix A.

Accordingly, the longitudinal tire forces F_{xf} and F_{xr} are calculated using Equation 3-16

$$\begin{aligned} F_{yf} &= C_f \alpha_f \\ F_{yr} &= C_r \alpha_r \end{aligned} \quad (3-16)$$

Moreover, because the tires operating in the linear region, the same small-angle approximation can be used to disregard the arctan-term from Equation 3-13 and express the slip angles as;

$$\alpha_f = \delta - \arctan\left(\frac{v_y + L_f \dot{\psi}}{v_x}\right) \approx \delta - \frac{v_y + L_f \dot{\psi}}{v_x} \quad (3-17)$$

$$\alpha_r = \arctan\left(\frac{v_y - L_r \dot{\psi}}{v_x}\right) \approx \frac{v_y - L_r \dot{\psi}}{v_x} \quad (3-18)$$

Combining the above equations with the earlier obtained equations of motions in 3-10, 3-11 and 3.12 will lead to the final equations that describe the longitudinal, lateral and yaw-dynamics of a single vehicle in the platoon. These are drafted in Equations 3-19, 3-20 and 3-21.

$$\dot{v}_x = \frac{1}{m}(F_{xf} + F_{xr}) + \dot{\psi}v_y \quad (3-19)$$

$$\dot{v}_y = -\frac{1}{v_x} \left(\frac{C_f + C_r}{m}\right) v_y + \left(\frac{1}{v_x} \left(\frac{-C_f L_f + C_r L_r}{m}\right) - v_x\right) \dot{\psi} + \left(\frac{C_f}{m}\right) \delta \quad (3-20)$$

$$\ddot{\psi} = \frac{1}{v_x} \left(\frac{-C_f L_f + C_r L_r}{I_z}\right) v_y + \frac{1}{v_x} \left(\frac{C_f L_f^2 - C_r L_r^2}{I_z}\right) \dot{\psi} + \left(\frac{C_f L_f}{I_z}\right) \delta \quad (3-21)$$

As in this work the aim is to design a lateral controller for a homogeneous platoon of vehicles, it is assumed that a constant forward velocity is maintained by another longitudinal, distance-keeping controller. In other words, throughout the rest of this thesis it is assumed $v_x = 0$. As a result, Equations 3-20 and 3-21 give a linear description of the lateral dynamics and v_x is considered a parameter rather than a vehicle state.

3-1-1 State-Space Equation for a single vehicle

To facilitate the control design, the obtained equations of motion are expressed in a continuous-time state-space equation of the conventional form;

$$\begin{aligned} \dot{x}(t) &= Ax(t) + Bu(t) \\ y &= Cx(t) + Du(t) \end{aligned}$$

Rewriting equations 3-20 and 3-21 as derived in the previous section and choosing v_y and $\dot{\psi}$ as vehicle states, the following state-space equation is drafted for a single platoon member;

$$\begin{bmatrix} \dot{v}_y \\ \dot{\psi} \end{bmatrix} = \begin{bmatrix} -\frac{1}{v_x} \left(\frac{C_f + C_r}{m}\right) & \frac{1}{v_x} \left(\frac{-L_f C_f + L_r C_r}{m}\right) - v_x \\ \frac{1}{v_x} \left(\frac{-L_f C_f + L_r C_r}{I_z}\right) & \frac{1}{v_x} \left(\frac{L_f^2 C_f - L_r^2 C_r}{I_z}\right) \end{bmatrix} \begin{bmatrix} v_y \\ \dot{\psi} \end{bmatrix} + \begin{bmatrix} \frac{C_f}{m} \\ \frac{C_f L_f}{I_z} \end{bmatrix} \delta \quad (3-22)$$

The output equation can be chosen arbitrarily, depending on the control objective.

3-2 Error dynamics

This section covers the derivation of the error dynamics, an element inseparable from path-following methods. With error dynamics, lateral- and heading-error of a platoon member i with respect to a reference trajectory \mathcal{T} and how they change over time are described. These errors, $y_{e,i}$ and $\psi_{e,i}$, are detected by embedded sensors in all AVs and used as input for the lateral controller to ensure the vehicle-following is done accurately.

Equivalent as in the situation for deriving the equations of motion from the single track bicycle model, both the world-fixed coordinate frame \mathcal{N} and a platoon member i 's body-fixed frame \mathcal{B}_i are used. In addition, to successfully derive the required expressions for error dynamics, the use of a third coordinate system is required. This reference frame, \mathcal{C} , consists from the orthogonal projection of the origin of \mathcal{B}_i on the reference trajectory \mathcal{T} and unit vectors, i.e. $\mathcal{C} = \{\mathcal{O}^C, \vec{e}_x^C, \vec{e}_y^C\}$. By definition, the unit vector \vec{e}_x^C is always tangent to \mathcal{T} and as a result unit vector \vec{e}_y^C is always perpendicular to reference trajectory \mathcal{T} . Furthermore, an angle φ is defined between the x -axis of the world-fixed frame, \vec{e}_x^g , and unit vector of the tangent-frame, \vec{e}_x^C . Similarly, the yaw-angle ψ_i is defined between a vehicle i 's unit vector, \vec{e}_x^i , and the unit vector of the tangent frame, \vec{e}_x^C . Lastly, in the same way as derived for the single track model, an angle β_i is defined for every vehicle i 's sideslip angle; $\beta_i = \arctan\left(\frac{v_{y,i}}{v_{x,i}}\right)$. In Figure 3-2, a schematic overview of all relevant parameters and conventions are illustrated.

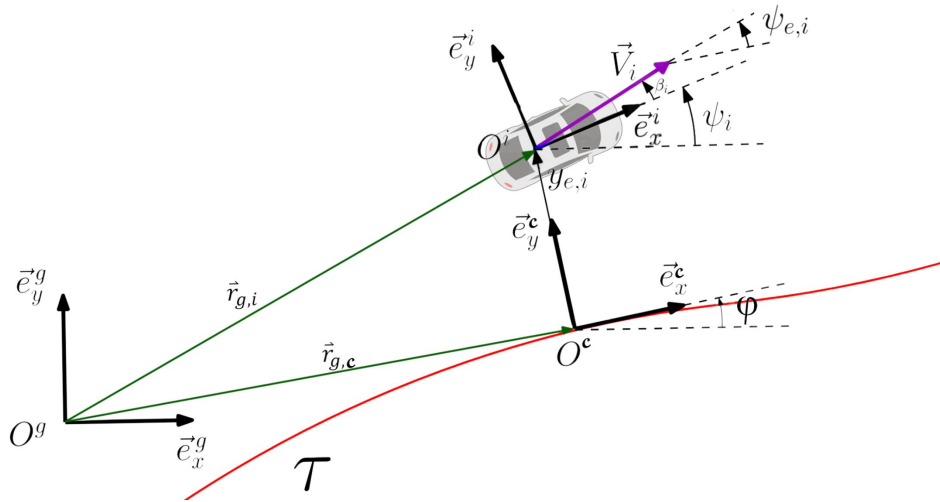


Figure 3-2: Relevant parameters and conventions for error dynamics

In the figure, one observes the two main components for error dynamics, errors $\psi_{e,i}$ and $y_{e,i}$. The heading error $\psi_{e,i}$ represents the rotational difference between the heading of the vehicle (i.e. the direction of the velocity vector \vec{V}_i) and the projected tangent line (\vec{e}_x^C) on reference trajectory \mathcal{T} . It is calculated using Equation 3-23.

$$\psi_{e,i} = \psi_i + \beta_i - \varphi \quad (3-23)$$

The lateral error $y_{e,i}$ defines the absolute offset from a vehicle i 's center of gravity to the reference trajectory, set by the preceding vehicle. In other words, the shortest (perpendicular) distance from the origin of coordinate frame \mathcal{C} to the origin of coordinate frame \mathcal{B}_i , denoted by vector $\vec{r}_{\mathcal{C},i}$. This error can be calculated using the inner product and is given in Equation 3-24.

$$y_{e,i} = \vec{r}_{\mathcal{C},i} \cdot \vec{e}_y^{\mathcal{C}} \quad (3-24)$$

However, in order to enable accurate path following, not only the errors themselves need to be derived, but also their derivative terms $\dot{\psi}_{e,i}$ and $\dot{y}_{e,i}$ are required. Both expressions will be derived in the upcoming sections, in which it will become clear $\dot{\psi}_{e,i}$ represents the rate of change in yaw-angle error of vehicle i and $\dot{y}_{e,i}$ describes the rate of change of the trajectory-following centerline deviation. These are also relevant terms since they serve as inputs for the lateral controller in order to ensure high performance tracking.

3-2-1 $\dot{\psi}_{e,i}$ -derivation

In Equation 3-23, the expression of heading error $\psi_{e,i}$ is given. Taking the first derivative with respect to time and applying the quotient rule for the β_i -term yields the following result;

$$\begin{aligned} \dot{\psi}_{e,i} &= \dot{\psi}_i + \dot{\beta}_i - \dot{\varphi} \\ \dot{\psi}_{e,i} &= \dot{\psi}_i + \frac{\dot{v}_{y,i}v_{x,i} - v_{y,i}\dot{v}_{x,i}}{v_{x,i}^2} - \dot{\varphi} \\ \dot{\psi}_{e,i} &= \dot{\psi}_i + \frac{\dot{v}_{y,i}}{v_{x,i}} - \frac{v_{y,i}\dot{v}_{x,i}}{v_{x,i}^2} + \dot{\varphi} \end{aligned} \quad (3-25)$$

Because at an earlier stage it has been assumed that $\dot{v}_x = 0$, and that for highway platooning conditions it follows that $v_y \ll v_x$, Equation 3-25 can be reduced to;

$$\dot{\psi}_{e,i} = \dot{\psi}_i + \frac{\dot{v}_{y,i}}{v_{x,i}} - \dot{\varphi} \quad (3-26)$$

in which the term $\frac{\dot{v}_{y,i}}{v_{x,i}}$ describes the rate of change in body slip angle and $\dot{\varphi}$ denotes the rate of change in road curvature of trajectory \mathcal{T} . Lastly, in the above obtained equation, the expression for \dot{v}_y from Equation 3-20 is substituted. This leads to the final expression for the heading error;

$$\dot{\psi}_{e,i} = -\frac{1}{v_x^2} \left(\frac{C_f + C_r}{m} \right) v_{y,i} + \frac{1}{v_x} \left(\frac{-L_f C_f + L_r C_r}{m} \right) \dot{\psi}_i + \frac{1}{v_x} \left(\frac{C_f}{m} \right) \delta_i - \dot{\varphi} \quad (3-27)$$

3-2-2 $\dot{y}_{e,i}$ -derivation

In Equation 3-24 the expression for lateral error $y_{e,i}$ is given. If we want to determine the rate of change in lateral error, we start again by taking again the first derivative with respect to time and applying the product rule. This yields;

$$\dot{y}_e = \dot{\vec{r}}_{\mathcal{C},i} \cdot \vec{e}_y^{\mathcal{C}} + \vec{r}_{\mathcal{C},i} \cdot \dot{\vec{e}}_y^{\mathcal{C}} \quad (3-28)$$

Because coordinate frame \mathcal{C} is assigned to move entirely along the unit vector $\vec{e}_y^{\mathcal{C}}$ on the reference trajectory, it immediately follows at all times that $\dot{\vec{e}}_y^{\mathcal{C}} = 0$. Therefore Equation 3-28 reduces to a simpler form;

$$\dot{y}_e = \dot{\vec{r}}_{\mathcal{C},i} \cdot \vec{e}_y^{\mathcal{C}} \quad (3-29)$$

Furthermore, the velocity vector of with frame \mathcal{C} with respect to \mathcal{B}_i , defined as $\dot{\vec{r}}_{\mathcal{C},i}$, is calculated using Equation 3-30;

$$\dot{\vec{r}}_{\mathcal{C},i} = \dot{\vec{r}}_{g,i} - \dot{\vec{r}}_{g,c} \quad (3-30)$$

Earlier in Equation 3-3, it was defined that;

$$\dot{\vec{r}}_{g,i} = [v_x \quad v_y] \underline{\vec{e}}^i \quad (3-31)$$

Or;

$$\dot{\vec{r}}_{g,i} = [v_x \quad v_y] \begin{bmatrix} \vec{e}_x^i \\ \vec{e}_y^i \end{bmatrix} \quad (3-32)$$

This equation can be rewritten using a rotation matrix from coordinate frame \mathcal{C} with respect to \mathcal{B}_i . However in this case a different rotation matrix is required; one such that $\psi_i - \varphi$ defines the orientation error; the angle between the vehicle and road. This leaves the following expression;

$$\dot{\vec{r}}_{g,i} = [v_x \quad v_y] R(\psi_i - \varphi)^T \begin{bmatrix} \vec{e}_x^i \\ \vec{e}_y^i \end{bmatrix} \quad (3-33)$$

In which, for the rotation matrix $R(\psi_i - \varphi)$ the following expression holds;

$$R(\psi_i - \varphi) = \begin{bmatrix} \cos(\psi_i - \varphi) & -\sin(\psi_i - \varphi) \\ \sin(\psi_i - \varphi) & \cos(\psi_i - \varphi) \end{bmatrix} \quad (3-34)$$

Combining Equation 3-33 with Equation 3-34 leads to;

$$\dot{\vec{r}}_{g,i} = [v_{x,i} \cos(\psi_i - \varphi) - v_{y,i} \sin(\psi_i - \varphi) \quad v_{x,i} \sin(\psi_i - \varphi) + v_{y,i} \cos(\psi_i - \varphi)] \begin{bmatrix} \vec{e}_x^{\mathcal{C}} \\ \vec{e}_y^{\mathcal{C}} \end{bmatrix} \quad (3-35)$$

Given geometrical relations as to be observed in Figure 3-1, it is possible to write $\psi_i - \varphi = \psi_{e,i} - \beta_i$. Then the rate of change in lateral error can also be expressed as;

$$\dot{y}_{e,i} = v_{x,i} \sin(\psi_{e,i} - \beta_i) + v_{y,i} \cos(\psi_{e,i} - \beta_i) \quad (3-36)$$

Lastly, once again small angles are approximated by assuming $\sin(\psi - \varphi) \approx \psi - \varphi$ and $\cos(\psi - \varphi) \approx 1$, disregarding the sin and cos terms and substituting in β . This yields the final expression for the derivative of lateral error of vehicle i , $\dot{y}_{e,i}$, to be observed in Equation 3-37;

$$\begin{aligned} \dot{y}_{e,i} &= v_{x,i} \left(\psi_{e,i} - \frac{v_{y,i}}{v_{x,i}} \right) + v_{y,i} \\ \dot{y}_{e,i} &= v_{x,i} \psi_{e,i} \end{aligned} \quad (3-37)$$

3-2-3 State-Space Equation including error dynamics

Having derived the state-space equation for every individual platoon member i including the error dynamics, it is possible to draft a new state-space equation with these error terms incorporated to complete the model description for a path-following approach. We use again an extended Linear Time Invariant (LTI) system including one vehicle i 's dynamics, error dynamics and disturbance term of the form:

$$\begin{aligned} \dot{x}_i(t) &= Ax_i(t) + Bu_i(t) + Ew(t) \\ y_i &= Cx_i(t) + Du_i(t) \end{aligned}$$

In the new description, the state vector $x_i(t)$, that contains vehicle- and error states is defined as;

$$x_i(t) = \begin{bmatrix} v_{y,i} & \psi_i & y_{e,i} & \psi_{e,i} \end{bmatrix}^T \quad (3-38)$$

Note: for the sake of brevity, the (t) -terms will be dropped from the state-space equation.

Furthermore, $u = \delta_i(t)$ represents the input vector that is represented by the steering angle of vehicle i . The 'uncontrolled input' vector $w = \dot{\varphi}(t)$ represents the change in reference trajectory. Equation 3-39 shows the complete state-space equation as derived until now.

$$\begin{bmatrix} \dot{v}_{y,i} \\ \dot{\psi}_i \\ \dot{y}_{e,i} \\ \dot{\psi}_{e,i} \end{bmatrix} = \begin{bmatrix} -\left(\frac{C_f + C_r}{mv_{x,i}}\right) & \left(\frac{-C_f L_f + C_r L_r}{mv_{x,i}} - v_{x,i}\right) & 0 & 0 \\ \left(\frac{-C_f L_f + C_r L_r}{I_z v_{x,i}}\right) & \left(-\frac{C_f L_f^2 + C_r L_r^2}{I_z v_{x,i}}\right) & 0 & 0 \\ 0 & 0 & 0 & v_{x,i} \\ -\left(\frac{C_f + C_r}{mv_{x,i}^2}\right) & \left(\frac{-C_f L_f + C_r L_r}{mv_{x,i}^2}\right) & 0 & 0 \end{bmatrix} \begin{bmatrix} v_{y,i} \\ \psi_i \\ y_{e,i} \\ \psi_{e,i} \end{bmatrix} + \begin{bmatrix} \frac{C_f}{m} \\ \frac{C_f L_f}{I_z} \\ 0 \\ \frac{C_f}{mv_{x,i}} \end{bmatrix} \delta_i + \begin{bmatrix} 0 \\ 0 \\ 0 \\ -1 \end{bmatrix} \dot{\varphi} \quad (3-39)$$

Once more, the output equation y can be chosen arbitrarily, depending on the control objectives.

One can observe that for this state-space equation configuration, a change in road curvature φ leads to a change in value of heading error. In turn, this leads to a change of value in lateral error $y_{e,i}$, implying the system is completely dependent on the disturbance-input $\dot{\varphi}$. The steering angle input δ_i for every vehicle i should then be chosen that these terms asymptotically go to zero.

3-3 Platoon model

In the previous section, the complete state-space equation for a single vehicle including its error model was derived. However, this state-space equation does not yet describe the coupling of dynamics between a vehicle i and its preceding vehicle $i - 1$. Therefore, in this section, the state-space description for a vehicle following method as well as the extension to the complete platoon model is derived. From the generalized platoon model it is clarified how a string of vehicles are interconnected in a dynamical sense.

For the Direct Vehicle Following approach, the reference trajectory to be followed by vehicle i is generated by vehicle $i - 1$. The goal of a Direct Vehicle Following method is to let the path driven by vehicle i resemble as closely as possible the reference trajectory from vehicle $i - 1$. Put more practically, we want a vehicle i to copy the states of vehicle $i - 1$ along its trajectory.

This can be achieved when we write the rate of change in road orientation for vehicle i at a given time, $\dot{\varphi}_i(t)$, in terms of the heading rate and sideslip rate of preceding vehicle $i - 1$ at an earlier time instant; i.e. $\dot{\psi}_{i-1}(t - \Delta t)$ and $\dot{\beta}_{i-1}(t - \Delta t)$. This relation is visualized in Figure 3-3 and described in Equation 3-40.

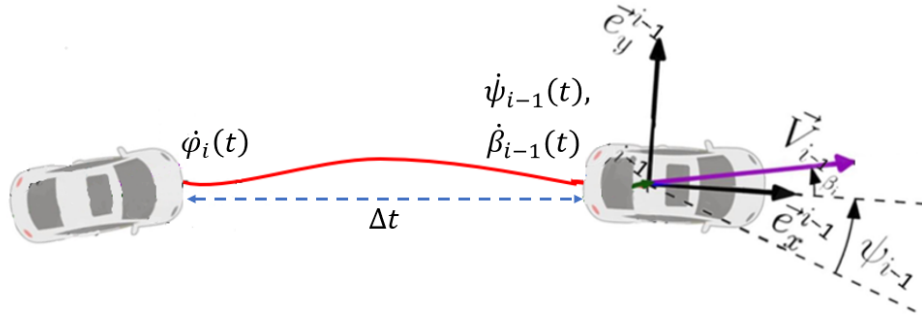


Figure 3-3: Relevant parameters and conventions for vehicle following

$$\dot{\varphi}_{i-1}(t) = \dot{\psi}_{i-1}(t - \Delta t) + \dot{\beta}_{i-1}(t - \Delta t) \quad (3-40)$$

In which the time delay Δt represents the inter-vehicle time, and is defined as the time it takes vehicle i to drive the inter-vehicle distance d_i at a certain constant forward velocity v_x , i.e., $\Delta t = \frac{d_i}{v_x}$.

Earlier in this chapter, the expression for $\dot{v}_{y,i}(t)$ has been derived. Moreover, we can again perform a small angle approximation for $\dot{\beta}_i$, to obtain $\dot{\beta}_i = \frac{\dot{v}_{y,i}(t)}{v_{x,i}(t)}$.

Plugging in the $\dot{v}_{y,i}(t)$ term, adding the $\dot{\psi}_{i-1}(t)$ term to Equation 3-40 and shifting for Δt provides us the relation that denotes the rate of change for trajectory orientation for vehicle i ;

$$\dot{\varphi}_i(t) = -\frac{1}{v_{x,i-1}^2} \left(\frac{C_f + C_r}{m} \right) v_{y,i-1}(t-\Delta t) + \frac{1}{v_{x,i-1}^2} \left(\frac{-C_f L_f + C_r L_r}{m} \right) \dot{\psi}_{i-1}(t-\Delta t) + \frac{1}{v_{x,i-1}} \left(\frac{C_f}{m} \right) \delta_{i-1}(t-\Delta t) \quad (3-41)$$

Notice how in this equation, the disturbance term $\dot{\varphi}_i$ depends exclusively on the states of the preceding vehicle $i - 1$. Therefore it is wise to express the disturbance term $Ew(t)$ from the earlier obtained state-space equation in terms of the state vector for preceding vehicle, $x_{i-1}(t - \Delta t)$ and an additional 'output'-matrix for the input vector $\delta_{i-1}(t - \Delta t)$, such that;

$$\dot{\varphi}_i(t) = S_{i-1}x_{i-1}(t - \Delta t) + V_{i-1}u_{i-1}(t - \Delta t) \quad (3-42)$$

in which the state vector x_{i-1} is drafted as;

$$x_{i-1} = \left[v_{y,i-1}(t - \Delta t) \quad \dot{\psi}_{i-1}(t - \Delta t) \quad \psi_{e,i-1}(t - \Delta t) \quad y_{e,i-1}(t - \Delta t) \right]^T$$

S_{i-1} a 'state'-matrix of a preceding vehicle $i - 1$ defined as;

$$S_{i-1} = \left[-\frac{1}{v_{x,i-1}^2} \left(\frac{C_f + C_r}{m} \right) \quad \frac{1}{v_{x,i-1}^2} \left(\frac{-C_f L_f + C_r L_r}{m} \right) \quad 0 \quad 0 \right]$$

and lastly, an 'output'-matrix V_{i-1} is used to include the preceding vehicle's steering angle;

$$V_{i-1} = \left[0 \quad 0 \quad 0 \quad \frac{1}{v_{x,i}} \left(\frac{C_f}{m} \right) \right]^T$$

3-3-1 State-Space Equation for preceding- and following vehicle

The equation that describes the interconnected lateral dynamics of two consecutive vehicles as derived in the previous section is added to the state-space equation from Equation 3-39 for further completion of the platoon model. In short-hand notation, we find this expression to be as;

$$\begin{aligned} \dot{x}_i(t) &= A_i x_i(t) + B u_i(t) + S_{i-1} x_{i-1}(t - \Delta t) + V_{i-1} u_{i-1}(t - \Delta t) \\ y_i &= C x_i(t) + D u_i(t) \end{aligned} \quad (3-43)$$

Further expanding this expression leads to;

$$\begin{aligned}
 \begin{bmatrix} \dot{\psi}_{y,i} \\ \dot{\psi}_i \\ \dot{y}_{e,i} \\ \dot{\psi}_{e,i} \end{bmatrix} &= \begin{bmatrix} -\frac{1}{v_x} \left(\frac{C_f + C_r}{m} \right) & \frac{1}{v_x} \left(\frac{-C_f L_f + C_r L_r}{m} - v_x \right) & 0 & 0 \\ \frac{1}{v_x} \left(\frac{-C_f L_f + C_r L_r}{I_z} \right) & -\frac{1}{v_x} \left(\frac{C_f L_f^2 + C_r L_r^2}{I_z} \right) & 0 & 0 \\ 0 & 0 & 0 & v_x \\ -\frac{1}{v_x^2} \left(\frac{C_f + C_r}{m} \right) & \frac{1}{v_x^2} \left(\frac{-C_f L_f + C_r L_r}{m} \right) & 0 & 0 \end{bmatrix} \begin{bmatrix} v_{y,i} \\ \psi_i \\ y_{e,i} \\ \psi_{e,i} \end{bmatrix} + \begin{bmatrix} \frac{C_f}{m} \\ \frac{C_f L_f}{I_z} \\ 0 \\ \frac{1}{v_{x,i}} \left(\frac{C_f}{m} \right) \end{bmatrix} \delta \\
 + \begin{bmatrix} 0 & 0 & 0 & 0 \\ 0 & 0 & 0 & 0 \\ 0 & 0 & 0 & 0 \\ -\frac{1}{v_{x,i-1}^2} \left(\frac{C_f + C_r}{m} \right) & \frac{1}{v_{x,i-1}^2} \left(\frac{-C_f L_f + C_r L_r}{m} \right) & 0 & 0 \end{bmatrix} \begin{bmatrix} v_{y,i-1}(t - \Delta t) \\ \psi_{i-1}(t - \Delta t) \\ y_{e,i-1}(t - \Delta t) \\ \psi_{e,i-1}(t - \Delta t) \end{bmatrix} + \begin{bmatrix} 0 \\ 0 \\ 0 \\ \frac{1}{v_{x,i}} \left(\frac{C_f}{m} \right) \end{bmatrix} \delta_{i-1}(t - \Delta t) \\
 (3-44)
 \end{aligned}$$

Once again the choice for the output equation y is arbitrary and depends on the control objectives.

3-3-2 Centralized Platoon Model

Following the reasoning in the previous section, we can derive the final, centralized platoon model that describes the full inter-dependency of lateral dynamics for all vehicles part of this platoon. This would become nothing more than an n -extended version of the state-space equation as found in Equation 3-44. One could rightfully reason that a platoon can be (theoretically) infinitely long, by consequently adding vehicles to this 'string' of vehicles. However, due to stability issues in the lateral domain, current literature reviewed n is usually limited between 5 and 10.

The centralized platoon model description is (obviously) especially useful when the centralized approach for the lateral controller is incorporated, and will therefore we used as the plant model for control design in Chapter 4. Due to the homogeneity of the platoon considered, all vehicles share the same system dynamics, physical actuator limits and thus input responses. As a direct result it follows that for the total platoon system, the assumption concerning the vehicle's system matrices A and B it holds that $A_1 = A_2 = \dots = A_n$ and $B_1 = B_2 = \dots = B_n$.

The final state-space equation that describes the total, generalized homogeneous platoon model is found in Equation 3-45;

$$\begin{aligned}
 \dot{x}_{tot}(t) &= A_{tot}x_{tot}(t) + B_{tot}u_{tot}(t) + S_{tot}x_{tot}(t - \Delta t) + V_{tot}u_{tot}(t - \Delta t) \\
 y_{tot}(t) &= C_{tot}x_{tot}(t) + D_{tot}u_{tot}(t)
 \end{aligned} \tag{3-45}$$

Or, after extending this equation, we find the following expression;

$$\begin{aligned} \dot{x}_{tot}(t) = & \begin{bmatrix} A_1 & 0 & 0 & 0 & 0 \\ 0 & A_2 & 0 & 0 & 0 \\ 0 & 0 & \ddots & 0 & 0 \\ 0 & 0 & 0 & \ddots & 0 \\ 0 & 0 & 0 & 0 & A_n \end{bmatrix} \begin{bmatrix} x_1(t) \\ x_2(t) \\ \vdots \\ x_n(t) \end{bmatrix} + \begin{bmatrix} B_1 & 0 & 0 & 0 & 0 \\ 0 & B_2 & 0 & 0 & 0 \\ 0 & 0 & \ddots & 0 & 0 \\ 0 & 0 & 0 & \ddots & 0 \\ 0 & 0 & 0 & 0 & B_n \end{bmatrix} \begin{bmatrix} u_1(t) \\ u_2(t) \\ \vdots \\ u_n(t) \end{bmatrix}^T \\ & + \begin{bmatrix} 0 & 0 & 0 & 0 & 0 \\ S_1 & 0 & 0 & 0 & 0 \\ 0 & S_2 & 0 & 0 & 0 \\ 0 & 0 & \ddots & 0 & 0 \\ 0 & 0 & 0 & S_{n-1} & 0 \end{bmatrix} \begin{bmatrix} x_1(t - \Delta t) \\ x_2(t - 2\Delta t) \\ \vdots \\ x_n(t - n\Delta t) \end{bmatrix} + \begin{bmatrix} 0 & 0 & 0 & 0 & 0 \\ V_1 & 0 & 0 & 0 & 0 \\ 0 & V_2 & 0 & 0 & 0 \\ 0 & 0 & \ddots & 0 & 0 \\ 0 & 0 & 0 & V_{n-1} & 0 \end{bmatrix} \begin{bmatrix} u_1(t - \Delta t) \\ u_2(t - 2\Delta t) \\ \vdots \\ u_n(t - n\Delta t) \end{bmatrix}^T \end{aligned} \quad (3-46)$$

in which x_{tot} represents the collection of all vehicle states, i.e. x_i for $i = \{1, \dots, n\}$, which in turn represent state vector for the i -th vehicle in the platoon, i.e. $x_i = [v_{y,i} \ \psi_i \ y_{e,i} \ \psi_{e,i}]^T$. Likewise, u_{tot} represents the collection of input vectors for $i = \{1, \dots, n\}$, containing in turn only the input signals of the steering angle for vehicle i , i.e. $u_i = \delta_i$. Once more, the output equation for y_{tot} can be chosen to one's preference, depending on the control objectives.

In Figure 3-4, one observes a visualization of the centralized platoon model as derived in Equation 3-46 including some relevant parameters.

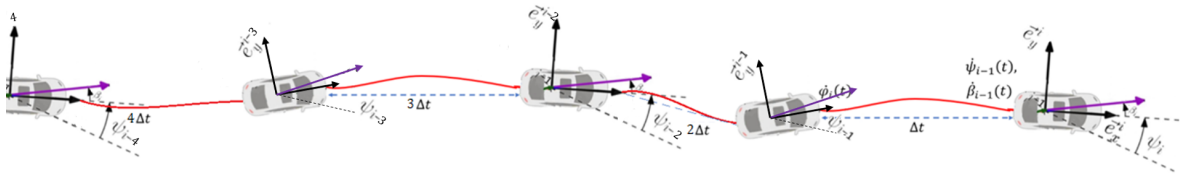


Figure 3-4: Relevant parameters and conventions for the centralized platoon model

Proposed control solution

In this chapter, the proposed control solution for a practically string stable, lateral dynamics controller for a homogeneous platoon of n vehicles, is discussed. In fact, two controllers are established based on the Direct Vehicle Following method, while incorporating two different Model Predictive Control approaches. These control approaches are tightly linked to the Information Flow Topologies as discussed in Section 1-2-1. The first controller follows a *centralized* strategy, and is based on the centralized platoon model from Equation 3-46. The second controller follows a *distributed* strategy and is applied to the state-space equation derived as in Equation 3-39.

First, Section 4-1 highlights the mathematical approach towards the concept of string stability and defines some of the commonly used methods for assessing string stable behaviour encountered in literature. The well-defined and widely adopted general definition of string stability as found in [35], [36] is analyzed to investigate whether it can be applied to the platoon model as derived in this work and to inspect whether Lateral String Stability for this application can be assured. Ploeg's definition is based on the propagation of initial conditions perturbations and utilizes the \mathcal{L}_∞ -norm to guarantee stability. Section 4-2 covers the practical implementation and application for this work; a novel definition of the concept, entitled Practical Lateral String Stability (PLSS) is introduced.

When the string stability requirements are known, we proceed in Section 4-3 by listing the control objectives the controller is required to meet. Herein, performance and stability criteria are further discussed. The difference between the two selected control strategies, centralized and distributed, is explained in preceding Section 4-4. Lastly, in Section 4-5, the process of designing both controllers' architecture is thoroughly elaborated.

4-1 String Stability: a mathematical definition

The issue of string stability has been studied as early as 1974 [37] and ever since, many different definitions of the concept have been formulated. Consequently, a vast amount of literature has also proposed different methods for assessing-methods for string stability. It has been stated in Chapter 1 that one general concept of String Stability is defined as *"the attenuation of errors propagating in an upstream direction of interconnected vehicles forming a platoon"*. This definition is deemed appropriate to fit the purposes in this work and will thus be considered as starting point, but need to be explored a bit deeper to lay the groundwork for developing a novel definition.

For Lateral String Stability, it can then be conceived that the propagation of *lateral* disturbances need to be attenuated in an upstream direction of the platoon. It is wise to construct the propagation of lateral disturbance, ε_i , as a variable such that it can be analyzed. Then, in order for this error not to amplify along the string of vehicles, $\|\varepsilon_i(t)\|_2 < \|\varepsilon_{i-1}(t)\|_2$ must hold for all vehicles $i \in \{1, \dots, n\}$ in the time domain. One way this can be achieved is by the modeling this propagation of the lateral error ε_i as a transfer function in terms of input and output in the complex frequency (i.e. Laplace) domain, $H(j\omega)$.

If the magnitude of this transfer function for $\omega \rightarrow \infty \leq 1$, the lateral error will not be amplified along the string and consequently, lateral string stability can be established. In other words, the transfer function must suffice the relation as described in Equation 4-1.

$$\begin{aligned} \|H(j\omega)\|_\infty &= \left\| \frac{\varepsilon_i(j\omega)}{\varepsilon_{i-1}(j\omega)} \right\|_\infty \leq 1, \quad \forall \omega \\ \|H(j\omega)\|_\infty &= \left| \frac{\varepsilon_i(j\omega)}{\varepsilon_{i-1}(j\omega)} \right| \leq 1, \quad \forall \omega \end{aligned} \tag{4-1}$$

However, the above mentioned H_∞ -method is most commonly used in platooning applications where a Robust Control approach is handled. Utilizing the same H_∞ -method to assess the stability would not be sensible for the application explored in this thesis, because in practice it is difficult to translate Equation 4-1 into constraints embedded in the MPC formulation. This indicates that is substantially harder to say something useful about the behaviour and stability of the system. Rather, we should investigate stability methods in the time domain from a more practical nature.

One method that investigates stability in the time domain is a method referred to as \mathcal{L}_∞ -stability and is directly related to maximum overshoot. It is based on the work of Ploeg [36] and Swaroop [38]. To understand the fundamentals of this method, first some remarks on the overarching concept of \mathcal{L}_p -stability should be made.

4-1-1 \mathcal{L}_p stability

In general, given a Lebesgue measurable signal $y(t)$, the \mathcal{L}_p stability for $1 \leq p \leq \infty$ is a form of Input/Output-stability and defines the set of all piecewise continuous functions into the Euclidian Space of \mathbb{R}^m , that is, $y : [0, \infty) \rightarrow \mathbb{R}^m$, such that for the output signal y ;

$$\|y\|_{\mathcal{L}_p} = \left(\int_0^\infty \|y(t)\|^p dt \right)^{\frac{1}{p}} < \infty \quad (4-2)$$

Consider the general description of an interconnected system, as derived in the previous chapter. Consider Equation 4-3 to be a linear, platoon of n vehicles written as cascaded system;

$$\begin{aligned} \dot{x}_0 &= f_r(x_0, u_r) \\ \dot{x}_i &= f_i(x_i, x_{i-1}), \quad i \in S_n \\ y_i &= h(x_i), \quad i \in S_n \end{aligned} \quad (4-3)$$

in which $S_n = \{i \in \mathbb{Z} \mid 1 \leq i \leq n\}$ is the set of all vehicles in the platoon of length $n \in \mathbb{Z}$. Moreover, $u_r \in \mathbb{R}^q$ denotes the set of external inputs to the system. For the state vector x_i , we have $x_i \in \mathbb{R}^n \quad \forall i \in S_n$. On output vector y_i , the conditions $y_i \in \mathbb{R}^l \quad \forall i \in S_n$ are set. Theorem 4.1 describes the conditions for \mathcal{L}_p string stability as found in [35].

Theorem 4.1 *Consider the interconnected system as found in equation 4-10. Let $x^T = (x_0^T \ x_1^T \ \dots \ x_n^T)$ be the lumped state vector and let $\bar{x}^T = (\bar{x}_0^T \ \dots \ \bar{x}_0^T)$ denote a constant equilibrium solution of 4-3 for $u_r \equiv 0$. The system 4-3 is \mathcal{L}_p string stable if there exists a class \mathcal{K} functions α and β , such that, for any initial state $x_0 \in \mathbb{R}^{(n+1)m}$ and any $u_r \in \mathcal{L}_p^q$.*

$$\|y_i(t) - h_0(\bar{x}_0)\|_{\mathcal{L}_p} \leq \alpha(\|u_r(t)\|_{\mathcal{L}_p}) + \beta(\|x(0) - \bar{x}\|), \quad \forall i \in S_n, \forall n \in \mathbb{Z} \quad (4-4)$$

if, in addition, with $x(0) = \bar{x}$ it also holds that

$$\|y_i(t) - h_0(\bar{x}_0)\|_{\mathcal{L}_p} \leq \|y_{i-1}(t) - h(\bar{x}_0)\|_{\mathcal{L}_p}, \quad \forall i \in S_n \setminus \{1\}, \forall n \in \mathbb{Z} \setminus \{1\} \quad (4-5)$$

the system is strictly \mathcal{L}_p string stable with respect to its input u_r .

It can be observed that the class-functions \mathcal{K} considers both the external disturbance u_r as well as initial conditions perturbations $x(0) - \bar{x}$, as opposed to other stability definitions [38]. These class-functions \mathcal{K} have the property of being continuous and strictly increasing on the domain $[0 \rightarrow \infty)$ and $f(0) = 0$.

With the condition for \mathcal{L}_p stability set, we proceed in the next section by posing an extension of this definition; i.e. going from \mathcal{L}_p to \mathcal{L}_∞ stability.

4-1-2 \mathcal{L}_∞ -stability

Consider again the linear, interconnected system as described in Equation 4-3. If such a system is assumed to be homogeneous, i.e., all vehicles have the same dynamics incorporated, the system can be rewritten with a lumped state vector as displayed in Equation 4-6. The notation used the work of [36] is slightly different but should look familiar from the centralized platoon model derived in Equation 3-46, but in this formulation the B -matrix only considers the platoon leader input.

$$\begin{bmatrix} \dot{x}_0 \\ \dot{x}_1 \\ \vdots \\ \dot{x}_n \end{bmatrix} = \begin{bmatrix} A_r & \dots & & O \\ A_1 & A_0 & & \\ \vdots & \ddots & \ddots & \vdots \\ O & \dots & A_1 & A_0 \end{bmatrix} \begin{bmatrix} x_0 \\ x_1 \\ \vdots \\ x_n \end{bmatrix} + \begin{bmatrix} B_r \\ 0 \\ \vdots \\ 0 \end{bmatrix} u_r \quad (4-6)$$

$$y_i = Cx_i + Du_i, \quad i \in S_n$$

in which A_r, A_0 and A_1 , up to A_n represent the corresponding state matrices that represents the vehicle dynamics for the host and following vehicles, as derived in Chapter 3. B_r denotes the input matrix for (only) the host vehicle.

We can take a small side-step to the Laplace domain to gain insights on the stability for the time domain. The output equation from Equation 4-6 as expressed in the Laplace domain yields;

$$y_i(s) = P_i(s)u_r + O_i x(0), \quad i \in S_n \quad (4-7)$$

In this equation, $P_i(s)$ represents the complementary sensitivity transfer function from external input to chosen output and is assumed to be a square matrix. It is calculated using $P_i(s) = C_i(sI - A)^{-1}B$. Furthermore, O_i denotes the initial condition-transfer function, from initial condition error to again chosen output and is calculated using $O_i = C_i(sI - A)^{-1}$. It follows directly from Equation 4-7 when it is assumed that $x(0) = 0$, the input/output relation for $y_i(s)$ may be reduced to;

$$y_i = \Gamma_i(s)y_{i-1}(s) \quad (4-8)$$

$\Gamma_i(s)$ is defined as string stability complementary sensitivity function and is calculated using;

$$\Gamma_i(s) = P_i(s)P_{i-1}^{-1}(s) \quad (4-9)$$

Then, Theorem 4.2 [35] is utilized to define \mathcal{L}_2 string stability using the earlier discussed H_∞ -framework.

Theorem 4.2 *Let 4-6 represent a linear, interconnected system of which the input-output behaviour is described by 4-7. Assume that the pair (C_i, A) is such that unstable and marginally modes are unobservable and that $P_i(s)$ is square and non singular for all $i \in \mathbb{N}$, thus guaranteeing the existence of $P_{i-1}(s)$. Then the system 4-6 is \mathcal{L}_2 string stable if and only if;*

1. $\|P_1(s)\|_{\mathcal{H}_\infty} < \infty$
2. $\|\Gamma_i(s)\|_{\mathcal{H}_\infty} \leq 1, \quad \forall i \in \mathbb{N} \setminus \{1\}$

However, the \mathcal{L}_2 -norm of a signal only captures the feature of 'dissipated energy' and guarantees boundedness for this aspect. In order to guarantee boundedness of maximum overshoot, we must further extend the definition to arrive at the \mathcal{L}_∞ -norm, which is found in a similar manner.

Reconsider the same interconnected system as for the \mathcal{L}_2 -case from Equation 4-3 and its lumped form in Equation 4-6.

$$\begin{aligned}\dot{x}_0 &= f_r(x_0, u_r) \\ \dot{x}_i &= f_i(x_i, x_{i-1}), \quad i \in S_n \\ y_i &= h(x_i), \quad i \in S_n\end{aligned}\tag{4-10}$$

We use the same system, but will apply a different norm; the \mathcal{L}_1 norm for the impulse response matrix, $p_i(t)$. This formulation is denoted in Equation 4-11. By doing so it is possible to guarantee \mathcal{L}_∞ for a signal, as is reviewed in Theorem 4.3. The proof for the Theorem can be found in Appendix B.

$$\|p_i(t)\|_{\mathcal{L}_1} = \max \frac{\|y_i(t)\|_{\mathcal{L}_\infty}}{\|u_i(t)\|_{\mathcal{L}_\infty}}\tag{4-11}$$

Theorem 4.3 *Let 4-6 represent a linear, interconnected system of which the input-output behaviour is described by 4-7. Assume that the pair (C_i, A) is such that unstable and marginally modes are unobservable and that $P_i(s)$ is square and non singular for all $i \in \mathbb{N}$. Then the system 4-6 is \mathcal{L}_∞ string stable if;*

1. $\|p_1(t)\|_{\mathcal{L}_1} < \infty$
2. $\|\gamma_i(t)\|_{\mathcal{L}_1} \leq 1, \quad \forall i \in \mathbb{N} \setminus \{1\}$

where $p_1(t)$ and $\gamma_i(t)$ are the impulse response functions corresponding to $P_1(s)$ and $\Gamma_i(s)$ that were derived in Theorem 4.2. The system is strictly \mathcal{L}_∞ if and only if conditions 1 and 2 both, if $\sup_{i \in \mathbb{N}} \|p_i(t)\|_{\mathcal{L}_1}$ exists and if the class \mathcal{K} functions as mentioned in section 4-1 can be chosen as: $\alpha(\|u_r(t)\|_{\mathcal{L}_\infty}) = (\sup_{i \in \mathbb{N}} \|p_i(t)\|_{\mathcal{L}_1}) \|u_r(t)\|_{\mathcal{L}_\infty}$.

From the above theorem, we learn that when looking at the dynamical output signals of the system in the time-domain, Lateral String Stability can be *guaranteed* if we treat boundedness by the \mathcal{L}_∞ -norm induced by the supremum (i.e. least upper bound of the overshoot) as a requirement. Therefore, in the next section, a more simplified, practical resolution to achieve Lateral String Stability for Model Predictive Controlled vehicular platoons and its implementation will be elaborated.

4-2 From Theoretical to Practical String Stability

The previous section essentially established the framework for a novel definition for the concept of Lateral String Stability. By the means of this new definition one can guarantee whether a vehicular platoon would stay string stable in the lateral sense during simulation or real-life application without the use of sophisticated mathematical analysis. Analysis of boundedness regarding the transfer function using one of the conventional Laplace-domain methods [39] would be simply cumbersome and unwise for this application. Furthermore, against the original definition of string stability, some amplification of a disturbance signal should be allowed if the complete string remains between the imposed bounds anyway.

We therefore rephrase the definition of \mathcal{L}_∞ -stability obtained in Theorem 4.3 to a more comprehensible definition regarding string stability. The novel definition (Definition 4.2) builds further on the conditions as described in Definition 4.1 from [38] and extends it to fit lateral control purposes for vehicular highway-platooning.

Definition 4.1 Consider the following interconnected system $\dot{x}_i = f(x_i, x_{i-1}, \dots, x_{i-r+1})$. The origin $x_i = 0$, $i \in \mathbb{R}^n$ is Time-domain String Stable (TSS), if given any $\gamma > 0$ there exists a $\xi > 0$ such that;

$$\|x_i(0)\|_\infty \leq \xi \Rightarrow \sup_i \|x_i(t)\|_\infty \leq \gamma, \quad \forall t > 0 \quad (4-12)$$

For proof of Definition 4.1 the reader is referred to [38]. This definition evaluates whether the magnitude of the largest element belonging to the vector x_i , the supremum (or least upper bound), exceeds the bound γ that is imposed on this set. With the largest element in the set, evidently the maximum overshoot value of this vector is implied. However, this theoretical description of the concept does was originally designed for longitudinal string stability. Nor does it provide insight on the upper limit for which n , using this definition, the string remains stable. Therefore, this definition is extended with two new terms; lateral and practical.

In order to establish the *lateral* aspect for the novel definition, it must hold for the vector x_i , not all elements in this vector but *only* the lateral error states of the platoon members, $y_{e,i}$, are evaluated. Furthermore, in order to establish the connection towards the *practical* aspect the new string stability definition, not only one single element in the output vector $y_{e,i}$, must respect the imposed bound γ but also the summation of lateral errors of all platoon members, $\sum y_{e,i}$, must remain bounded by ξ . Practical Lateral String Stability (PLSS) can be guaranteed if conditions 1 and 2 are satisfied;

$$1. \sum_i \|y_{e,i}(0)\|_\infty \leq \xi \Rightarrow \sup \|y_{e,i}(t)\|_\infty \leq \gamma, \quad \forall t > 0 \quad (4-13)$$

$$2. \sum_i \|y_{e,i}(0)\|_\infty \leq \xi \Rightarrow \sup \|y_{e,i}(t)\|_\infty \rightarrow 0, \quad t \rightarrow \infty \quad (4-14)$$

In simpler words, when the maximum value of lateral error of a vehicle i is less or equal to γ **and** the summed maximum value of lateral errors for all n platoon members is less or equal to ξ during simulations or real-life applications, Lateral String Stability is a guarantee in the practical sense.

Furthermore, it is important to realize, in contrast to the classical definition of string stability, (slight) amplification of the output vector **is** allowed in this definition, as long as the imposed bounds (i.e., lane width) are not exceeded.

The attentive reader might notice the similarity between the mathematical expressions from Equations 4-13 and 4-14, and the state- or output constraints that are imposed on a dynamical system when handling Model Predictive Control, as explained in Section 2-2. Moreover, the comparison can be justified considering the imposed bounds can be physically (thus practically) limited due to actuators in real-life, ensuring certain undesirable states can not be reached. In that sense, guaranteeing PLSS and thus internal stability for this platooning application (i.e. highway driving at constant forward velocity) would imply nothing more than constraining the platoon's coupled dynamics, without the use of complex mathematical analysis while yielding the same results.

We implement the PLSS conditions by adding two more (discretized) constraints to the optimization problem formulation and impose a terminal set and terminal cost to the cost function. If these three constraints are satisfied along with the terminal costs, PLSS by definition, is guaranteed. The conditions are enumerated in Definition 4.2.

Definition 4.2 A vehicle platoon of n members incorporating a Model Predictive Control approach is deemed Practically Lateral String Stable (PLSS), if given any $\gamma > 0 \wedge \xi > 0$ the following two constraints are respected:

1. $-\gamma \leq y_{e,i}(k) \leq \gamma \quad [m] \quad \forall k, \quad \forall i \in \{1, 2, \dots, n\}$
2. $-\xi \leq y_{e,0}(k) - y_{e,n}(k) \leq \xi \quad [m] \quad \forall k, \quad \forall i \in \{1, 2, \dots, n\}$

Note that the practical aspect of the definition does *not* include a condition on the amplification of the lateral disturbance, as we have seen in the classical definition of (theoretical) string stability. However, the attenuation of the lateral error is still a welcome property for the controller. A third condition can therefore be added that reinforces the definition, but is not a requirement for PLSS. A system for which all three conditions hold would be titled Absolute Lateral String Stability (ALSS), and is given in Definition 4.3.

Definition 4.3 A vehicle platoon of n members incorporating a Model Predictive Control approach is deemed Absolutely Lateral String Stable (ALSS), if given any $\gamma > 0 \wedge \xi > 0$ the following three conditions hold:

1. $-\gamma \leq y_{e,i}(t) \leq \gamma \quad [m] \quad \forall t, \quad \forall i \in \{1, 2, \dots, n\}$
2. $-\xi \leq y_{e,0}(t) - y_{e,n}(t) \leq \xi \quad [m] \quad \forall t, \quad \forall i \in \{1, 2, \dots, n\}$
3. $\max |y_{e,i-1}(t)| \leq \max |y_{e,i}(t)| \quad [m] \quad \forall t, \quad \forall i \in \{1, 2, \dots, n\}$

Here strictness of bounds depends on the control objectives and desired performance. The values for decision variables γ and ξ for this application are discussed in Section 5-1. The rest of Chapter 4 will clarify how the above definitions are used and implemented in the design of a lateral control strategy.

4-3 Control Objectives

The main control objective of the lateral platoon controller designed in this work, is to let a homogeneous platoon of $n = 5$ vehicles track a desired reference trajectory \mathcal{T} by adjusting the steering wheel angle δ . In other words, the controller must ensure that errors definitions as derived in Chapter 3, the lateral offset $y_{e,i}$ and heading error $\psi_{e,i}$ for every platoon member i are asymptotically reduced to zero. This implies that the main objective for the controller is drafted as:

$$\begin{aligned} \lim_{t \rightarrow \infty} y_{e,i}(t) &= 0 \quad \forall \mathcal{T} \\ \lim_{t \rightarrow \infty} \psi_{e,i}(t) &= 0 \quad \forall \mathcal{T} \end{aligned} \quad (4-15)$$

Furthermore, the controller must also;

- Generate a control action that is physically possible to be executed by every vehicle in the platoon, i.e. respect input constraints on the steering wheel and comply with system dynamical bounds.
- Satisfy closed-loop performance specifications for both single vehicles as for the complete platoon.
- Respects the Practical Lateral String Stability conditions posed in Definition 4-2.
- Succeed to remain at least Practically Lateral String Stable after noise- and disturbance conditions are added to the simulations.

Lastly, it is also extremely desirable (but not mandatory) if the controller;

- Respects the Absolute Lateral String Stability conditions posed in Definition 4-3.

4-4 Centralized- vs. Distributed strategy

The nature of the plant model applied to an MPC is of great significance to the eventual system performance. In Section 1-2-1, several Information Flow Topologies were briefly discussed. The method in which vehicles share data with the other vehicles and whether they incorporate V2V-communication is tightly linked with the actual plant model that can be adopted for an MPC. In literature, it has been found the two most commonly used control structures for linear MPC structures in platooning applications are the *centralized* and *distributed* approach.

Centralized strategy

In general, the centralized approach implies one centralized MPC (conventionally embedded inside the platoon leader) calculates the optimal control actions for *all* vehicles in the platoon. At every time step, the platoon leader (wirelessly) receives data from all following vehicles' states and calculates the optimal steering input for all its members based the reference of its own driven trajectory.

This data is then broadcasted back to each individual platoon member, after which this control action is executed. Simultaneously, the new state variables for all platoon members are again exchanged towards the leader for calculation of the next timestep. Throughout the whole vehicle following procedure this process is repeated. The centralized control topology is visualized in Figure 4-1.

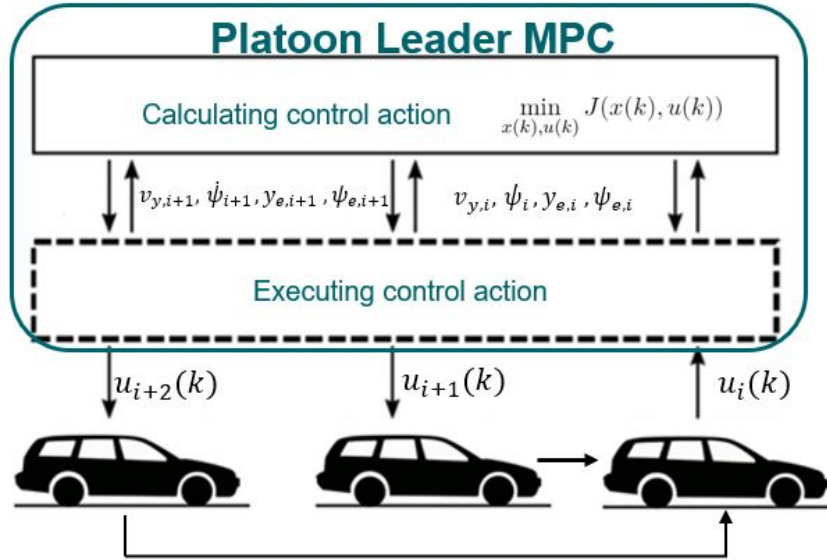


Figure 4-1: Centralized control topology for platooning application

The main advantage that can be achieved by incorporating the centralized approach is extremely high tracking performance. As the platoon leader is repeatedly updated on every vehicle's states, it implies a perfect overview of the complete platoon's (coupled) lateral dynamics is always available. By this virtue, dynamical inter-dependency of platoon members will counter-effect Lateral String Stability issues. Furthermore, the cutting corner phenomenon as discussed in Section 1-4-2 is expected to be absent due to platoon members not relying exclusively on the preceding vehicle.

However, the centralized method also experiences a few drawbacks. Since the complete platoon system embodies only a single MPC, the optimization step performed by the controller becomes a computational demanding task. In addition, a more complex plant model representing the system dynamics is needed. As a direct result, increased computational efforts for the centralized approach can drastically increase the computation time. In situations where high speeds are attained, such as highway driving considered in this thesis, strict computation time conditions must be set.

Another major drawback present for this type of control structure, lies in the fact that perfect wireless inter-vehicle communication is an indisputable requirement. Ultra fast, latency-free, data exchange between vehicles must be guaranteed in order for such an approach to properly function. Unfortunately, such a guarantee is practically infeasible when adapting for real-life application, however some performance bounds can be adopted. Therefore, for the purposes of this thesis, the centralized approach is more treated as a 'benchmark' controller against which the distributed shall be compared.

Distributed strategy

Oppositely, the distributed approach operates around the concept that each vehicle calculates *only* its own control action using the embedded MPC, based on the states of *only* the preceding vehicle. Also for this approach, the state information is collected by the means of wireless communications. However, applications exist ([40], [27]) where no V2V-communication at all is adopted, in which the platoon uses forward looking RADAR and LiDAR sensors to determine the preceding vehicle's states. Figure 4-2 depicts the control topology for such a distributed approach.

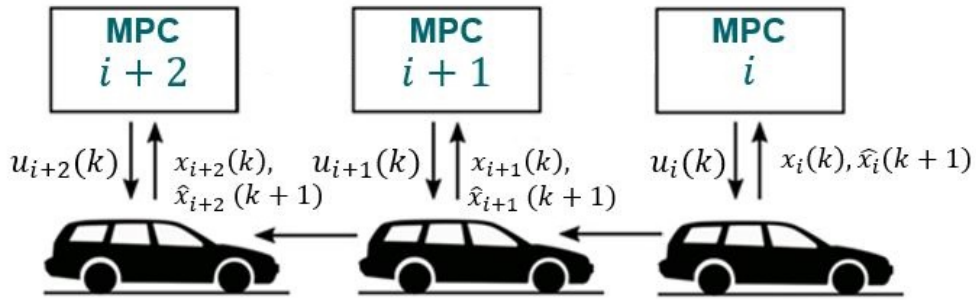


Figure 4-2: Distributed control topology for platooning application

The distributed strategy's main benefit arises from the same nature as the main drawback from the centralized approach. As each individual platoon member has its own MPC embedded, the required plant model utilized by the MPC becomes far less complex as opposed to the centralized strategy. Moreover, as in practice these controllers run in parallel, significantly shorter computation times seem viable. Furthermore, the fallback option can be seen as a valuable asset.

On the other hand, it is expected that tracking performance of the complete platoon for this method are not as adequate as compared to the centralized approach. This is a result from possessing information only on its direct predecessor rather than every other member in platoon; the (lateral) dynamic inter-dependency for this method is far greater. As an accompanying result, it is still likely that Lateral String Stability effects as well as the corner cutting phenomenon might be present when assessing the results for this strategy.

4-5 Designing controller architecture

This section covers a step-by-step walkthrough along the controller architecture as they will be embedded in the MPCs. Each design choice is elaborated briefly, explaining how the feature was established. At the end of this section, a complete overview of the control system that will attempt to safely navigate a platoon of n vehicles in highway driving applications should be clear to the reader.

The first step into designing an MPC is to complete the discretization of the continuous time vehicle- and platoon model as obtained in Equations 3-39 and 3-46.

4-5-1 Discretization of the system matrices

The discretization is carried out on the plant model in order for the MPC to successfully adopt the receding horizon framework. The discretized state space equation incorporates a certain sampling time (t_s) that determines the step-size of k in the discrete time domain. The expression of a state-space equation in discretized form is denoted in Equation 4-16.

$$\begin{aligned}\dot{x}(k+1) &= A_d x(k) + B_d u(k) + w(k) \\ y(k) &= C_d x(k) + D_d u(k) + v(k)\end{aligned}\quad (4-16)$$

in this equation, A_d, B_d, C_d and D_d denote the discretized system matrices of continuous time system matrices $A(t), B(t), C(t)$ and $D(t)$. $w(k)$ and $v(k)$ represent the disturbance terms caused by the truncation error during the process of discretization.

In this work, a value of $t_s = 0.01$ s ($\approx 20\%$ of controller rise-time, t_{rise}) has been selected, as it has shown to be sufficient for handling both the dynamics during the simulations as well to make the simulations run within an acceptable time. The rise-time is discovered by observing the system dynamics when a step response is applied. For completing the discretization, assuming Zero Order Hold, the discretized system matrices A_d, B_d, C_d and D_d are obtained the using the Equations of 4-17.

$$\begin{aligned}A_d &= e^{A(t)t_s} \\ B_d &= \int_0^{t_s} (e^{A(t)t_s})B(t)dt \\ C_d &= C(t) \\ D_d &= \left(\int_0^{t_s} e^{A(t)t_s} dt \right) D(t)\end{aligned}\quad (4-17)$$

Then, by the working principles of a discretized systems, we find the system response by writing the state vector $x(k)$ as function of the discretized system matrices A_d, B_d and initial conditions of the known state vector $x(0)^T$ at the current time step k . This step is required in order for the MPC to be able to reconstruct and predict the future states. By expressing the states in terms of the discretized system matrices, we derive the relation as can be found in Equation 4-18;

$$\begin{aligned}x(1) &= A_d x(0) + B_d u(0) \\ x(2) &= A_d x(1) + B_d u(1) \\ &= A_d^2 x(0) + A_d B_d u(0) + B_d u(1) \\ x(3) &= A_d^3 x(0) + A_d^2 B_d u(0) + A_d B_d u(1) + B_d u(2) \\ &\vdots \\ x(k) &= A_d^k x(0) + A_d^{k-1} B_d u(0) + \dots + A_d B_d u(k-2) + B_d u(k-1)\end{aligned}\quad (4-18)$$

Or equivalently, the response from time instant k over the complete prediction horizon N , we find [41];

$$x(k + N) = A^k x(N) + \sum_{i=0}^{k-1} A^{k-i-1} B u(i + N) \quad \forall i = [1, \dots, N - 1] \quad (4-19)$$

When the discretized system is known in terms of the system matrices, we can start designing the controller architecture. First, the cost function is drafted to maximize controller tracking performance. Needed next is the predictor, i.e. the algorithm behind the receding horizon and reconstruction of future states. Hereafter, the constraints are determined and added to the system to enhance once more system performance and simulate physical system bounds.

4-5-2 Cost function

The first attribute in the design process of an MPC is the cost function. The cost function is used to minimize the difference between the reference states and the measured/predicted states over the complete prediction horizon. When designed properly, in the process of minimizing this cost function implies that the output state approaches the desired reference value. Conventionally, designing the weights that are incorporated in the cost function is a matter of trade-off between controller settling time and performance. The cost function devotes a penalty to reference states or input signals if the weight on that particular state or input is higher. Conversely, the state with the lowest normalized weight is deemed most important and thus tracked in the most accurate fashion.

When discretizing the cost function as found in Equation 2-2 and adding weight matrices, the cost function at a time instant k can be denoted as displayed in Equation 4-20;

$$J(k) = \sum_{i=1}^N \Omega y(k + i|k)^2 + \lambda u(k + i - 1|k)^2, \quad \forall i = \{0, 1, \dots, N\} \quad (4-20)$$

In this cost function Ω represents the weighing matrix on the state vector and λ represents weighing matrix on the input signal. The optimal control action to be applied to the plant is then calculated solving the quadratic cost function for every time instant k over the complete prediction horizon N . The values on the diagonal of the state vector matrix Ω identify as;

$$\Omega = \begin{bmatrix} \Omega_1 & 0 & 0 & 0 \\ 0 & \Omega_2 & 0 & 0 \\ 0 & 0 & \Omega_3 & 0 \\ 0 & 0 & 0 & \Omega_4 \end{bmatrix}$$

As the weighing matrix is multiplied with the state vector it directly follows that Ω_1 corresponds with the first element of that state; $v_{y,i}$. Ω_2 is associated with the second state, yaw rate $\dot{\psi}_i$. Ω_3 influences the importance of the lateral error $y_{e,i}$ and lastly, Ω_4 penalizes deviation from the heading error $\psi_{e,i}$. For the input weights, as we have only one input signal it also follows that we have only one single λ .

From Section 4-3 where the control objectives were declared, it became clear the controller's main objective is to asymptotically reduce the heading- and lateral error to zero. Therefore these two states are deemed of higher relative importance compared to the other two states and will therefore be tracked in a more accurate way. The yaw rate is a direct result from the implemented steering angle at a certain timestep, thus in order to achieve high performance tracking, deviation from the reference yaw angle will be medium-severely penalized. Smooth tracking of lateral velocity is mostly important for comfort purposes, and less performance-wise. For this reason this state is tracked with the least relative importance. Finally, because we don't want the controller to respond too nervous (i.e. much oscillations), controller input weight is medium penalized using λ .

It has to be noted that both controllers have a different plant model incorporated; the centralized approach features the platoon model as found in Equation 3-46, whereas the distributed approach utilizes the vehicle model from Equation 3-39. As an evident result one could deduct different tuning values (i.e. state- and input weights) are therefore handled by the controllers. Following the above reasoning in conjunction with some tuning using Trial & Error, the controller weights for both controllers Ω_i , λ for $i = \{1, 2, 3, 4\}$ and N were chosen as;

Control strategy	Ω_1	Ω_2	Ω_3	Ω_4	λ	N
Centralized	100	25	0.5	8	1	15
Distributed	17	10	1	3	1	15

These values differ significantly in order of magnitude as the obtained values for the states and input also greatly differ in order of magnitude. To compensate for this, the weights are normalized to a factor of 1 and hereafter weighed on their relative importance. The value of $N = 15$ was selected by the virtue of the balance between speeding up computation and still having enough time to react to certain inputs. It has been verified using Trial & Error that larger N 's had no effect.

4-5-3 Predictor

When the cost function is drafted with the weights included, needed next are respectively the prediction matrices of the future states and future outputs over the prediction horizon, $\hat{x}(k + N)$ and $\hat{y}(k + N)$. These are required in order to allow the MPC to anticipate future behaviour and choose a series of control action that asymptotically approach the reference state. It is this characteristic that makes MPC stand out against most of its competitors and explains the widespread application in all branches of engineering. The prediction step in the receding horizon framework starts by predicting the future states using the discretized system matrices A_d and B_d . The vector containing all the predicted states over N is calculated using Equation 4-21.

$$\begin{bmatrix} \hat{x}(k + 1|k) \\ \vdots \\ \hat{x}(k + N|k) \end{bmatrix} = \begin{bmatrix} A_d \\ \vdots \\ A_d^N \end{bmatrix} x(k) + \begin{bmatrix} B_d & 0 & \dots & 0 \\ \vdots & \ddots & \ddots & \vdots \\ \vdots & \ddots & \ddots & 0 \\ A_d^{N-1}B_d & \dots & \dots & B_d \end{bmatrix} \begin{bmatrix} \hat{u}(k|k) \\ \vdots \\ \hat{u}(k + N - 1|k) \end{bmatrix} \quad (4-21)$$

Using the predicted state vector, we can also obtain the predicted output vector up to N , $\hat{y}(k + N|k)$. This is done using the relation found in Equation 4-22.

$$\begin{bmatrix} \hat{y}(k+1|k) \\ \vdots \\ \hat{y}(k+N|k) \end{bmatrix} = \begin{bmatrix} C_d & 0 & \dots & 0 \\ 0 & \ddots & \ddots & \vdots \\ \vdots & \ddots & \ddots & 0 \\ 0 & \dots & 0 & C_d \end{bmatrix} \begin{bmatrix} \hat{x}(k+1|k) \\ \vdots \\ \hat{x}(k+N|k) \end{bmatrix} + \begin{bmatrix} D_d & 0 & \dots & 0 \\ 0 & \ddots & \ddots & \vdots \\ \vdots & \ddots & \ddots & 0 \\ 0 & \dots & 0 & D_d \end{bmatrix} \begin{bmatrix} \hat{u}(k|k) \\ \vdots \\ \hat{u}(k+N-1|k) \end{bmatrix} \quad (4-22)$$

With the newly derived state- and output predictions over N , it is necessary to rewrite the cost function as derived in Equation 4-20 in terms of these prediction matrices. This leads to a new expression for the cost function that is handled by the MPC. The expression can be examined in Equation 4-23 (**Note:** for the sake of brevity the subscript d for the system matrices has been dropped).

$$\begin{aligned} J(k) &= \Omega \hat{y}^T \hat{y} + \lambda \hat{u}^T \hat{u} \\ &= x^T(k) \hat{A}^T \hat{C}^T \hat{C} \hat{A} x(k) + 2 \hat{u}^T \hat{B}^T \hat{C}^T \hat{C} \hat{A} x(k) + \hat{u}^T (\hat{B}^T \hat{C}^T \hat{C} \hat{B} + \lambda I_N) \hat{u} \end{aligned} \quad (4-23)$$

Now the plant model, cost function and predictor for the MPC are available, still one important feature for a complete, functioning MPC is missing; the constraints imposed on the dynamics of the model will be discussed in the next section.

4-5-4 Constraints

The constraints used for Model Predictive Control are typically bounds imposed on system variables to ensure high performance and to resemble physical limits on actuators. Because of this system-enhancing property the constraints verify that the optimized control actions do not enter the infeasible region. The constraints can be directly imposed on both the vehicle states as well as the input signal to coincide with the given model information. For platooning applications, the satisfaction of constraints might be exceptionally important because the efficiency demands operating points on, or close to, the boundary of the set of admissible states and controls.

Furthermore, a distinction can be made between hard constraints and soft constraints. Hard constraints imply that once set, the values of vehicle states and input signal *cannot* override the bounds, i.e. the cost function must always respect them. Hard constraints usually take the form of physical limits on the actuator dynamics as well as frictional limits on the tires and engine saturations. Oppositely, soft constraints are bounds that *can* be overridden, although the optimization will preferably choose a control action that does not override the constraint and move away from the bound. Imposed soft constraints usually aim to achieve certain system performance by setting upper or lower bounds on state or input signals.

Input constraints

As mentioned in the previous section, the constraints imposed on the input signal take the form of actual physical limitation on the steering actuators. For the selected platooning application involving highway driving, a maximum angle on the steering *wheel* of $\pm 90^\circ$, (i.e. $\frac{\pi}{2}$ rad) is imposed. In a similar manner, the steering wheel rate constrained to a value of $60^\circ/s$, (i.e. $\frac{\pi}{3}$ rad/s). These values should be translated to the actual steering angles the by incorporating the steering ratio ($\frac{1}{17}$ for the selected vehicles). Both constraint values are based on findings in Human Factor research on the topic of driving comfort and motion sickness, minimizing the effects of jerk for passengers [42] and for minimizing oscillations in steering angle during simulation.

Each platoon member i is then subjected to the following two constraints;¹

$$-\frac{\pi}{34} \leq \delta_i(k) \leq \frac{\pi}{34} \quad [rad] \quad \forall k \quad (4-24)$$

$$-\frac{\pi}{51} \leq \dot{\delta}_i(k) \leq \frac{\pi}{51} \quad [rad/s] \quad \forall k \quad (4-25)$$

State constraints

By adding the (hard) state constraints to the controller, it is generally restricted for values of any of the vehicle states to approach system bounds. Rather would the controller choose a control action that ensures high-performance as far away as possible from these values. All vehicles are therefore constrained in the simulation by the following values:

$$-0.5 \leq v_{y,i}(k) \leq 0.5 \quad [m/s] \quad \forall k \quad (4-26)$$

$$-0.25 \leq v_{y,i}(k) - v_{y,i+1}(k) \leq 0.25 \quad [m/s] \quad \forall k \quad (4-27)$$

$$-0.1 \leq \dot{\psi}_i(k) \leq 0.1 \quad [rad/s] \quad \forall k \quad (4-28)$$

$$-0.2 \leq \psi_{e,i}(k) \leq 0.2 \quad [rad] \quad \forall k \quad (4-29)$$

Constraint number 4-27 ensures that the lateral velocity during the simulation stays bounded, complying with the guidelines for driver comfort. Likewise, this is the case for the lateral acceleration, seen in constraint number 4-28. The yaw rate constraint, as a direct result of the input constraint δ_i operates as an additional checkup, as can be seen in constraint number 4-29. Lastly, the heading error constraint in 4-30 protects the error of deviation to the preceding vehicle's trajectory, and by setting it strict, aiming to improve performance.

String Stability constraints

Definition 4.2 discussed the practical definition to Lateral String Stability. It was mentioned that the imposed bounds on the lateral error signals could practically be applied by adding constraints to the MPC, which in turn limits system actuators to exceed the constraints. Therefore, when the MPC finds an optimal solution and the lateral error bounds are respected, string stability is guaranteed and thus the requirement of vehicles staying within their respective lane is satisfied.

¹Because a sampling rate of 100 Hz is adapted, the constraints were scaled accordingly. Therefore, the constraint bounds for stepsize k as implemented in `Matlab` were 100x larger in magnitude to comply with the simulation.

The two posed conditions for PLSS, now found as constraints number 4-30 and 4-31 for PLSS will be added to the full problem formulation:

$$-\gamma \leq y_{e,i}(t) \leq \gamma \quad [m] \quad \forall t, \quad \forall i \in \{1, 2, \dots, n\} \quad (4-30)$$

$$-\xi \leq y_{e,0}(t) - y_{e,n}(t) \leq \xi \quad [m] \quad \forall t, \quad \forall i \in \{1, 2, \dots, n\} \quad (4-31)$$

4-5-5 Terminal sets and terminal costs

Finally, the terminal set and terminal cost that ensure stability for the system are added to the full problem formulation. In Section 2-2 it was mentioned a conventional choice for $F(x)$ is the solution to the DARE (Equation 2-4) where N approaches infinity. Therefore, in this work $F(x) = x(N)^T P_N x(N)$ is chosen, where P_N represents this solution. The terminal set X_f is chosen such that it represents the same system bounds that are used for the state constraints as seen in constraint numbers 4-26 to 4-29. Therefore the terminal set does not add extra stability but could be chosen stricter to enhance performance (e.g. 90% of state the state bounds).

4-5-6 Full problem formulation

Having derived the discretized system matrices, predictor, cost function, constraints and terminals, ultimately we convert the general optimization problem formulation from Equation 2-3 to the full problem formulation to be solved by the MPC for this platooning application. We are left with the problem as can be observed in Equation 4-32:

$$\begin{aligned} \min_{u(k)} \quad & x^T(k) \hat{A}^T \hat{C}^T \hat{C} \hat{A} x(k) + 2\hat{u}^T \hat{B}^T \hat{C}^T \hat{C} \hat{A} x(k) + \hat{u}^T (\hat{B}^T \hat{C}^T \hat{C} \hat{B} + \lambda I_N) \hat{u} + x(N)^T P_N x(N) \\ \text{s.t.} \quad & \\ & x_i(k+1|k) = A_d x_i(k|k) + B_d u_i(k|k) + w(k) \\ & y_i(k|k) = C_d x_i(k|k) + D_d u_i(k|k) \\ & x(k|k) = x(0) \\ & -\frac{\pi}{34} \leq \delta_i(k) \leq \frac{\pi}{34} \\ & -\frac{\pi}{51} \leq \delta_i(k) - \delta_i(k-1) \leq \frac{\pi}{51} \\ & -0.5 \leq v_{y,i}(k) \leq 0.5 \\ & -0.25 \leq v_{y,i}(k) - v_{y,i}(k-1) \leq 0.25 \\ & -0.1 \leq \psi_i(k) - \psi_i(k-1) \leq 0.1 \\ & -0.2 \leq \psi_{e,i}(k) \leq 0.2 \\ & -\gamma \leq y_{e,i}(k) \leq \gamma \\ & -\xi \leq y_{e,0}(k) - y_{e,n}(k) \leq \xi \\ & k = 1, \dots, N-1 \end{aligned} \quad (4-32)$$

Solver

To determine which solver for the MPC should be utilized, let us examine once more the full optimization problem. The first step to determine whether the is optimization problem is convex or not. A set can be denoted as convex if it suffices the conditions as given in Definition 3.1 [43].

Definition 3.1 *A set \mathcal{C} in \mathbb{R}^n is convex if for each pair $x, y \in \mathcal{C}$ and for all $\lambda \in [0, 1]$, it holds that;*

$$(1 - \lambda)x + \lambda y \in \mathcal{C} \quad (4-33)$$

Then, a *function* is also convex if;

- a) *The domain of f is a convex set.*
- b) *Inequality 3-XX holds for all $x, y \in \text{dom}(f)$ and $0 \leq \lambda \leq 1$;*

$$f((1 - \lambda)x + \lambda y) \leq (1 - \lambda)f(x) + \lambda f(y) \quad (4-34)$$

An optimization problem is fully convex if;

- a) *The conditions above are satisfied.*
- b) *The constraints (if present) are linear.*

As can be observed in the full problem formulation in Equation 4-32, the cost function used within this controller is quadratic, and existing from only linear matrix multiplications. We therefore conclude the cost function suffices these conditions by definition. Furthermore, all the constraints as posed are exclusively linear constraints, which can also be examined in the full problem formulation. We may then conclude that we have a convex, constrained optimization problem. Due to the nature of convex problems, we can also safely assume that the optimum found by the solver is not only a local but also a global optimum, i.e., truly the optimal value.

For this type of optimization problems, several different solvers can be used handling convex problems. In this work, we will consider the Matlab built-in command `quadprog` that handles the interior-point method by default. This solver essentially rephrases the full problem formulation as found in Equation 4-34, and transforms it to a Quadratic Programming (QP) problem that handles a Hessian H for the quadratic terms and a gradient ∇f for the linear terms. A general constrained QP-problem takes the form to be viewed in Equation 4-35.

$$\begin{aligned} \underset{x}{\text{minimize}} \quad & \frac{1}{2}x^T Hx + f^T x \\ \text{s.t.} \quad & Ax \leq b \\ & A_{eq}x = b_{eq} \\ & lb \leq x \leq ub \end{aligned} \quad (4-35)$$

in which the H -matrix represents the Hessian, defined as the $(\hat{B}^T \hat{C}^T \hat{C} \hat{B} + \lambda I_N)$ -term from the cost function. The f matrix is defined as $(x^T(k) \hat{A}^T \hat{C}^T \hat{C} \hat{A} x(k))$. lb and ub respectively denote the lower- and upper bounds of the states and hold for each component. For the MPC application, the algorithm outputs a vector of all optimal future input controls over the complete prediction horizon to be implemented at every timestep by the use of this vector $\hat{u}(k) = [u(k), u(k+1), \dots, u(k+N-1)]$.

Simulation and results

To assess whether the developed lateral controllers perform well enough to meet the strict autonomous driving requirements robustly, the methodology behind the experimental simulation is discussed in this chapter. Section 5-1 discusses the simulation setup, explaining the intended scenarios under normal and disturbed conditions. Also, some attention is devoted on Siemens' simulation software. Section 5-2 provides the results of the simulations for all three scenarios under both conditions and contains a thorough discussion of the obtained results. At the end of the section a comparison between the two control approaches is made to determine the superior solution.

5-1 Simulation setup

Simulation modeling solves real-life problems in a safe and efficient manner. In this work, three different testing scenarios are proposed that could occur in everyday traffic to resemble every day situations. Additionally, both controllers will be tested first under 'normal' driving conditions as well as 'disturbed' driving conditions. The disturbances will be added to all three scenarios in the form of measurement/communication noise and a gust of wind to test both controllers' noise- and disturbance rejection properties. The simulations will be carried out using Siemens' *Simcenter Prescan*.

5-1-1 Simcenter Prescan

This software application embodies a physics based real-time simulation platform which is widely used in the automotive industry for the development of ADAS systems. The software features models for vehicle dynamics, roads and sensors but can be used for evaluating the Vehicle-To-Vehicle (V2V) and Vehicle-To-Infrastructure (V2I) communication, making it an attractive option for assessing platooning applications. Moreover the realistic physics engine also allows for the realistic testing, cutting the costs and speeding up the process of development of the ADAS.

Experiments are constructed in the 2D Graphical User Interface by placing vehicles, road segments objects and other road users in the plane. After the experiment has been run, a 3D rendering of the scenario is generated and visualized as the vehicles states are updated per sampling instant. This has lead to a high-fidelity testing environment that allows for reliable development of ADAS-systems. A number of screenshots of the experiment are depicted in Figure 5-1

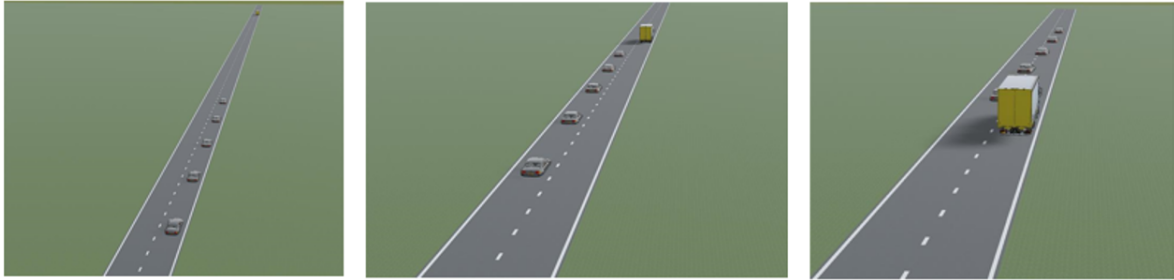


Figure 5-1: Screenshots of a double lane change scenario simulation

5-1-2 Test Vehicles

The homogeneous platoon considered in this thesis consists from five Audi A8 vehicles, as they are implemented in Simcenter Prescan. Figure 5-2 features all the vehicle parameters for this type of vehicle, applied to the single track bicycle model derived in Chapter 2.

Parameter	Value	Unit	Description
m	1820	[kg]	Vehicle mass
L	2.94	[m]	Wheelbase
L_f	1.17	[m]	COG to front axle
L_r	1.77	[m]	COG to rear axle
C_f	72653	[N/rad]	Front tire stiffness
C_r	121449	[N/rad]	Rear tire stiffness
I_{zz}	3746	[kgm ²]	Rotational Inertia Z-axis

Figure 5-2: Parameter values used in simulation

Computer hardware specification

The simulations are carried out on a remote HP desktop-computer running at the Siemens Digital Industries office in The Hague, Netherlands. The desktop specifications are listed below so one could have a sense of the computation time needed to perform the simulation.

- Windows 10 Enterprise x64
- Intel Xeon (R) E-2144G CPU @ 3.60GHz
- 64 GB RAM

5-1-3 Scenario 1: Double Lane Change (DLC)

In the first scenario, a platoon of 5 vehicles (i.e. one leader and four followers) is driving on a two-lane highway at a forward velocity of $v_x = 100$ km/h, at an inter-vehicle distance of $d_i = 20$ m. At some point, the platoon leader notices a truck standing still on the right-most lane and plans an overtaking manoeuvre. The first lane change is initiated when a safe distance between the platoon leader and truck is secured. Hereafter, all four following vehicles will follow the platoon leader's trajectory. After a platoon member has safely passed the truck, the second lane change is initiated, back into the original lane. This scenario is included to determine how the controller handles obstacle avoidance unaccounted for in the prediction matrices of future states. The scenario as it is intended can be observed in Figure 5-3. Note that this plot reviews the vehicle y -position against time rather than the absolute trajectory and that the aspect ratio for x and y are distorted.

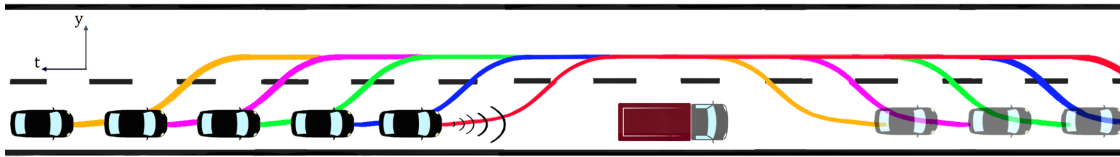


Figure 5-3: Scenario 1: Double Lane Change at $v_x = 100$ km/h

5-1-4 Scenario 2: Highway Turn

The second scenario involves again a vehicle platoon of 5 members driving with a constant forward velocity of $v_x = 80$ km/h, maintaining an inter-vehicle distance of $d_i = 20$ m on a straight road. At some point, the aim for the platoon is to navigate a turn of constant radius of $r = 400$ m after which another straight-road segment is followed. In [44], the corresponding value for radius is defined as minimum corner radius for a vehicle driving this velocity based on admitted lateral accelerations. This second scenario is primarily incorporated to investigate how the controller acts to a certain steady state value for all vehicle states. Figure 5-4 visualizes the intended scenario, again with a distorted aspect ratio.

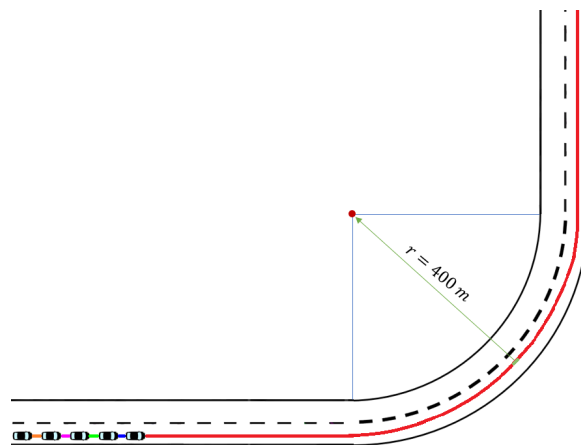


Figure 5-4: Scenario 2: Constant Curve ($r=400$ m) at $v_x = 80$ km/h

5-1-5 Scenario 3: Double Lane Change during constant curve

Finally, a third scenario is proposed that combines the characteristics of both the first and second scenario. Herein, once again a platoon of 5 vehicles maintains a forward velocity of $v_x = 80$ km/h, at an inter-vehicle distance of $d_i = 20$ m. The same constant curve is initiated from Scenario 2, but this time halfway through the curve, a double lane change is executed. Moreover, this scenario primarily tests both the steady-state conditions of the controllers as well as how easily the controller can deviate from and return to its steady state.

5-1-6 Noise and disturbance conditions

After running the tests first under normal driving conditions, the tests are also ran under noised- and disturbed conditions to see how the controller would handle these situations that could occur in real life. Once more it must be stated that due to the strict requirements on the developments in autonomous driving, faults cannot be tolerated and safety must be guaranteed at all times.

Wireless communication noise

Under such conditions, measurement noise is added directly to the communicated vehicle states in the form of Zero Mean White Noise (ZMWN). This type of noise is a property of a stochastic signal, i.e. a signal with a Gaussian probability density function. Put more specifically, a noise-signal $e(k)$ is stochastic if the following two conditions hold [41].

1. Signal mean is zero at all times; $m_e(k) = 0$,
2. Auto-covariance function $E[e(k)e(k - \tau)] = \sigma_e^2 \Delta(\tau)$, and 0 otherwise.

Hence, the information on other vehicle's state variables received through wireless communication now takes the form of $x_{i-1}(k)^T = [x_{i-1}(k)^T + e(k)^T]$. Figure 5-5 depicts the disturbed signal of e.g. the yaw rate, as received by a preceding vehicle.

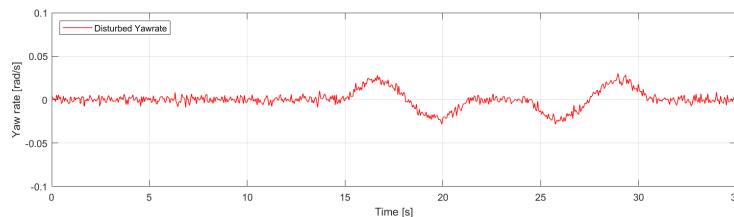


Figure 5-5: Disturbed signal (e.g. yaw rate)

These kinds of situations can for example occur under extraordinary weather circumstances causing the on-board sensors to make very unreliable predictions on vehicle states. Another possibility exists when driving through an area where numerous radio signals cause interference to the communicated vehicles states, making the measurements and communication unreliable.

5-1-7 Gust of wind

In this disturbance scenario it is assumed while driving suddenly a strong crosswind is temporarily acting on all following vehicles. The crosswind acts directly on every vehicle's center of gravity, being applied for a certain amount of time [45]. Correspondingly, this leads to an additional lateral acceleration caused by the lateral wind force, following Newton's second law of motion, $F = ma$. Rewriting this leads to;

$$a_y = \frac{F_{y,wind}}{m} \quad (5-1)$$

The magnitude of the applied lateral crosswind-force is calculated using Equation 5-2;

$$F_{y,wind} = \frac{1}{2} C_{d,y} A_y \rho_{air} v_{wind}^2 \quad (5-2)$$

In this equation, $C_{d,y}$ is the lateral drag coefficient, A_y is the side-area of the vehicle, ρ_{air} the ambient air density and v_y the windspeed in m/s. A Beaufort-scale 7 wind is considered delivering a windspeed of 15 m/s. Substituting the parameters of the Audi A8 test vehicles and considering a strong crosswind, a lateral force of approximately $F_{y,wind} = 430\text{N}$ was found, corresponding to an additional (rounded) lateral acceleration of $a_y = 0.25\text{m/s}^2$ applied to the model for three seconds halfway during the simulation.

5-1-8 Decision variables for guaranteeing Practical Lateral String Stability

The conditions for Lateral String Stability set in Section 4-2 ensure that certain bounds are not overridden. The selected values for γ and ξ in this work are determined by the requirement that the complete platoon of test vehicles do **not** enter a neighbouring lane or swerve off the road, reinforcing the definition of practicality. In Figure 5-6 one can observe the dimensions roads and test vehicles as used in this simulation.

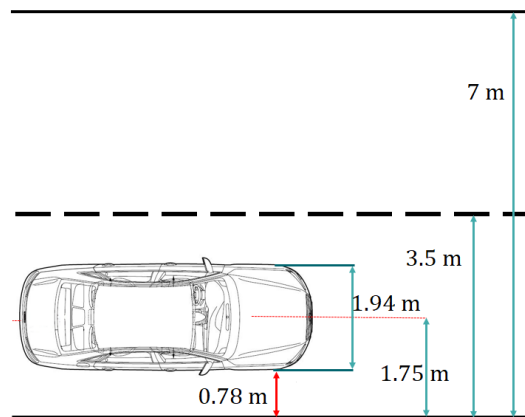


Figure 5-6: Relevant dimensions for road and test vehicles

The requirement to stay in the designated lane implies a value of $\xi = 0.78$ is selected. Additionally, considering $n = 5$, $\gamma = 0.2$ is chosen to comply with the first condition and desired performance strictness.

5-2 Simulation Results

In this section the results of the simulation are thoroughly discussed. For each scenario and for all conditions, the results of vehicle trajectories, individual lateral error, (i.e. shortest distance from vehicle i to the trajectory of vehicle $i - 1$) and total lateral error (i.e. shortest distance from final following vehicle n to platoon leader trajectory) will be depicted side-by-side so a valuable comparison can be performed. Other, slightly less relevant plots concerning the yaw rates and steering angles can be retrieved in Appendix C. The results, from top to bottom are depicted as distributed and centralized, respectively.

Double Lane Change scenario, normal driving conditions, $v_x = 100$ km/h

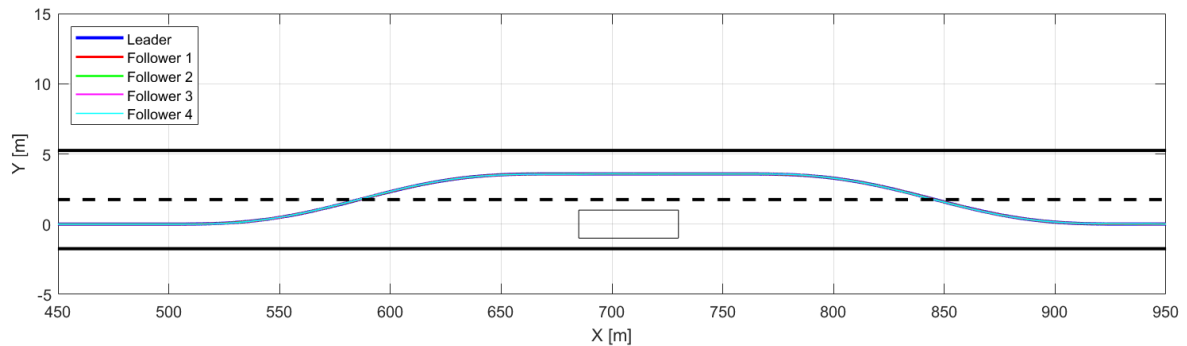


Figure 5-7: Distributed controller, trajectories under normal driving conditions

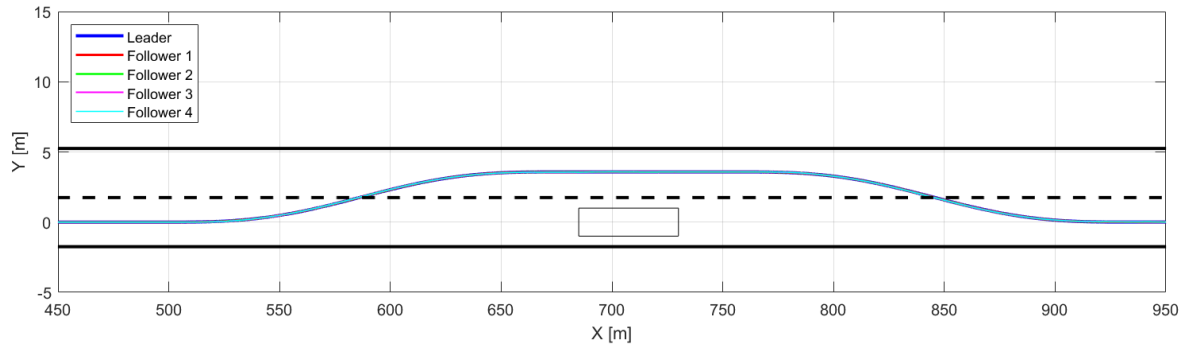


Figure 5-8: Centralized controller, trajectories under normal driving conditions

The trajectory plots in Figures 5-7 and 5-8 visualize the vehicle-following performance of both controllers during the double lane change scenario excluding noise or disturbance. One can easily observe that the plots look indistinguishable, suggesting both controllers perform extremely efficient in terms of reference tracking by producing a minuscule deviation from the platoon leaders' trajectory. We may therefore assume, by safely executing the double lane change, both controllers' tracking performance produce satisfying results. Though in order to say something useful on the string stability properties of the platoon, we must look at the corresponding lateral error plots over these trajectories. These plots are depicted in Figures 5-9 and 5-10.

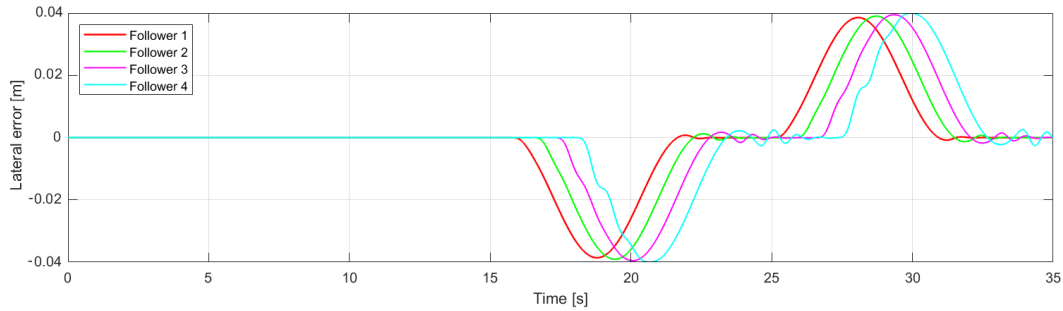


Figure 5-9: Distributed controller, individual lateral error under normal driving conditions

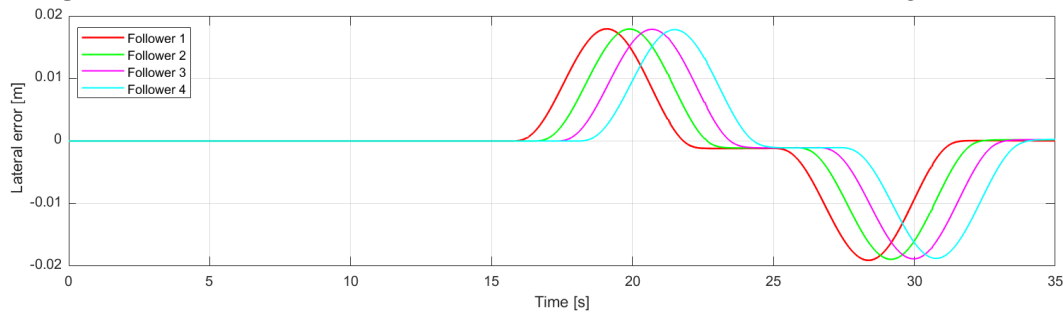


Figure 5-10: Centralized controller, individual lateral error under normal driving conditions

As was assumed the controllers perform extremely efficient tracking by observing the trajectory plots, Figures 5-9 and 5-10 confirm this assumption by indeed producing minuscule lateral errors over the complete trajectory. Peak values of lateral deviation for each individual platoon member using the distributed controller lay around 0.04 m. Whereas for the centralized controller, this error is only half this value. Furthermore the plots verify a very smooth overtaking manoeuvre for both controllers as could be seen from the previous trajectory plots, showing only very slight oscillations for the distributed controller.

At the first glance one could notice how for the distributed controller the plot is 'mirrored' as compared to the centralized controller. By zooming far into the trajectory plots from Figure 5-7 and 5-8, we observe that with the distributed controller slightly 'undercuts' the path of the platoon leader; suggesting suffering (negligible) from the cutting corner phenomenon as discussed in Section 1-4-2. By undercutting the path of the preceding vehicle, a following vehicle ends to the left of the reference trajectory. Whereas for the centralized controller, the opposite is true, ending up to the right of the reference trajectory.

Maximum overshoot of individual platoon member i 's lateral error stay bounded, implying Condition 1, formulated as;

$$-0.2 \leq y_{e,i}(t) \leq 0.2 \quad [m] \quad \forall t, \quad \forall i \in \{1, 2, \dots, n\}$$

is satisfied for both control approaches. Furthermore, it is of great important to notice that for the centralized controller, the obtained values of lateral error for a vehicle i does not further amplify upstream, to vehicle $i - 1$.

In other words, the definition of Absolute Lateral String Stability might be applicable to the centralized approach, as condition 3;

$$\max |y_{e,i-1}(t)| \leq \max |y_{e,i}(t)| \quad [m] \quad \forall t, \quad \forall i \in \{1, 2, \dots, n\}$$

is also satisfied. For the distributed controller on the other hand, we do observe amplification in the lateral error upstream, albeit in the order of magnitude ≈ 0.005 m.

However, to rightfully guarantee Practical Lateral String Stability for the current application, one more condition is required to be satisfied. The total lateral error, i.e. the lateral deviation from the last follower as compared to the reference trajectory set by the platoon leader, is required to stay bounded by ξ . The total lateral error plot for both controllers is visualized in Figures 5-11 and 5-12.

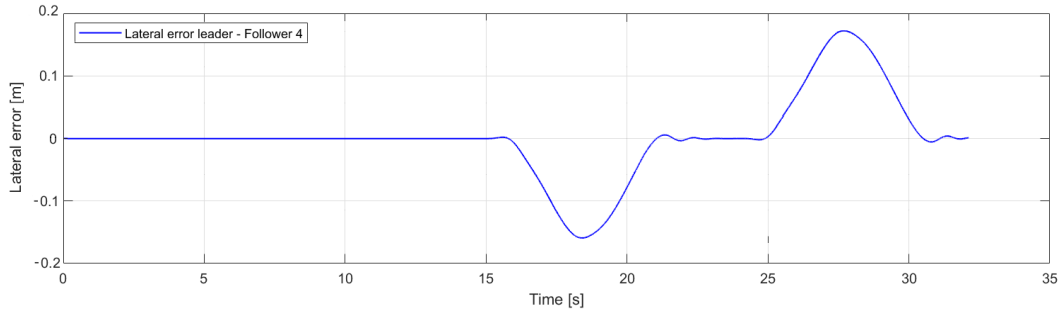


Figure 5-11: Distributed controller, total lateral error

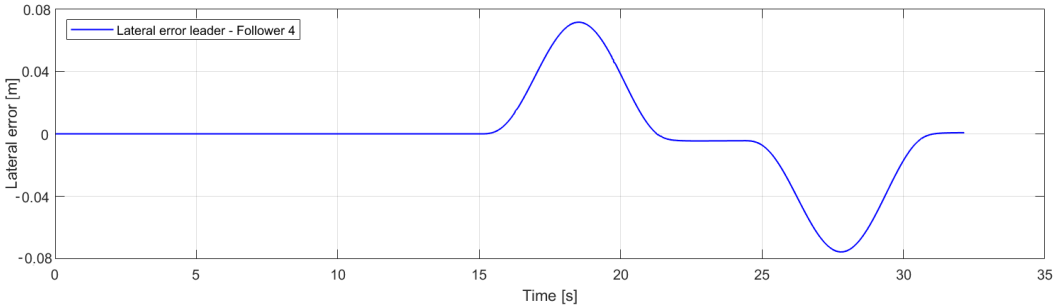


Figure 5-12: Centralized controller, total lateral error under normal driving conditions

The total lateral error implies the lateral error between the reference trajectory set by the platoon leader and the trajectory driven by the last follower, and is essentially a summation of all the individual plots from Figures 5-9 and 5-10. With the total lateral error plot available, we can finalize the assessment of PLSS by inspecting whether Condition 2 is satisfied for both controllers.

By examining the plot, we can easily conclude that the second required condition for Practical String Stability, formulated as;

$$-0.78 \leq y_{e,0}(t) - y_{e,n}(t) \leq 0.78 \quad [m] \quad \forall t, \quad \forall i \in \{1, 2, \dots, n\}$$

is also satisfied for both controllers for this scenario under normal driving conditions.

Aside from the figures that depict the trajectories and lateral errors, a fair amount of information is also to be obtained from the plots found in Appendix C. Evidently, the steering angle and corresponding yaw rate are also of significant relevance when assessing controller performance.

Figure C-1 and C-2 depict the steering angles over the trajectories against time. Along with the smooth trajectories found in Figures 5-7 and 5-8, the steering angle plots look smooth for both controllers and stay easily bounded between the constraint values of $\frac{\pi}{34}$ (i.e. $\approx 3.5^\circ$ on the wheels). For the distributed controller, the 4th follower starts oscillating towards the end, but also this phenomenon stays bounded for the steering rate. Therefore for both controllers, input constraints are respected. Accordingly, values of the yaw rate, a direct result from the steering angle, stay bounded (Figures C-3 and C-4).

Double Lane Change scenario, including measurement/communication noise

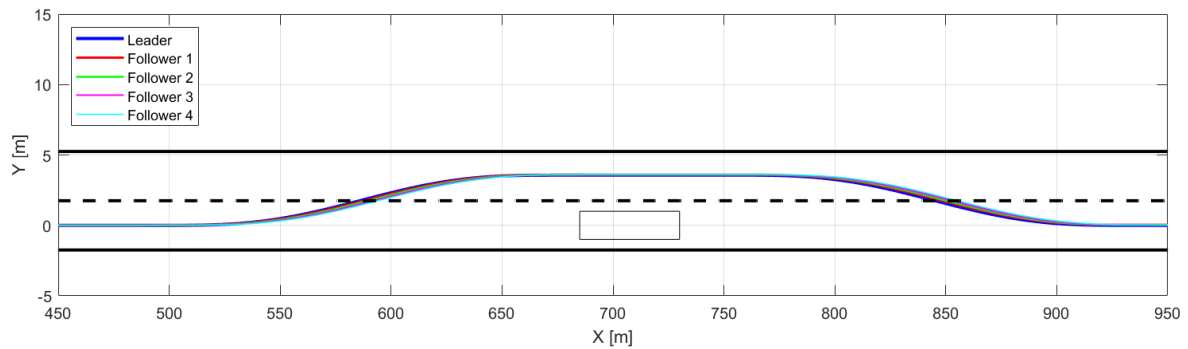


Figure 5-13: Distributed controller, trajectory including measurement noise

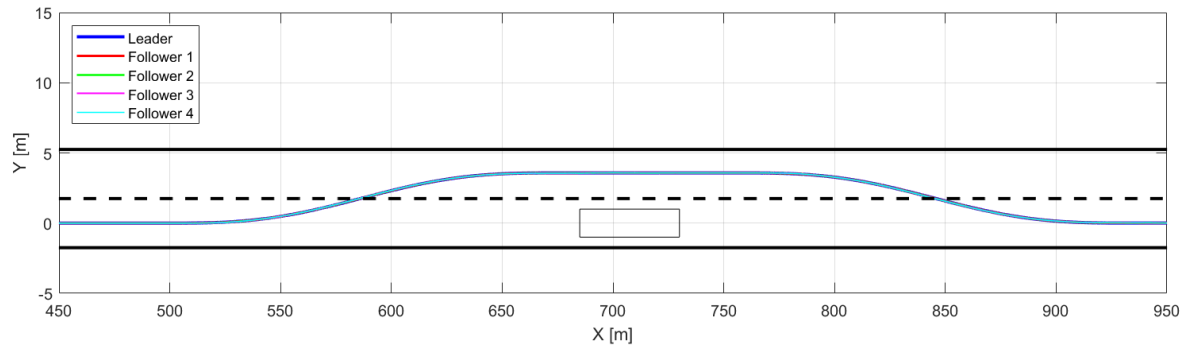


Figure 5-14: Centralized controller, trajectories including communication noise

When looking at the trajectory plots of Figures 5-13 and 5-14, one can comfortably reason that no major effects of the noise are to be distinguished. However, the actual effects of the noise become clear when we observe the lateral error plots for both the individual platoon members as for the complete platoon.

The distributed controller is noticeably more effected by the noise than the centralized controller, as can be observed from reviewing Figures 5-15 and 5-16, plotting the individual lateral errors for the platoon members.

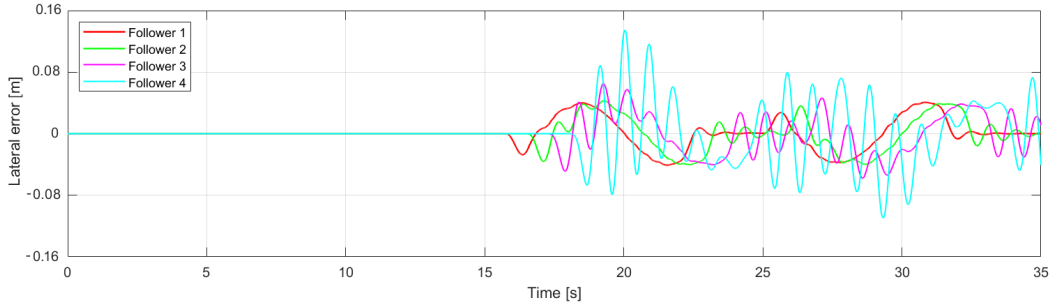


Figure 5-15: Distributed controller, individual lateral error including measurement noise

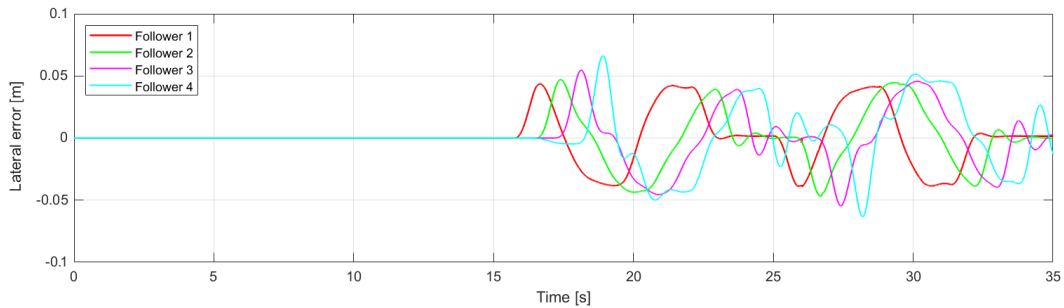


Figure 5-16: Centralized controller, individual lateral error including communication noise

Not only is the distributed controller clearly more susceptible to the noise by the means of introduced oscillations, but again also in terms of the maximum overshoot. Moreover, we clearly observe the string instability issue at work for both controllers, showing an amplification of the oscillations of the previous lateral error. This can most be probably explained due to the fact that the communicated/measured states of lateral error, are also noised. In turn the controller might try to 'overcompensate' for this effect, leading to larger amplifications.

For the last follower this results in a peak value of approximately 0.14 m for the distributed approach, against a maximum overshoot of around 0.06 m for the centralized approach. This implies that even under noised conditions, the first criteria for assessing the first condition of PLSS, is satisfied for both controllers.

For satisfying Condition 2, we must look again at the total summed lateral error. These plots are depicted in Figures 5-17 and 5-18. One notices that the smooth trajectory under normal driving conditions is no longer present; once more the oscillations for the distributed approach to be of greater magnitude as compared to the centralized approach.

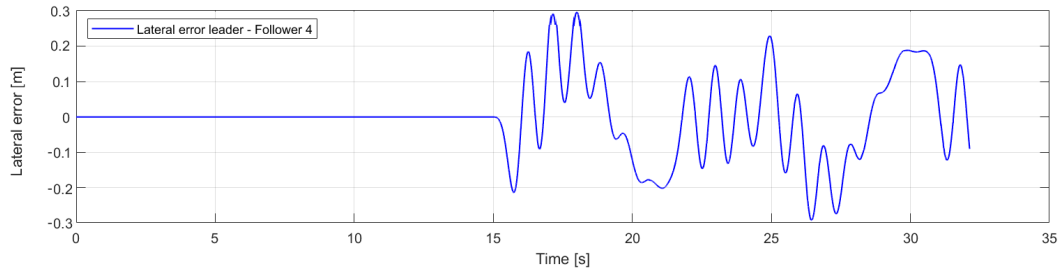


Figure 5-17: Distributed controller, total lateral error including measurement noise

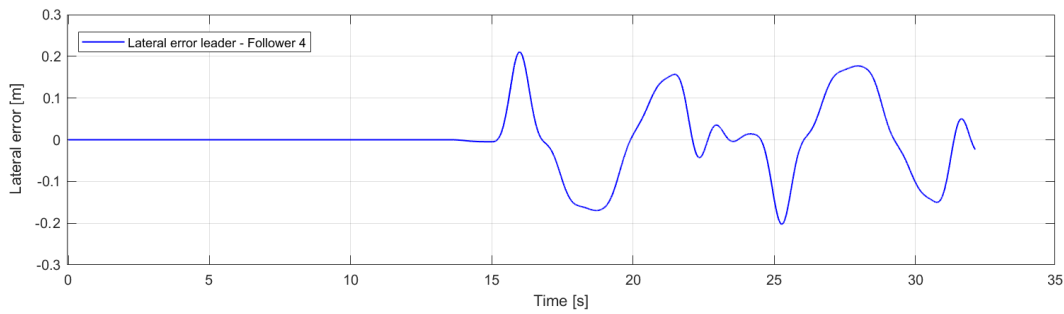


Figure 5-18: Centralized controller, total lateral error including communication noise

However, both controllers remain easily bounded between the constraint values of $\xi = 0.78$, as the maximum overshoot of lateral error from platoon leader to last follower reach peak values of 0.3 m and 0.21 m for respectively the distributed and the centralized controller. Furthermore it is important have a sense of scale for the errors in this plot; leader vehicle and last follower are 100 m apart in longitudinal distance whereas their centers of gravity differ only 0.3 m in lateral distance.

Double Lane Change scenario, including wind disturbance

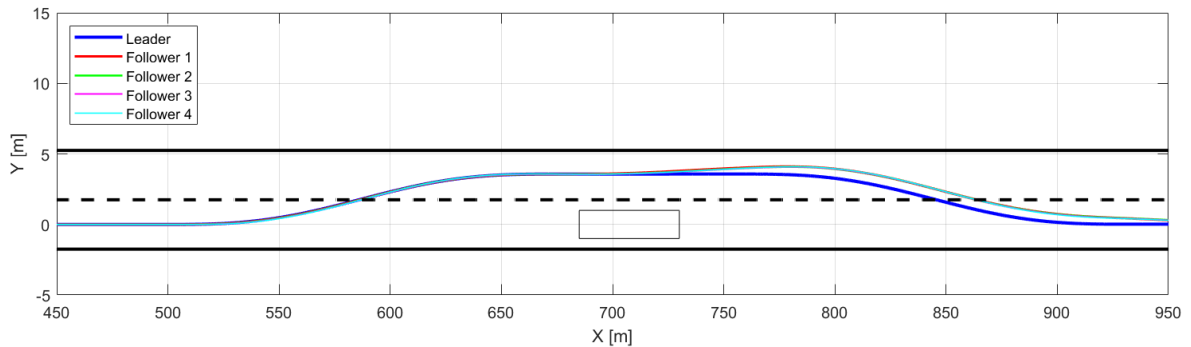


Figure 5-19: Distributed controller, trajectories including gust of wind

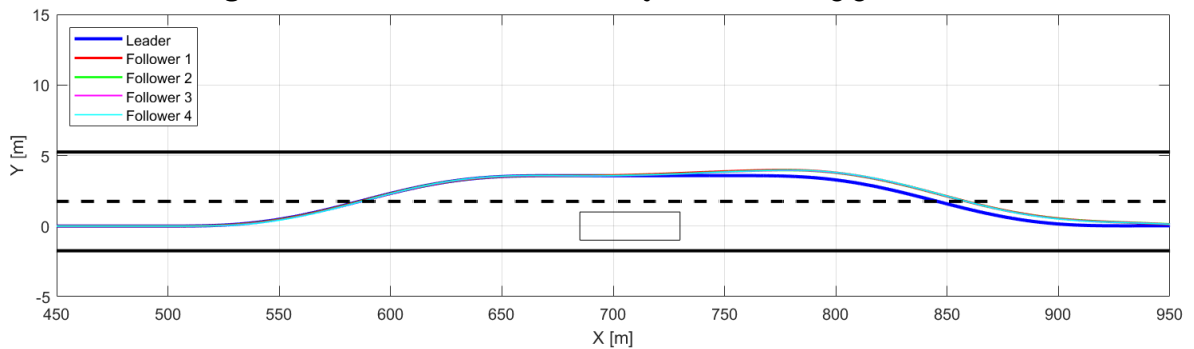


Figure 5-20: Centralized controller, trajectories including gust of wind

Evidently, the results from the wind disturbance scenario are easier to distinguish from the trajectory plots as compared to the previous noise scenario. Halfway through the double lane change, the crosswind acts on all follower's center of gravity for three seconds. As an effect, the following vehicles are slightly blown of the reference trajectory, after which the controller tries to recover by adjusting the steering angles. Figures 5-19 and 5-20 show the driven trajectories.

For the centralized approach we observe a slightly quicker recovery onto the reference trajectory as compared to the distributed controller, although one must observe closely to distinguish the subtle difference. Furthermore we notice how the overshoot for the centralized approach is smaller, as apparently during the wind scenario the centralized controller already works hard recovering from the wind effects even during the gust, implying more aggressive control. The distributed approach steers the vehicles back onto the reference trajectory 'one-by-one', whereas the centralized controller can steer the vehicles back simultaneously.

Therefore once more it can be concluded that the distributed approach is affected more by the noise as compared to the centralized approach, thus may we assume for the selected scenario, noise rejection properties are of higher efficiency when the centralized controller is embedded.

Constant Curve scenario, normal driving conditions, $v_x = 80$ km/h

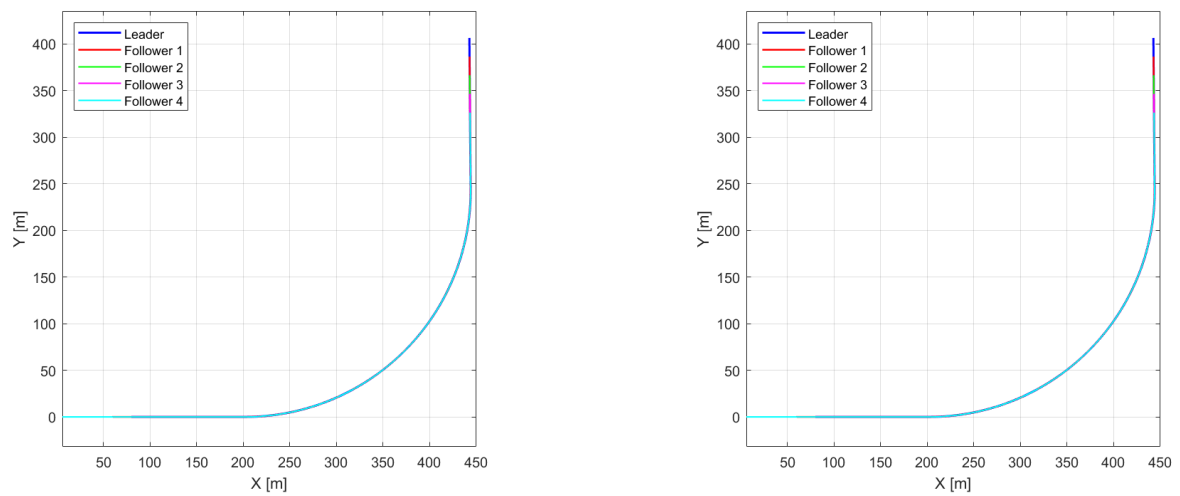


Figure 5-21: Distributed (left) and Centralized (right), normal driving conditions

Likewise as for the DLC scenario, from the trajectory plots in Figure 5-21 it can be observed controller tracking performance seems reliable at the first glance. Let us therefore examine more closely the individual lateral error plots in Figures 5-22 and 5-23.

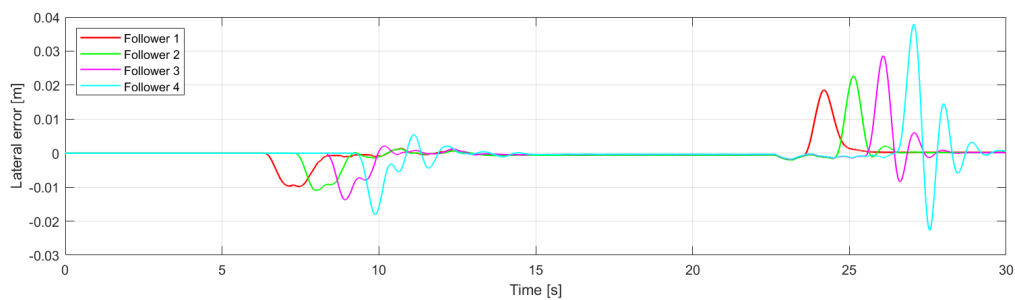


Figure 5-22: Distributed controller, individual lateral error under normal driving conditions

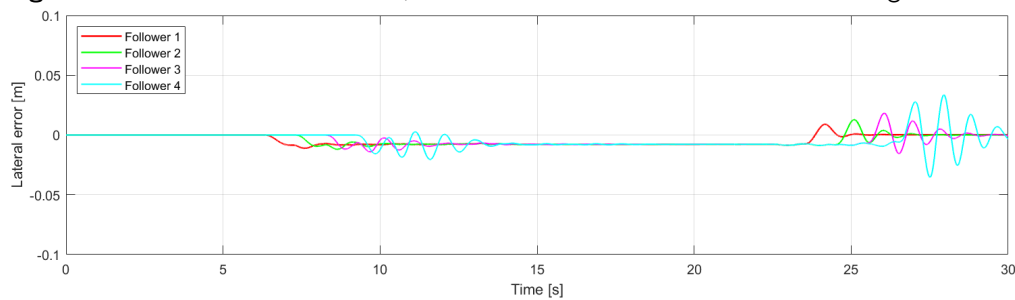


Figure 5-23: Centralized controller, individual lateral error under normal driving conditions

When analyzing the reference tracking performance of both controllers, the first thing one might notice is that for this scenario again performance is rather similar. Both controllers show excellent reference tracking performance. Maximum overshoot of lateral error for both controllers produced a value of approximately 0.038 m for the distributed controller and 0.012 m for the centralized controller, verifying that Condition 1 for PLSS for the constant curve scenario, comfortably hold for both approaches.

Furthermore, both controllers experience minor oscillations produced by the step-function of steering angle. The attentive reader might notice that these oscillations appear in the same frequency, indicating that (due to the absence of dampers) this an Eigenfrequency of the system model. For both cases, the oscillations are instantaneously damped.

It was stated in Section 5-1-4 that the constant curve scenario was introduced to assess the controllers' steady state characteristics. While having another look at Figures 5-22 and 5-23, it is perceived that the distributed controller produces no steady state error, whereas its competitor, the centralized controller, does. It must be noted though, that this steady state value of ≈ -0.004 m per vehicle is rather negligible. To verify if Condition 2 for PLSS is satisfied, we will examine the total lateral error plots as depicted in Figures 5-24 and 5-25.

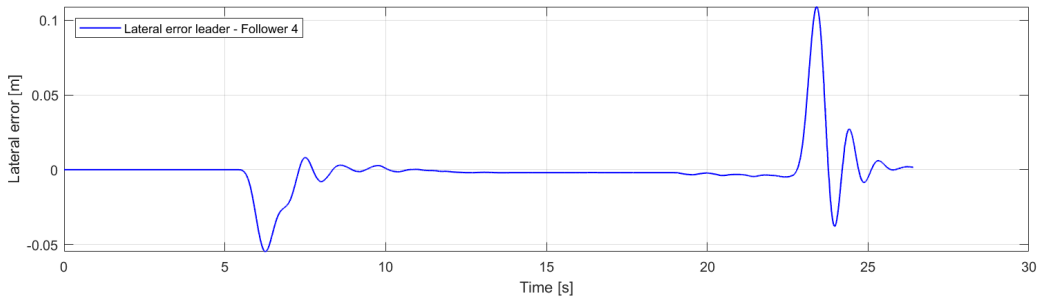


Figure 5-24: Distributed controller, total lateral error under normal driving conditions

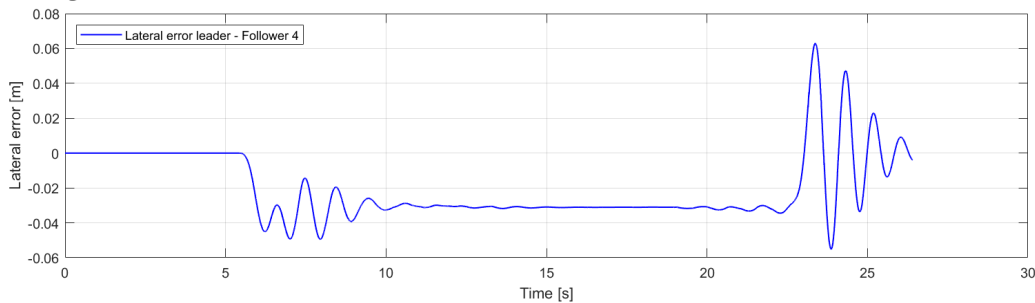


Figure 5-25: Centralized controller, total lateral error under normal driving conditions

In the plots we see that indeed the steady state error for the complete platoon while employing the distributed approach stays zero. Whereas for the centralized controller, we see that the summed steady state error for the complete platoon over this trajectory reaches ≈ -0.03 m. On the other hand, as compared to the centralized controller, the maximum values for overshoot are greater. This suggests that the tuned weights in the MPC controller for a situation where a steady state error is introduced, a different trade off between tracking performance and damping is made. When verifying if for this scenario the controller satisfies condition 3 for ALSS, as we see slight (order of magnitude of approx. 0.0025 m) amplification, therefore is by the strict definition, not satisfied.

Constant Curve scenario, including measurement noise

The trajectory plots for the noised constant curve scenario, produces identical plots as the plots depicted in Figure 5-21 due to the aspect ratio of the axes. In order to say something useful on the noise rejection properties in a steady-state environment, once more we look at the individual lateral error plots in Figures 5-26 and 5-27.

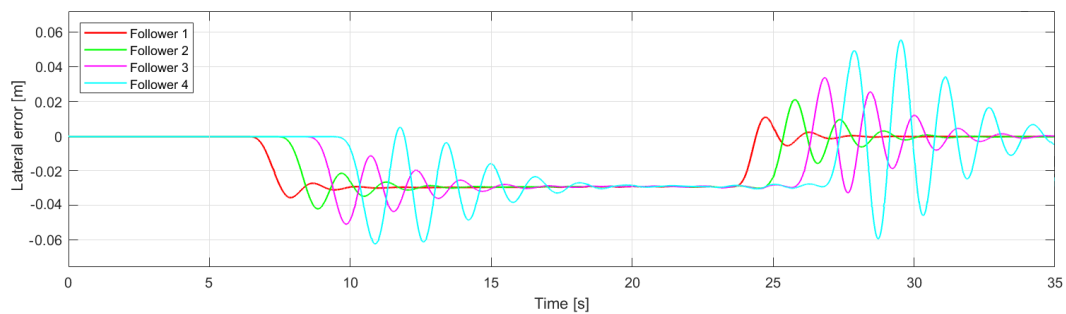


Figure 5-26: Distributed controller, individual error including measurement noise

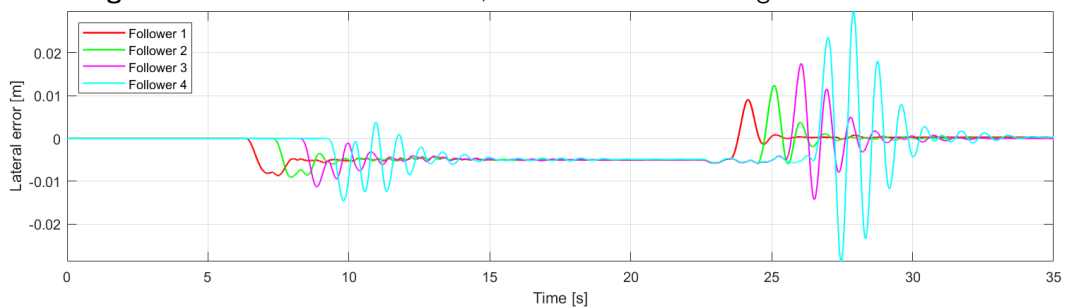


Figure 5-27: Centralized controller, individual error including measurement noise

For the distributed controller, performance in the noised scenario is (evidently) worse than for the noiseless scenario due to the oscillations introduced at the end not being damped but rather amplified; showcasing the string instability effect. However, even with these oscillations the individual lateral error remains between the imposed bounds with enough margin.

We also notice that a steady state error has been introduced because of the measurement noise, albeit a steady state error of 0.03 m for each individual platoon member. Throughout this 'steady state' also very slight oscillations are again recognized.

For the centralized controller, we see that the first 25 seconds show similar behaviour as in the noiseless scenario, with the exemption of a slightly larger steady state error for each platoon member (≈ 0.01 m). From this we can assume that the centralized controller undergoes little effects from the noise. However, after 25 seconds, suddenly a great amplification in oscillations are interestingly produced. However, these are very quickly damped out by the system. Once more it can be concluded both controllers satisfy the requirements for PLSS.

Constant Curve scenario, including wind disturbance

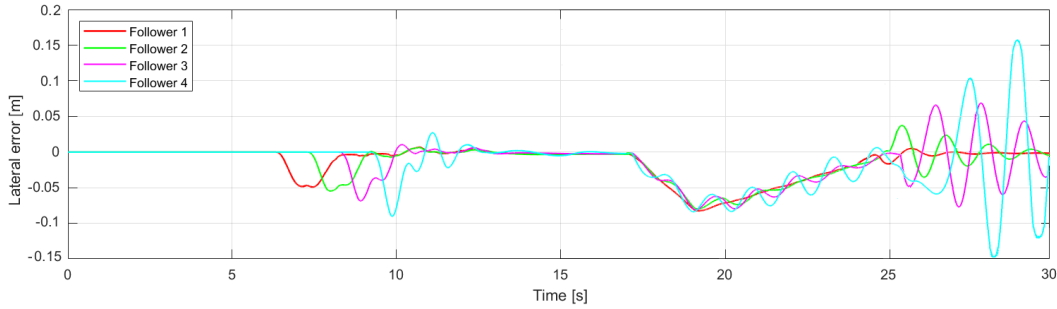


Figure 5-28: Distributed controller, individual lateral error including gust of wind disturbance

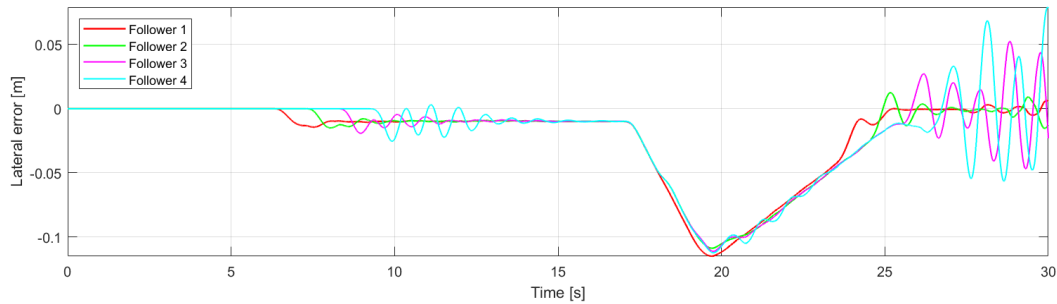


Figure 5-29: Centralized controller, individual lateral error including gust of wind disturbance

In this scenario the vehicles are also subjected to the crosswind, however it is acting from the other side trying to push the vehicle further off the road rather than cooperating against the centrifugal force introduced by the curve. The wind is initiated halfway through the curve (at $t = 17$ s), as one can see from the plot.

Consider Figure 5-28. The distributed controller endures no steady state error when the turn is negotiated. After the wind was applied, a maximum lateral deviation of 0.08 m was found, after which the controller needs about 6-7 seconds to recover. After 'recovering' rather large amplification of oscillation amplitude is found. No overshoot either, slow but certain recovery.

The peak value in lateral overshoot caused by the wind is interestingly larger for the centralized controller showing a value of 0.11 m in Figure 5-29. Also for this controller, 'recovering' from the initial offset takes again about 6 seconds. Oscillations are then again introduced, but do not amplify as much as for the distributed scenario.

Additionally, notice the difference between the lateral error values for this scenario as compared (Figure 5-28/29, ≈ 0.1 m) to the double lane change scenario (Figure 5-19/20 ≈ 0.6 m) after the crosswind was applied. This significant difference can most probably be explained by the difference in yaw angle at the instant the force was applied. During the double lane change scenario, the crosswind was applied at a time when the lateral acceleration was 0, as the vehicles were driving straight halfway through the overtaking manoeuvre, i.e. $\psi_i = 0$. During the constant curve scenario the lateral acceleration already reached a steady state value and was halfway through the corner, i.e., $\psi_i \approx \frac{\pi}{4}$ when the additional acceleration was applied. As a result, the additional 'force' would be divided over the longitudinal and lateral component of the tire forces, and thus level out the effect of the gust.

Lane Change in Curve scenario, normal driving conditions, $v_x = 80$ km/h

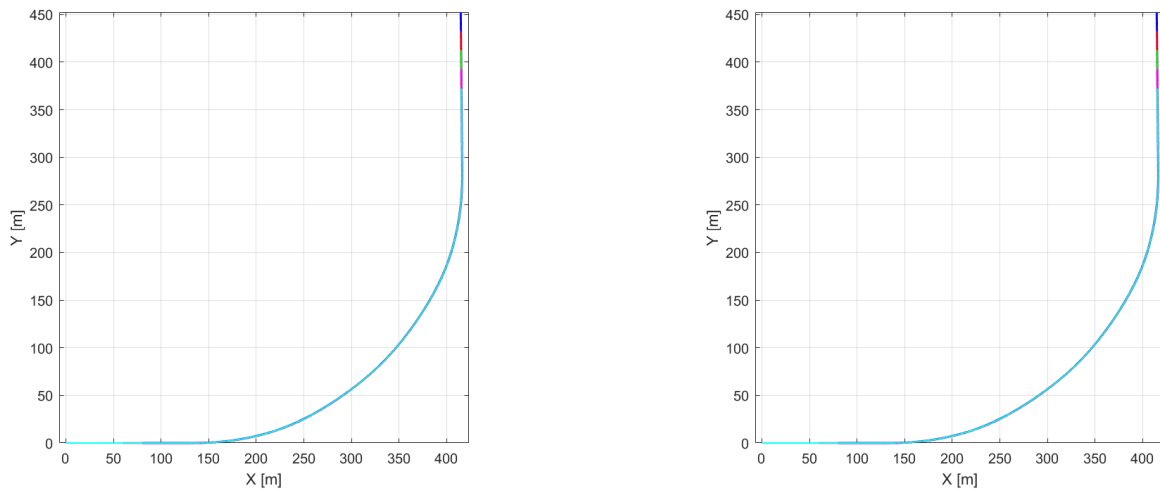


Figure 5-30: Distributed (left) and Centralized (right), trajectories, normal driving conditions

Reviewing the trajectory plots in Figure 5-30, it seems at first sight the third scenario is no different from the previous scenario. Nonetheless, after carefully reviewing the trajectory plots of both scenarios, a subtle difference in the smoothness of the curve can be distinguished.

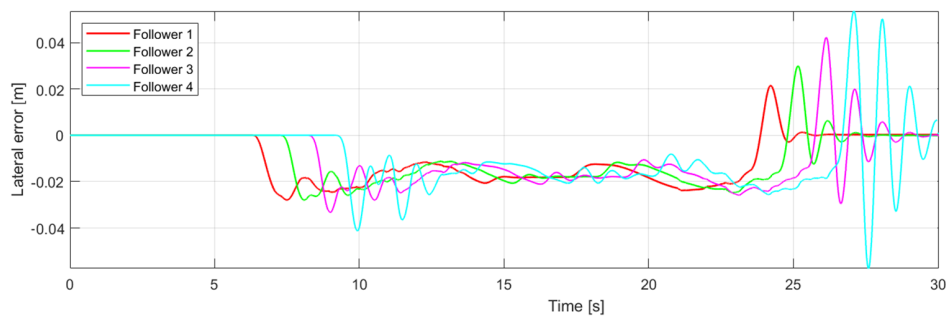


Figure 5-31: Distributed controller, individual lateral error under normal driving conditions

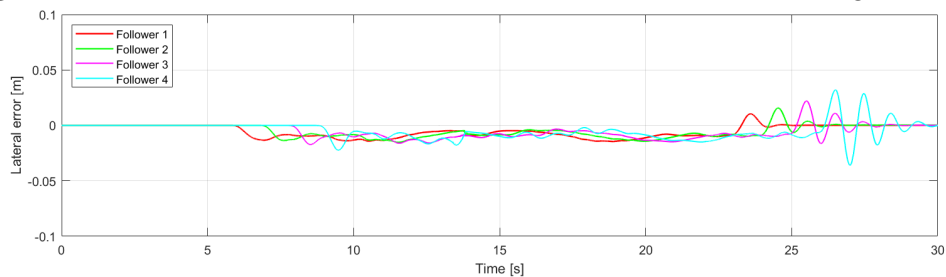


Figure 5-32: Centralized controller, individual lateral error under normal driving conditions

When comparing the individual lateral errors in Figures 5-31 and 5-32 with the individual errors found in the constant curve scenario, one perceives the same trend in excited oscillations due to the step-input on steering angle when executing the constant curve. Sadly, in this scenario the oscillations cannot be damped as quickly and efficiently due to another step input signal for the double lane change is initiated.

On the first glance, performance of both controllers look rather similar. However this time we also observe a steady state error for the distributed controller, that is in fact larger than for the centralized controller. Moreover, the oscillations observed from the distributed controller are, (slightly) higher.

The first condition for PLSS is satisfied by the virtue of peak valued of maximum overshoot for the distributed and centralized controller showing to be respectively, 0.045 m and 0.03 m.

The third condition for ALSS cannot be satisfied, as we observe an amplification of the lateral error signal, which immediately damps out after. However, we must be strict in assessing the behaviour in order to rely on safe autonomous driving. When observing the total lateral error for the complete platoon, we capture the results as depicted in Figures 5-33 and 5-34.

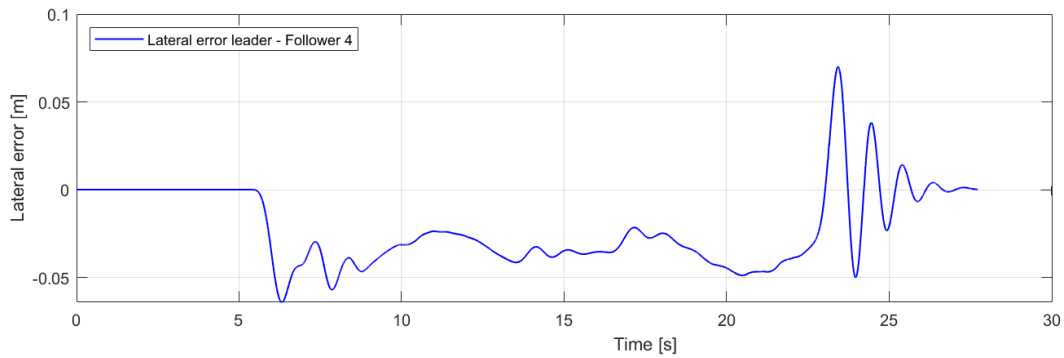


Figure 5-33: Distributed controller, total lateral error under normal driving conditions

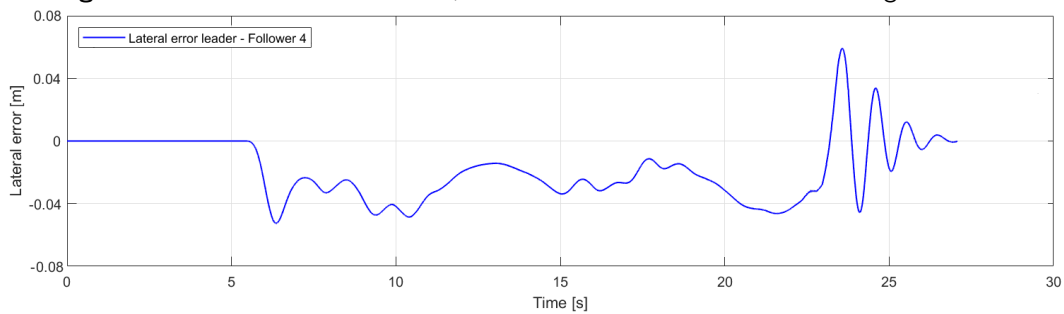


Figure 5-34: Centralized controller, total lateral error under normal driving conditions

One can observe once more that these two plot look much the same, as was mentioned that a similar trend was observed compared to the previous scenario. When assessing Condition 2 for PLSS, we see values of maximum overshoot to be far below the given bounds, meaning safe platooning can be ensured.

Lane Change in Curve scenario, including measurement noise

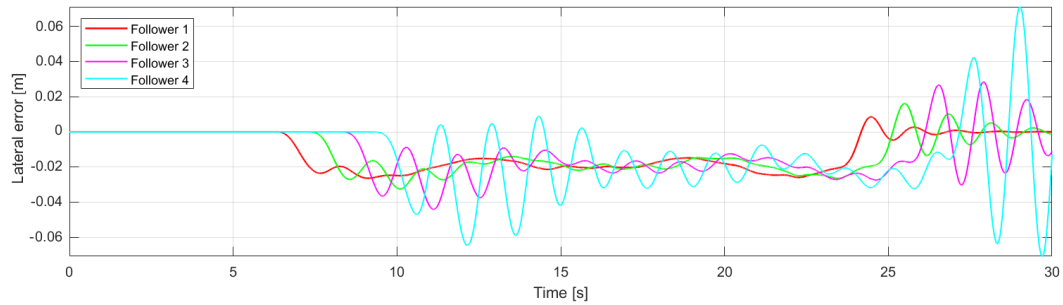


Figure 5-35: Distributed controller, individual lateral error including measurement noise

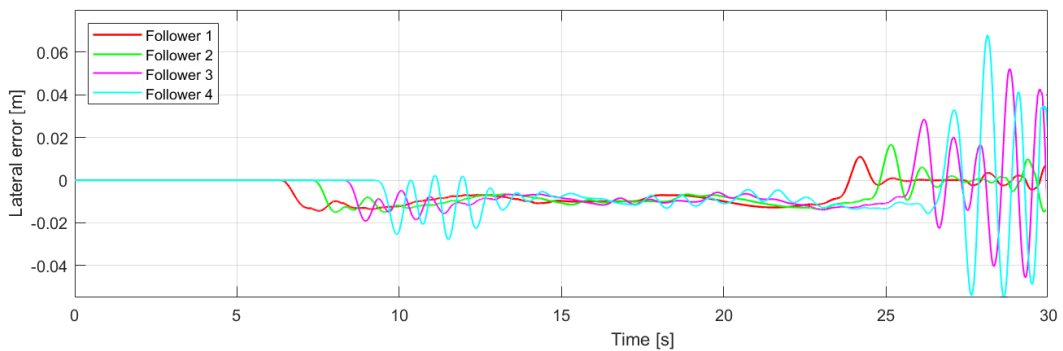


Figure 5-36: Centralized controller, individual lateral error including communication noise

For the noised scenario, evidently the trend we observe is the same as for the previous scenario under noised conditions. The distributed controller tracking performance is similar to the one found in Figures 5-26, but with marginally larger-magnitude oscillations. The controller furthermore behaves more 'nervous' around the steady state and during the lane change, but we do see the trend of amplification and immediate damping.

Again, the centralized controller produces an nearly identical graph compared to 5-27 in which a small steady state error is produced of the same magnitude. During the lane change, there is slight fluctuation around this steady state after which we find repeatedly the same oscillations pattern, where no trend can be identified.

Still, it can be concluded that the centralized controller does not handle noise well in this situation. The presumed cause for this is that the noise and chosen tuned weights cause the system dynamics to become unstable in situations around the steady state. Nevertheless, when assessing if PLSS is the case for this scenario, we detect $y_{e,i}$ for both approaches to remain spaciouly bounded between the allowed values γ and ξ .

Lane Change in Curve scenario, including wind disturbance

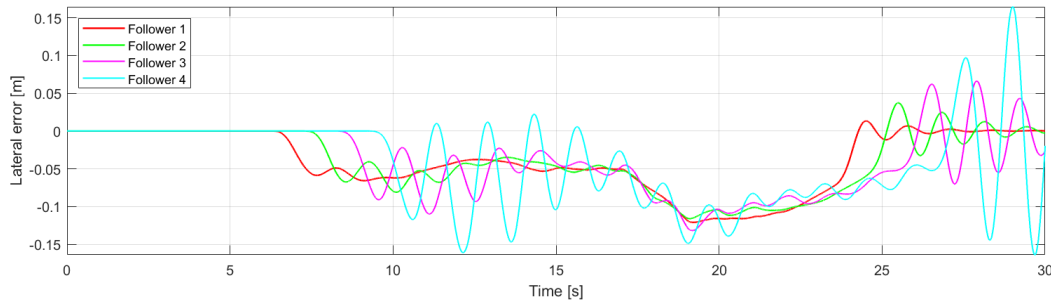


Figure 5-37: Distributed controller, individual lateral error including gust of wind disturbance

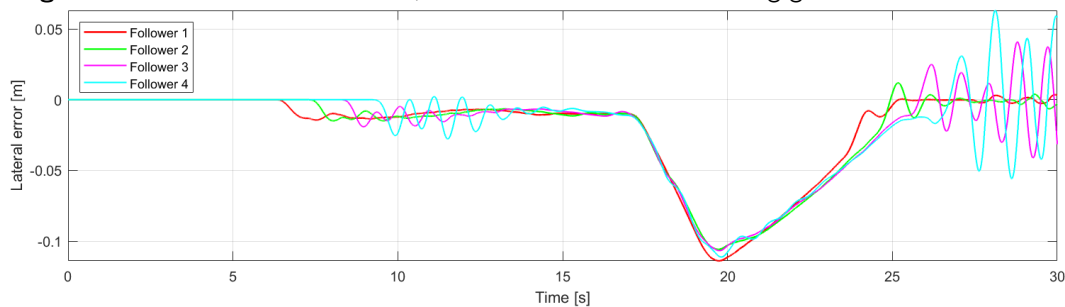


Figure 5-38: Centralized controller, individual lateral error including gust of wind disturbance

Finally, the last scenario for which scenarios have been carried out is the wind disturbance acting on the vehicles while performing the double lane change in the constant curve. Figures 5-37 and 5-38 display the retrieved plots from the simulation. These plots correspond strongly to the plots found in the constant curve excluding the double lane change, showing the same behaviour for both controllers.

The distributed controller's tracking performance in this situation is somewhat nervous, showing very shaky tracking performance, but while still maintaining its boundedness. It has to some extent difficulty with trying to recover from the gust; 'one-by-one' they are steered back on the reference trajectory, but while oscillating. When back in the original lane, the string instability phenomenon can once more be identified; by showing amplification of the lateral error signal.

However it must be noted that a scenario like this would test almost limit conditions; a strong crosswind on a double lane change in a steady state condition. Nonetheless, the controllers should be able to cope with these kinds of scenarios.

The tracking behaviour of the centralized controller is found to be more smooth; significantly less oscillation around the steady state. Moreover, the controller seems to recover in a more strict manner; steering all the vehicles back onto the reference trajectory at once rather than 'one-by-one', and does so in seemingly less time. When the vehicles are back in their lane, oscillations are excited again and for this approach damped out slowly rather than amplified.

Both Conditions 1 and 2 for PLSS are satisfied, implying that even under such heavy conditions, the platoon succeeds to safely perform such manoeuvres.

5-3 Discussion and comparison

In this section, the results that have been obtained by performing the simulations under all sorts of conditions will be further discussed. Hereafter a comparison between the two different control approaches is performed to determine the superior solution. Certain aspects of the controller performance are critically highlighted and some further remarks are made in order to lay the basis for the conclusion that will be drawn in the next chapter.

Tracking performance

By reviewing the trajectory- and lateral error plots, one can comfortably deduce that both controllers show excellent reference trajectory tracking performance. For all three scenarios, and under all driving conditions, the controllers managed to stay within the imposed bounds by great margins. At no point during the simulations, a vehicle either got 'lost' from the platoon or came close to swerve into a neighbouring lane while performing the manoeuvres.

When comparing the tracking performance of both controllers, one can conclude the 'benchmark' centralized controller outperforms its competitor, but not by a great margin. For almost all scenarios and under all conditions, the values of maximum overshoot and overall smoothness of tracking was better for the centralized controller. Moreover, noise was better handled by this controller. This can likely be explained by the virtue of having the state information of all the vehicles available at every time instant and therefore possesses a more detailed overview of the scenario.

It can be concluded that although the centralized controller performed better during the simulations, its practical implementation remains a point of attention. Ultra-fast, noiseless 5G communication is an absolute requirement, especially for highway driving conditions. In [46] it was stated 5G can deliver a data transmission of 20 Gb/s at a maximum latency of 3 ms. Therefore, if fast enough processors controllers and actuators are embedded in the AV, such an approach could be viable.

Noise- and disturbance rejection

Assessing the controllers' robustness is done by verifying how well noised- and disturbance are rejected by the controller. From the plots in Section 5-1 it can be derived that both controllers are affected, but that tracking performance remains of high efficiency.

The distributed approach endured greater effects of both the measurement noise as the added disturbance, compared to the centralized approach. The measurement noise introduced oscillations that further amplified the propagation of lateral error along the string of vehicles. However, these amplifications remained in the order of magnitude mostly below 0.1 m, after which they were conventionally damped out by the system dynamics. When pushed off the reference trajectory by the gust of wind, the distributed controller successfully recovered without additional overshoot, but took some time; indicating more robust control rather than aggressive.

The centralized controller reacted similar to the additional disturbances, hence we observe somewhat the same behaviour but with less overshoot and different frequency oscillations.

Furthermore, it also recovers 'quicker' from the gust of wind scenario by steering the vehicles back in place at the same time, rather than 'one-by-one'. It was assumed this difference lies at the heart of the centralized controller; having the overview of all state-variables for all platoon members available. Moreover it is also assumed some difference can be explained by the difference in tuning variables for both controllers, as they incorporate two completely different system models.

String stability results

The aim of this thesis was to design a string stable, lateral controller for a homogeneous platoon. A novel definition was introduced to ensure stability not the theoretical sense by the use of complex mathematics, but rather in the practical sense by limiting the maximum overshoot on the lateral error output of the system by imposing constraints on the MPC. Recall Definition 4.2:

Definition 4.2 A vehicle platoon of n members incorporating a Model Predictive Control approach is deemed Practically Lateral String Stable (PLSS), if given any $\gamma > 0 \wedge \xi > 0$ the following two conditions hold:

1. $-\gamma \leq y_{e,i}(t) \leq \gamma$ [m] $\forall t, \forall i \in \{1, 2, \dots, n\}$
2. $-\xi \leq y_{e,0}(t) - y_{e,n}(t) \leq \xi$ [m] $\forall t, \forall i \in \{1, 2, \dots, n\}$

For this application, γ and ξ were chosen as respectively 0.2 and 0.78 in order to ensure vehicles stay within their respective lane. It has been shown in the results section this has been the case for all scenarios under both normal and noised conditions, thus may it be concluded both controllers, for this application and for $n = 5$, are PLSS. In fact, during the normal driving conditions, the lateral errors were still comfortably clear of the imposed bounds, implying high-level PLSS. Under disturbed conditions, this margin became less comfortable but still easily acceptable. The values obtained are collected and can be observed in Figure 5-39 for a clean overview.

Individual Maximum overshoot of $y_{e,i}$ [m]											
$\gamma = 0.2$	Scenario 1			Scenario 2			Scenario 3			PLSS?	ALSS?
	normal	noise	wind	normal	noise	wind	normal	noise	wind		
Centralized	0.02	0.06	0.07	0.03	0.06	0.01	0.03	0.06	0.01	Yes	No
Distributed	0.04	0.14	0.07	0.04	0.07	0.05	0.05	0.07	0.06	Yes	No

$\xi = 0.78$											
Total Maximum overshoot of $y_{e,i}$ [m]											
	normal	noise	wind	normal	noise	wind	normal	noise	wind	PLSS?	ALSS?
Centralized	0.07	0.21	0.41	0.06	0.28	0.4	0.06	0.31	0.4	Yes	No
Distributed	0.17	0.29	0.62	0.11	0.17	0.36	0.08	0.37	0.48	Yes	No

Figure 5-39: Summary of results for String Stability Assessment

Unfortunately, the controllers were not able to ensure the attenuation of lateral errors throughout the platoon and therefore we must conclude the controllers do not suffice the conditions set in Definition 4.3, and thus are not Absolute Lateral String Stable.

Platoon length

The results that have discussed been in the previous section have indicated that for a platoon of $n = 5$ vehicles, PLSS under normal- and disturbed conditions could be guaranteed for both control approaches. However, when observing the trend of amplification along the string of vehicles, together with the 'safe margin' that is still left, it is assumed the platoon could safely be extended with more vehicles and remain PLSS.

As the centralized approach showed no amplification of lateral error during the double lane change, the distributed controller was investigated once more while extending the platoon to nine followers, i.e. $n = 10$. This supplied the following result under normal driving conditions.

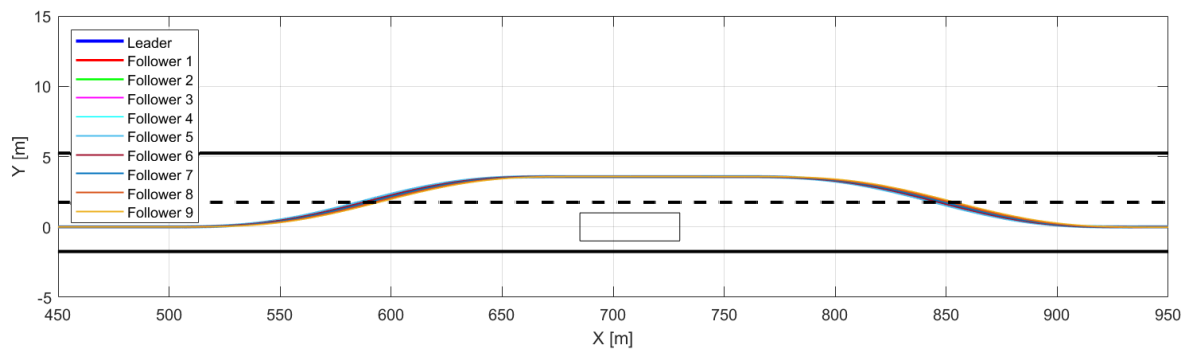


Figure 5-40: Trajectory plot for $n = 10$ vehicles

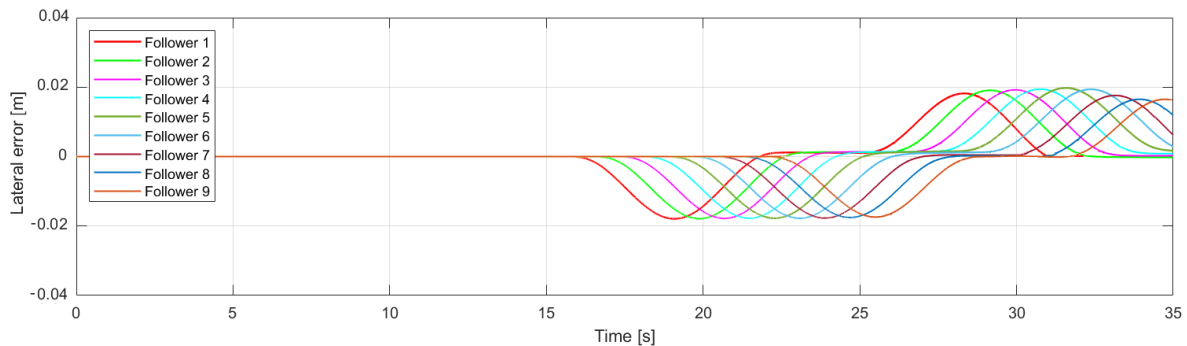


Figure 5-41: Individual lateral errors for $n = 10$ vehicles

One observes that the amplification trend has now been extended for $n = 10$ vehicles. The slight amplification has made sure the total lateral error has gradually increased to ≈ 0.38 m, therefore still easily respecting all restrictions and stay PLSS. However in order to determine for which n a platoon would become unstable is highly dependent on the type of application, system model, strictness in constraining and would therefore require further research.

Controller comparison

The above discussion of results is summarized in the table of Figure 5-42.

	Tracking Performance	Noise Rejection	Computation time	Model Complexity	Practical Feasibility	PLSS?
Distributed	●	◐	◐	◐	◐	Yes
Centralized	●	◐	◐	◐	◐	Yes

● = very high ◐ = high ◑ = moderate ◒ = low

Figure 5-42: Controller comparison

Both controllers showed excellent tracking behaviour with negligible difference during normal conditions. During the disturbed conditions, the centralized controller performed slightly better, and therefore scores higher on noise- and disturbance rejection. In terms of computation time, once more the centralized controller scores higher, but a note must be placed here on how this would hold for real life applications. This can be read in Section 6-1. The distributed model model incorporates only its own vehicle model as state-space equation with the reference of its predecessor. Therefore, it is far less complex as compared to the centralized controller, that incorporates the state-space equations of all followers. Due to the limitations on the wireless communication speeds and latency, it is expected the centralized controller has low practical feasibility. It was therefore treated as a 'benchmark' controller throughout this thesis. Whereas the distributed relies only on measurements, the practical feasibility, a very important aspect, is far more feasible.

To finalize the comparison, considering the distributed MPC approach did not greatly underperform, it is therefore perceived to be a worthy solution or substitute to overcome the issue of practical implementation for the centralized controller.

Additional remarks: Communication loss

Chapter 4 devoted a section to the differences between the two handled control approaches in this work. For this application under normal driving conditions, all wireless communication were assumed perfect. In the noised scenario, high frequency deviations were added to these signals to resemble real life disturbances.

However, a situation in which a sudden loss of communication or sensor malfunctioning occurs, in which case no state variables at all are fed to the MPC, has not been treated in this work as it fell outside of the scope. Therefore it is unknown how either controller would respond in such a situation where lateral control is no longer active.

A possible solution could be to incorporate an emergency-braking function, since a longitudinal controller is already assumed present. In such a scenario, the platoon could attempt to slow down to a complete stop without steering. Another possibility could be to rely on other fall-back methods, e.g. discussed in [47].

Additional remarks: Multiple velocity testing

For the double lane change scenario, testing has been performed at a constant velocity of 100 km/h to comply with highway guidelines. Whereas for the curve scenarios, 80 km/h was endorsed for safe cornering reasons. In addition, it is interesting to see how the controllers would perform when other velocities are handled. Tests were performed on the double lane change scenario at both lower (80 km/h) and higher velocities (120 km/h), excluding noise. The result can be observed in Figures 5-43 and 5-44.

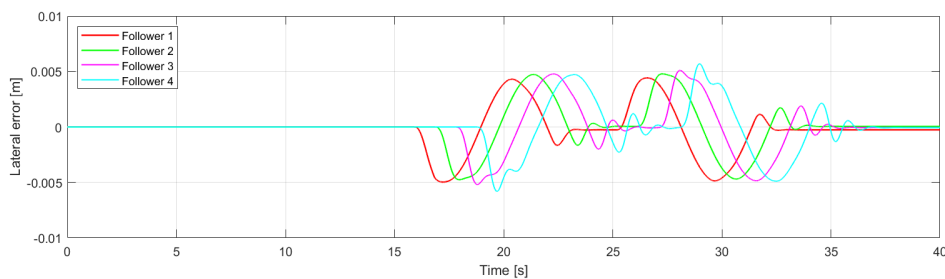


Figure 5-43: Distributed controller, double lane change at 80 km/h

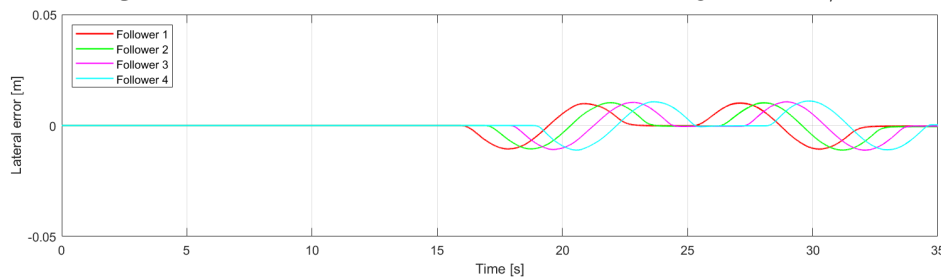


Figure 5-44: Centralized controller, double lane change at 80 km/h

The test performed at 80 km/h showed little difference; tracking performance was still excellent, yielding even better results (maximum $y_{e,i} = 0.005$ because the controller apparently has more time to anticipate. The distributed controller introduces some shakiness for the fourth follower, but clearly PLSS conditions are still satisfied.

Conversely, the tests performed at 120 km/h yielded slightly worse performance, as expected. In Figures 5-45 and 5-46, we observe the opposite effect; clearly the controller has less time to anticipate due to the inter-vehicle time having decreased from 0.72 s to 0.6 s. As a result, bigger oscillations have been introduced for both controllers. Furthermore, notice how the plots look different from the plots performed at 100 km/h, as the in-and-out merging of the lane is done at a faster rate in this experiment.

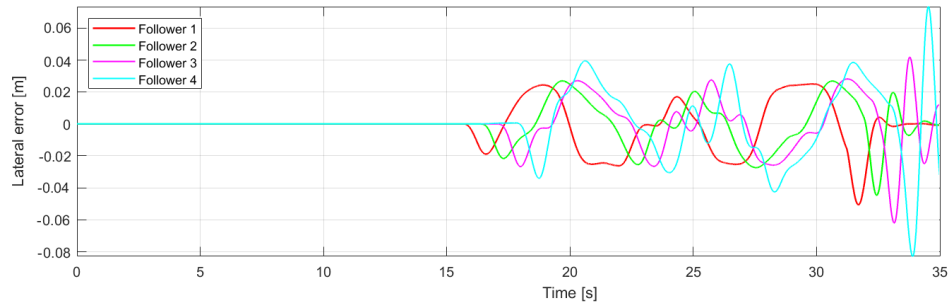


Figure 5-45: Distributed controller, double lane change at 120 km/h

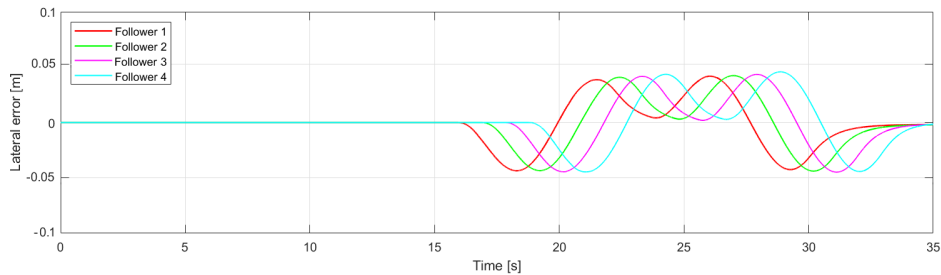


Figure 5-46: Centralized controller, double lane change at 120 km/h

Additional remarks: Controller tuning

Controller tuning is merely a matter of adjusting the state- and input weights, but is of great influence to system performance. Essentially a trade-off between reference tracking vs. fast settling and control freedom has to be made. For this application the chosen weights were selected such to ensure high-performance reference tracking was deemed most important, while a balance between performance and robustness was sought. As the obtained results are satisfactory to the author, a notion must be made on the selected tuning variables. In the results section one has observed the controllers experience oscillations. Simulations of the scenarios have also been ran using other tuning variables in which these oscillations were damped but led to significantly poorer tracking results. Likewise in the constant curve scenario; using different tuning variables has resulted in slightly better tracking, but a steady state error remained for the distributed controller. It can thus be concluded tuning weights do highly influence controller behaviour.

Additional remarks: Ride comfort

The results have indicated high frequency oscillations are introduced during most of the experiments. These oscillations can most probably explained by the controllers not responding properly to the step functions introduced during the curve scenarios. The sudden transition from a straight road into a curve, and vice-versa cause the system dynamics to excite. Even though the amplitudes of the oscillations are of a low order of magnitude, humans experience such oscillations in this frequency band to be annoying [48]. Therefore, ride comfort can decrease for this application using the embedded controllers. However, designing ride comfort did not fell in the scope of this thesis and was therefore not relevant.

Conclusions and Future Work

6-1 Conclusions

The continuous technological advancements in transportation demand continuous solutions for smart mobility. Vehicular platooning is regarded as such a promising solution. By allowing vehicles to cruise at a short inter-vehicle distance, many benefits could be achieved. Amongst these benefits are, first and foremost, the increase of existing road network capacity. More and more vehicles enter the road every day leading to severe congestion. A well-designed platooning solution would increase traffic flow, without ever increasing road infrastructure. Secondly, environmental benefits are to be obtained by a reduction of global fuel consumption and emissions. This is accomplished due to the decrease of aerodynamic drag and efficient speed control. Another substantial asset brought forward by (cooperative) autonomous driving, is its proven contribution to a reduction of accidents by filtering out the human error.

Unfortunately, still some technical challenges need to be overcome in order for platooning to become a widespread application. In the aspect of longitudinal control most bottlenecks have been resolved, whereas for the lateral aspect of control, complications remain. One of these obstacles is the issue of Lateral String Stability that arises when one incorporates a vehicle following approach for lateral control. In principle, Lateral String Stability connotes the amplification of lateral errors in an upstream platoon direction. While executing certain lateral manoeuvres (e.g. a lane change) it is of major importance the fleet of vehicle remains stable and does not swerve off the road or into neighbouring lanes, possibly leading to severe accidents. This issue could possibly be resolved by analyzing the interconnected dynamics of a platoon and identifying control objectives to minimize these effects.

The aim of this master thesis was to design a string stable, lateral controller for a homogeneous platoon of vehicles using a Model Predictive Control approach. During the process, two different control strategies were proposed to determine which would be the superior solution and whether string stability could be achieved in the lateral sense using either of these strategies.

Chapter 1 started by listing the motivation on why platooning is regarded as a promising solution. Hereafter, a brief definition and introduction to the concept of vehicular platooning including the topics of string stability and information flow topology were given. Furthermore, the problem statement, scope, limitations, outline and how this MSc contributes to the State Of The Art were provided of this thesis were provided to set expectations for the reader.

Chapter 2 continued with a review of lateral control methods available in the current literature. The review was completed to identify where a contribution to the State Of The Art could be discovered, and on what ways lateral automation for a platoon could be achieved efficiently. It was concluded a Direct Vehicle Following approach would be most suited for the selected highway-platooning application. Hereafter, a brief overview of the theory behind Model Predictive Control was given along with the accompanying motivation for the method.

The dynamical analysis of a platooning system was performed in Chapter 3. Using the linearized bicycle model, including error dynamics and incorporating a vehicle's dynamical properties in relation to a preceding vehicle, the generalized platoon model that defines the interconnected (lateral) dynamics of the complete platoon could be established.

In Chapter 4, the proposed solution for the problem statement as defined in Chapter 1 was introduced. The chapter started with a further exploration on the concept of String Stability. First, the concept was elaborated in a rather mathematical manner to open insights on developing a novel definition. This novel definition along with its practical implementation, entitled as Practical Lateral String Stability (PLSS), was elaborated after. Essentially, if a vehicular platoon of n vehicles satisfies two conditions posed on the lateral errors, it can guarantee string stability in the lateral domain. This definition provides a guideline and gives sense for practical (in this work, highway) implementation, rather than proving theoretical boundedness. It could therefore be concluded that Definition 4.2 imposes more specified conditions on the vehicle (lateral) behaviour compared with Definition 4.1, and making it a more 'conservative' definition. When further research is performed, using Definition 4.2 would be beneficial because one knows where to start designing, what conditions should be used and up to what n stability holds for a given application. A third definition was introduced that incorporates also the amplification of lateral errors, denoted as Absolute Lateral String Stability (ALSS).

The chapter proceeded with listing the required control objectives. Then, properties of the compared control strategies, Centralized and Distributed were reviewed, discussing the pros and cons for both methods. Essentially, the Centralized approach implies the platoon leader calculates all the control actions for all platoon members based on their vehicle states. Whereas for the distributed approach, each vehicle calculates its own control action based on only its preceding vehicle. Lastly, the complete controller architecture as embedded for this system including all of the MPC-features (discretization, cost function, predictor, constraints, terminal set and cost) were thoroughly discussed.

The simulation setup and accompanying results have been discussed in Chapter 5. First, three scenarios were proposed that would test different controller properties. A double lane change manoeuvre was selected for assessing the platoon's 'obstacle avoiding' capability. Secondly, a constant curve scenario was initiated investigating the controllers' steady-state behaviour. A third scenario was proposed that combines the characteristics of both Scenarios 1 and 2. First, the simulations were run under normal driving conditions. Results have indicated that both controllers performed excellent reference tracking; high accuracy path following

while satisfying all imposed constraints has been achieved. Hereafter, noise- and disturbance conditions were introduced to investigate the controllers' disturbance rejection properties. The noise added to the system was modeled in the form of ZMWN on the communicated vehicle states. Applying these conditions showed no great effects on tracking performance; however steering input became slightly more oscillatory.

The disturbance scenario was modeled as a gust of wind acting on all the vehicles. While blown off the reference trajectories, the controllers showed they were able to recover to the reference trajectory. Even under noised- and disturbed conditions, the lateral errors remained comfortably between the imposed bounds. Therefore, PLSS could be guaranteed. Unfortunately, the controllers did not succeed to also guarantee ALSS behaviour.

When comparing both controllers towards the end of Chapter 5, it was deduced the centralized controller outperformed the distributed controller, but not by a great margin. Considering the practical limitations for the centralized approach, the distributed approach is therefore perceived to be a worthy solution for the selected, highway-platooning application. When taking into account the assumptions and limitations as described in the introduction, one could conclude a sufficient basis for further research is laid in this work.

6-2 Recommendations for further research

Even though this work attempted to contribute the current State Of The Art by proposing a lateral control solution for vehicular platooning, still more knowledge in this field is to be gained by the means of further, more extent research. As a recommendation for the required further research, the following points should be taken into consideration;

- This work has proposed a solution based on the assumption of a linearized bicycle model to describe the lateral vehicle dynamics. Despite the fact for this application the linearization has showed to be sufficiently accurate, for further research it is recommended to use a non-linearized vehicle model instead. This would imply that the assumptions made in tire behaviour, as well as the small angle approximations, no longer hold. In this way even more reliable results can be obtained, but would also imply implementation of a Non-linear MPC is a necessity.
- While running the simulations, longitudinal velocity is assumed constant by the presence of a longitudinal controller. This suggests that the string stable result that was verified, but only for this velocity (and probably lower). In order to safely guarantee string stability for all velocities, one could opt to either incorporate a longitudinal controller to obtain a combined controller, or perform more open loop testing at varying velocities.
- The controller as designed in this work is applied to a homogeneous platoon of vehicles. The assumption of homogeneity for a platoon signifies identical dynamic behaviour for all platoon members. However, for real life applications this would almost never be the case. To attain more credible results, one could for example pose conditions on the homogeneity and leave some room for uncertainty. On the other hand, one could consider a heterogeneous platoon and compare results to this work.

- The results in this work have indicated Lateral String Stability in this work is achieved, but by the means of a novel definition (Practical Lateral String Stability). However, re-evaluating the string stability properties of the system and approaching the novel definition from a different direction would undoubtedly give insights on how this condition can be improved. There is room for extra conditions or rephrasing some of the conditions as proposed in this work, possibly leading to even better results.
- The selected solver to perform optimization steps in this work was chosen to be `Matlab`'s built-in `quadprog` algorithm. The centralized controller simply outperformed the distributed controller. For an average simulation run (of 35 seconds) in the `Matlab-Simulink` environment of Prescan, the distributed controller took ≈ 410 s, whereas the centralized controller lasted ≈ 280 on average. This is explained by the fact that the distributed controller runs five MPCs simultaneously, whereas the centralized controller merely one. The computation time values are acceptable, but can surely be done faster. Therefore, one could consider implementing a different solver for even achieving even shorter computation times. When one chooses to keep using a linear model, a solver such as `CVX` or `CVXGEN` could be used. However, when one chooses to incorporate a non-linear model, employing a non-linear solver such as `FORCES Pro` or `ACADO` would be judicious.
- The controller has been tested by implementing three scenarios that could occur in every day situations. The assessed controller properties such as unforeseen input (obstacle avoidance) and steady state behaviour (constant curve) were taken into account. However, other scenarios or manoeuvres (e.g. platoon merging) that assess other controller properties can also be implemented. Moreover, more noised- and disturbance scenarios can be adopted for even more reliable results. E.g., the concept of communication loss or latency have not been reviewed in this work due to time constraints. It is interesting to investigate how the controller would behave when the state variables are (temporarily) no longer communicated.
- The introduced high frequency oscillations during the simulations are perceived by humans as annoying, [48] concluded. Therefore, if passengers are present in the platoon, ride discomfort may be experienced. To avoid such issues in future research, one could attempt to introduce a clothoid curve between the straight sections and curves to establish a smooth transition rather than using a step input. Otherwise, different tuning weights, cost function and constraints can be incorporated such that ride comfort is also improved for the selected application.
- The results in this work have been obtained by the means of simulation. Even though Simcenter Prescan is a high-fidelity testing environment due to the extensive physics-based platform, it will never be as reliable as performing experiments in everyday life. Therefore, if one bears sufficient confidence in the distributed or centralized MPC approach, it is highly encouraged to perform testing in a (controlled) testing environment.

Linear Tire Behaviour

A tire consists of a set of rubber blocks with two friction mechanisms working on it: shearing and sliding. In shearing, the rubber block deforms without sliding with respect to the ground. A resistance force proportional to deformation is generated. When this force reaches a maximum value, called the Coulomb force, the rubber block rubs on the ground and start sliding. If slip value continue growing, the tire suffers from a loss of potential, which causes the instability of the vehicle. The friction force maximum value is then very important to predict [3]. It depends on two varying-parameters: the vertical load applied by the vehicle and the coefficient of friction that characterizes the condition of both the road and tire rubber. Furthermore, longitudinal adhesion and lateral adhesion are competing: they must share the tire friction potential, i.e. the overall adhesion is delimited by the “friction ellipse”.

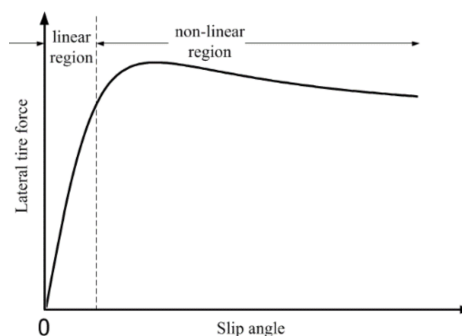


Figure A-1: Lateral tire force against slip [3]

Two regions are distinguished:

- **Linear region:** the curve is linear and increasing, the rubber blocks are deforming without sliding (shearing). Elastically returns to resting state when forces are removed.
- **Non-linear region:** the curve is non-linear and increasing, and ends up reaching a maximum. A portion of the contact area begins to slide. Then, the curve is decreasing, and there is the sliding of the tire. Tire behavior is unstable.

Appendix B

Proof of \mathcal{L}_∞ -stability

Expressing the factorization of $P_i(s)$, $i \geq 2$, as described in Theorem 4.1 in the time domain results in;

$$y_i(t) = (p_i * u_r) \tag{B-1}$$

$$= (\gamma_i * \gamma_{i-1} * \dots * \gamma_2 * p_i * u_r)(t), \quad i \in \mathbb{N} \setminus \{1\}, \tag{B-2}$$

where $*$ denotes the convolution operator. Applying Young's inequality for convolutions, the following inequality is obtained:

$$\|p_i(t)\|_{\mathcal{L}_1} \leq (\prod \|\gamma_k(t)\|_{\mathcal{L}_1}) \|p_i(t)\|_{\mathcal{L}_1}, \quad i \in \mathbb{N} \tag{B-3}$$

from which it follows that $\sup_{i \in \mathbb{N}} \|p_i(t)\|_{\mathcal{L}_1}$ exists, under the conditions 1 and 2 in Theorem 4.1. Since it is also assumed that the pair (C_i, A) is such that unstable and marginally stable modes are unobservable for all $i \in \mathbb{N}$, it thus follows that the linear system is \mathcal{L}_∞ string stable, according to definition X. Moreover, using the \mathcal{L}_∞ -stability gain definition of the system with the impulse response $\gamma_i(t)$ and condition 2 yields;

$$\|y_i(t)\|_{\mathcal{L}_\infty} \leq \|\gamma_i(t)\|_{\mathcal{L}_1} \|y_{i-1}(t)\|_{\mathcal{L}_\infty} \tag{B-4}$$

$$\leq \|y_{i-1}(t)\|_{\mathcal{L}_\infty}, \quad \forall i \in \mathbb{N} \setminus \{1\}, \tag{B-5}$$

implying that the interconnected system is strictly \mathcal{L}_∞ string stable. Clearly, conditions 1 is necessary for both \mathcal{L}_∞ and strict \mathcal{L}_∞ . Moreover, if condition 2 is not satisfied, there exists an $i \in \mathbb{N} \setminus \{1\}$ such that $\|\gamma_i(t)\|_{\mathcal{L}_2} > 1$, yielding $\|y_i(t)\|_{\mathcal{L}_\infty} \geq \|y_{i-1}(t)\|_{\mathcal{L}_\infty}$ which contradicts the string stability requirement in Definition 4.1. Therefore, condition 2 is also a necessary condition for \mathcal{L}_∞ string stability.

Appendix C

Simulation result plots

C-0-1 Double Lane Change Scenario, normal conditions, $v_x = 100$ km/h

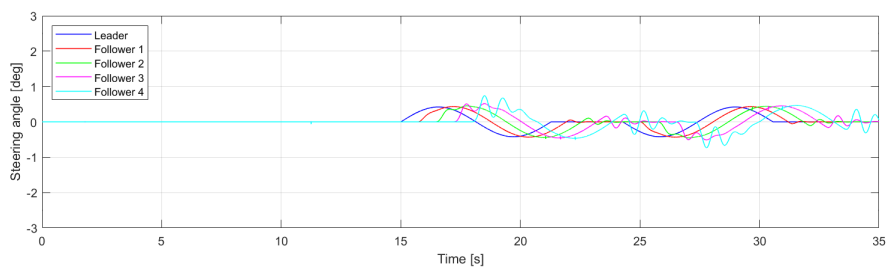


Figure C-1: Distributed controller, steering angle under normal driving conditions

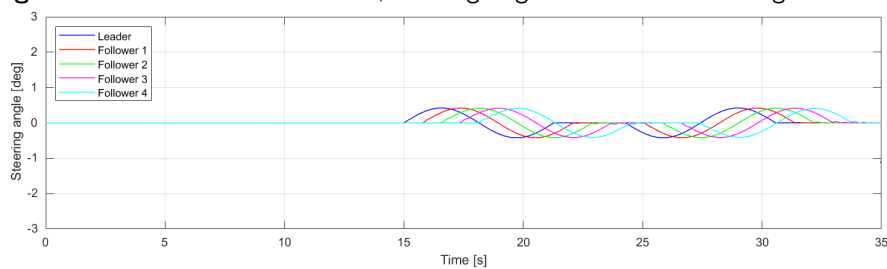


Figure C-2: Centralized controller, steering angle under normal driving conditions

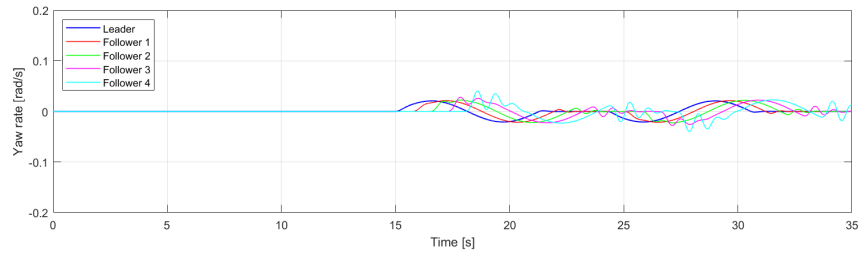


Figure C-3: Distributed controller, yaw rate under normal driving conditions

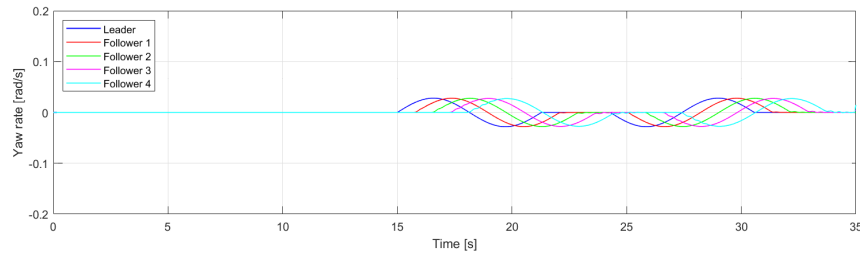


Figure C-4: Centralized controller, yaw rate under normal driving conditions

C-0-2 Constant Curve Scenario, normal conditions, $v_x = 80$ km/h

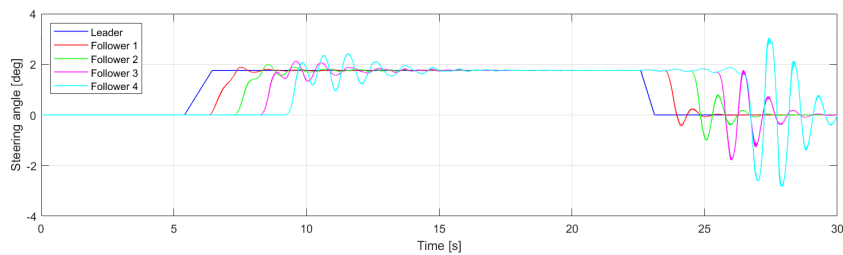


Figure C-5: Distributed controller, steering angle under normal driving conditions

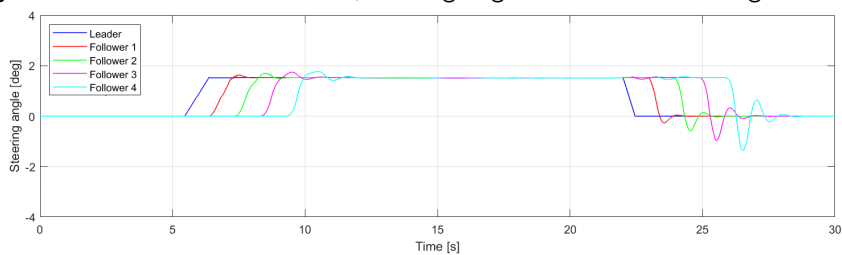


Figure C-6: Centralized controller, steering angle under normal driving conditions

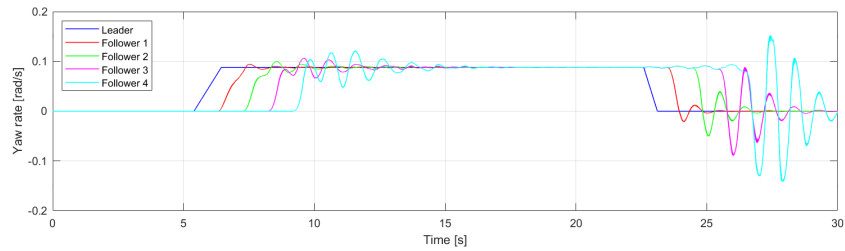


Figure C-7: Distributed controller, yaw rate under normal driving conditions

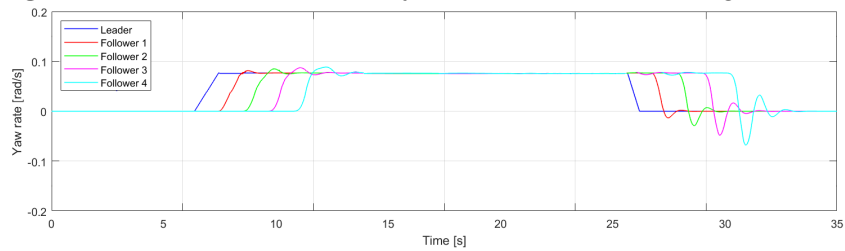


Figure C-8: Centralized controller, yaw rate under normal driving conditions

C-0-3 Lane Change in Constant Curve, normal conditions, $v_x = 80$ km/h

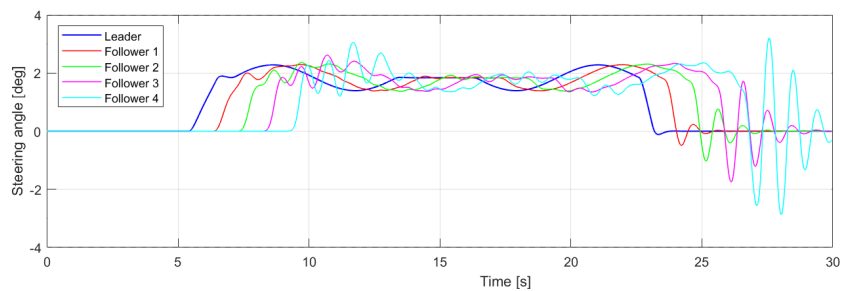


Figure C-9: Distributed controller, steering angle under normal driving conditions

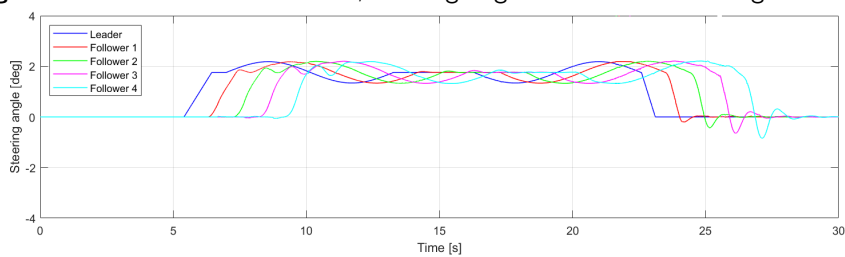


Figure C-10: Centralized controller, steering angle under normal driving conditions

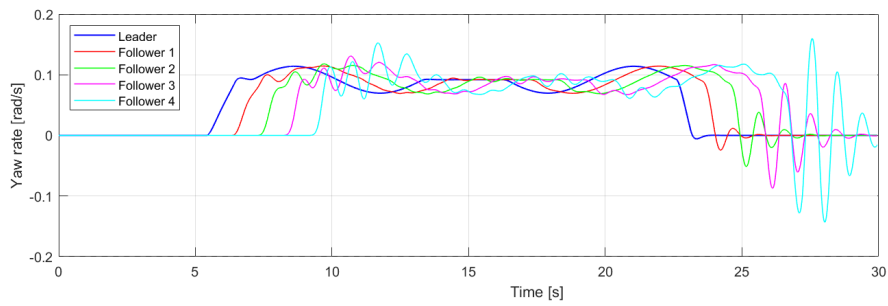


Figure C-11: Distributed controller, yaw rate under normal driving conditions

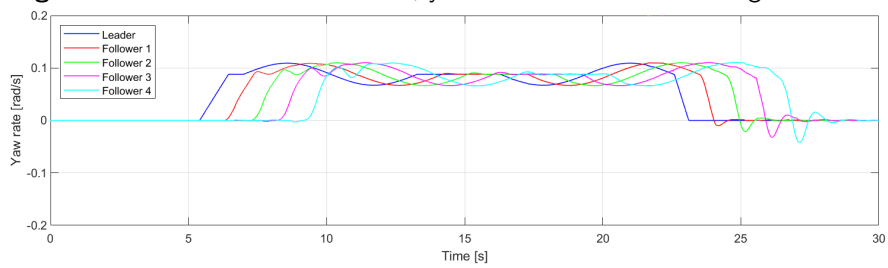


Figure C-12: Centralized controller, yaw rate under normal driving conditions

Bibliography

- [1] Y. Zheng, S. Li, J. Wang, and D. Cao, “Stability and Scalability of Homogeneous Vehicular Platoon: Study on the Influence of Information Flow Topologies,” *IEEE Transactions on Intelligent Transportation Systems*, vol. 3, pp. 205–209, 2016.
- [2] A. Bemporad and M. Morari, “Robust model predictive control: A survey,” *Robustness in identification and control*, pp. 201–226, 2007.
- [3] H. Pacejka, “Tire and vehicle dynamics,” *Elsevier*, 2005.
- [4] K. Salari and J. Ortega, “Experimental Investigation of the Aerodynamic Benefits of Truck Platooning,” *SAE Technical Paper 2018-01-0732*, p. 11, 2018.
- [5] A. Davila and E. Del Pozo, “Environmental Benefits of Vehicle Platooning,” *SAE Technical Paper 2013-26-0142*, p. 6, 2013.
- [6] M. Nombela and A. Davila, “Platooning: Safe and Eco-Friendly mobility,” *SAE Technical Paper 2012-01-0488*, p. 6, 2012.
- [7] K. Hymel, A. Small, and K. Dender, “Induced demand and rebound effects in road transport,” *Transportation Research Part B: Methodological*, vol. 44, pp. 1220–1241, 2010.
- [8] S. Ishikawa and S. Arai, “Evaluating advantage of sharing information among vehicles toward avoiding phantom traffic jam,” *2015 Winter Simulation Conference (WSC)*, vol. 44, pp. 1220–1241, 2015.
- [9] V. Turri, B. Besselink, and J. Martensson, “Fuel-efficient heavy-duty vehicle platooning by look-ahead control,” *Proceedings of the IEEE Conference on Decision and Control*, pp. 654–660, 2015.
- [10] S. Tsugawa, S. Jeschke, and S. Shladover, “A Review of Truck Platooning Projects for Energy Savings,” *IEEE Transactions on Intelligent Vehicles*, vol. 1, pp. 68–77, 2016.
- [11] J. Treat, “A study of pre-crash factors involved in traffic accidents,” *Highway Safety RI Research Review*, vol. 6, pp. 10–15, 1980.

- [12] U. S. Dept. of Transportation, “Traffic Safety Facts,” *National Highway and Traffic Safety Administration, Washington DC*, 2015.
- [13] S. Li and Y. Zheng, “Influence of information flow topology on closed-loop stability of vehicle platoon with rigid formation,” *IEEE Transactions on Intelligent Transportation Systems*, 2014.
- [14] T. C. Ng and J. Guzman, “Autonomous Vehicle Following System - A Virtual Trailer Link Approach,” *International Conference on Intelligent Robots and Systems*, 2005.
- [15] P. Cook, “Conditions for String Stability,” *Systems and Control letters*, vol. 54, pp. 991 – 998, 2003.
- [16] J. A. de Geus, “Lateral Vehicular Platoon Control: A literature review,” *TU Delft*, 2020.
- [17] S. Stankovic and M. Stanojevic, “Decentralized overlapping control of a platoon of vehicles,” *IEEE Transactions on Control Systems Technology*, 2000.
- [18] L. Shengbo and Y. Zheng, “Stability Margin Improvement of Vehicular Platoon Considering Undirected Topology and Asymmetric Control,” *IEEE Transactions on Control Systems Technology*, vol. 24, pp. 1253–1265, 2015.
- [19] R. Hall and C. Chin, “Vehicle sorting for platoon formation: Impacts on highway entry and throughput,” *Transportation Research Part C: Emerging Technologies*, vol. 13, pp. 405–420, 2005.
- [20] L. Davis, “Comment on ‘Analysis of optimal velocity model with explicit delay’,” *PHYSICAL REVIEW E*, 2002.
- [21] “Veilig Verkeer Nederland, <https://verkeersregels.vvn.nl/situatie/afstand-houden>,”
- [22] R. Rajamani, H. Tan, L. Boon, and W. Zhang, “Demonstration of Integrated Longitudinal and Lateral Control for the Operation of Automated Vehicles in Platoons,” *IEEE Transactions on Control Systems Technology*, vol. 8, pp. 695–701, 2000.
- [23] K. Lee and M. Han, “Lane-following method for high speed autonomous vehicles,” *International Journal of Automotive Technology*, vol. 9, pp. 607–613, 2008.
- [24] J. Goldbeck and B. Huertgen, “Lane following combining vision and DGPS,” *Image and Vision Computing*, vol. 18, pp. 425–433, 2000.
- [25] A. Schmeitz, J. Zegers, J. Ploeg, and M. Alirezeai, “Towards a generic lateral control concept for cooperative automated driving,” *IEEE Conference on Models and Technologies for Intelligent Transportation Systems*, 2017.
- [26] R. Castro, A. Schaub, and C. Satzger, “A Vehicle Following Controller for Highly Actuated Vehicles,” *International Conference on Intelligent Transportation Systems*, 2016.
- [27] S. Solyom, A. Idelchi, and B. Bin-Salaman, “Lateral Control of Vehicle Platoons,” *International Conference on System, Man and Cybernetics*, 2013.
- [28] S. Gehrig and F. Stein, “A trajectory-based approach for the lateral control of car following systems,” *IEEE Conference on Systems, Man and Cybernetics*, 1998.

-
- [29] F. Espinosa, A. Awawdeh, and M. Mazo, “Non-Linear Trajectory Generation and Lateral Control New Algorithms to Minimize Platoon’s Oscillations,” *American Control Conference*, 2004.
- [30] C. Chen and L. Shaw, “On receding horizon feedback control,” *Automatica*, vol. 18, pp. 349–352, 1982.
- [31] D. Bertsekas, “Dynamic Programming and Suboptimal Control: A Survey from ADP to MPC,” *European Journal of Control*, vol. 11, pp. 310–334, 2005.
- [32] D. Hrovat, S. Di Cairano, and H. Tseng, “The development of Model Predictive Control in automotive industry: A survey,” *2012 IEEE International Conference on Control Applications*, 2013.
- [33] R. Rajamani, “Vehicle Dynamics and Control,” *Mech. Eng. Series Springer, US*, 2011.
- [34] M. Abe, “Vehicle handling dynamics: Theory and Application,” *Butterworth-Heinemann*, 2015.
- [35] J. Ploeg, “Lp String Stability of Cascaded Systems: Application to Vehicle Platooning,” *International IEEE Conference on Control System Technology*, pp. 786 – 793, 2013.
- [36] J. Ploeg, “Analysis and design of controllers for cooperative and automated driving (Doctorial Master thesis),” *TU/e Ripository*, 2014.
- [37] L. Peppard, “String stability of relative-motion PID vehicle control systems,” *IEEE Transactions on Automatic Control*, vol. 19, pp. 579 – 581, 1974.
- [38] D. Swaroop and J. Hendrick, “String stability of interconnected systems,” *IEEE Transactions on Automatic Control*, vol. 3, pp. 1806–1810, 1995.
- [39] S. Feng, S. Li, and Z. Cao, “String Stability for vehicular platooning: Definitions and analysis methods,” *Annual Reviews in Control*, 2019.
- [40] R. Kianfar, P. Falcone, and J. Fredriksson, “A distributed model predictive control approach to active steering control of a string stable cooperative vehicle platoon,” *IFAC AAC*, 2013.
- [41] M. Verhaegen and V. Verdult, “Filtering and Identification, A least squares approach,” *Cambridge University Press*, 2007.
- [42] C. Diels and J. Bos, “Self-driving carsickness,” *Applied Ergonomics*, pp. 374–382, 2016.
- [43] B. De Schutter and T. Van Den Boom, “Optimization in Systems and Control,” 2018.
- [44] J. Vos, “Richtlijn Ontwerp Autosnelwegen 2017 (ROA2017),” *Ministerie van Infrastructuur en Milieu, Rijkswaterstaat Grote Projecten en Onderhoud (RWS, GPO)*, pp. 64–69, 2017.
- [45] Y. Maruyama and F. Yamazaki, “Driving simulator experiment on the moving stability of an automobile under strong crosswind,” *Journal of Wind Engineering and Industrial Aerodynamics*, vol. 191-205, p. 94, 2004.

-
- [46] C. Ping-Li, W. Chen, and T. Ti, “5G ultra-reliable and low-latency systems design,” *European Conference on Networks and Communications*, 2017.
- [47] S. Sheikholeslam and C. Dasoer, “Longitudinal control of a platoon of vehicles with no communication of lead vehicle information: a system level study,” *IEEE Transactions on Vehicular Technology*, 1993.
- [48] D. Pelargus and A. Schmidt, “The influence of oscillations on the ride comfort of passenger cars—a study to correlate objective data with subjective perceptions.,” *14th FISITA Congress*, pp. 19–28, 1992.